

**Thermostamping of Long-Fiber Thermoplastic Composites:
Consideration of Wrinkles, Distortions, and Cost**

Samuel Ste-Marie

A Thesis
In
The Department
of
Mechanical and Industrial Engineering

Presented in Partial Fulfillment of the Requirements
For the Degree of
Master of Applied Science (Mechanical Engineering) at
Concordia University
Montreal, Quebec, Canada

April 2018

© Samuel Ste-Marie, 2018

CONCORDIA UNIVERSITY
School of Graduate Studies

This is to certify that the thesis prepared

By: Samuel Ste-Marie

Entitled: Thermostamping of Long-Fiber Thermoplastic Composites: Consideration of
Wrinkles, Distortions, and Cost

and submitted in partial fulfillment of the requirements for the degree of

Master of Applied Science (Mechanical Engineering)

Complies with the regulations of the university and meets the accepted standards with respect to
originality and quality.

Signed by the final examining committee:

_____Chair
Dr. Chevy Chen

_____Examiner
Dr. Zhibin Ye

_____Examiner
Dr. Mehdi Hojjati

_____Supervisor
Dr. Suong Van Hoa

Approved by

Dr. Chair of Department of Mechanical and Industrial Engineering

Dr. Dean of Faculty of Engineering and Computer Science

Date: _____

Abstract

Thermostamping of Long-Fiber Thermoplastic Composites: Consideration of Wrinkles, Distortions, and Cost

Samuel Ste-Marie

Thermostamping is a popular manufacturing method to form thermoplastic composites because of its fast cycle time, allowing production at low cost. As any manufacturing method, obtaining a defect-free part which respects the geometry tolerance is a challenge.

The goal of this study is to use simulations to evaluate and optimize the manufacturing process of thermostamped parts in order to avoid or minimize defects. The defects analyzed here are shape distortions and wrinkles. In addition, a cost analysis method is developed to estimate composite manufacturing costs.

A detailed characterization of PPS/Carbon pre-impregnated material in order to identify the specific heat, the coefficient of thermal expansion and the mechanical properties over a wide range of temperature was conducted. Those temperature related properties are then used in a finite element analysis using a sequential thermal-mechanical approach to predict shape distortion. The model is evaluated for spring-in of an angled part. A sensitivity analysis showed that CTE is the most influential parameter compared to the friction coefficient and mechanical properties.

A methodology to optimize the initial manufacturing set-up and to minimize or to remove wrinkles using different methods is done using a commercial finite element software. It was found that removing redundant material, adding springs and changing springs tension are successful methods to eliminate wrinkles in a double curved part manufactured with thermostamping.

Finally, a cost analysis methodology is presented. The method is applied to a case study comparing thermostamping of long fiber reinforced thermoplastics, resin transfer molding of a thermoset with long fiber and compression molding using short fibers.

Résumé

Thermoformage de composite thermoplastique à fibres longues : Considération de la formation de replis, des distorsions géométriques et du coût

Samuel Ste-Marie

Le thermoformage est une méthode de fabrication populaire pour former des composites thermoplastiques en raison de son temps de cycle rapide, permettant la production à faible coût. Comme avec tout procédé de fabrication, une pièce sans défaut qui respecte les tolérances géométriques est un défi.

Le but de cette thèse est d'utiliser des simulations pour évaluer et optimiser le processus de fabrication de pièces faites par thermoformage afin d'éviter ou de minimiser les défauts tels que les distorsions géométriques et les replis. De plus, une analyse des coûts est élaborée pour estimer les coûts de fabrication de pièce en composite pour le milieu de l'aérospatiale.

Une caractérisation détaillée du matériau pré-imprégné PPS / Carbone est faite afin d'identifier la chaleur spécifique, le coefficient de dilatation thermique et les propriétés mécaniques sur une large plage de température. Ces propriétés sont ensuite utilisées dans une analyse par éléments finis en utilisant une approche séquentielle thermique-mécanique afin de prédire la déformation géométrique. Le modèle est évalué sur une pièce angulaire. Une analyse de sensibilité a montré que le coefficient de dilatation thermique est le paramètre le plus influent par rapport au coefficient de frottement et aux propriétés mécaniques.

Une méthodologie pour optimiser le processus de fabrication minimisant les replis a été développée en utilisant un logiciel d'éléments finis. Il a été constaté que l'élimination de matériaux redondants, l'ajout de ressorts et la modification de la rigidité des ressorts sont des méthodes efficaces d'élimination des replis.

Enfin, une méthodologie d'analyse des coûts est présentée. La méthode concerne le thermoformage de composite thermoplastiques à fibres longues, le moulage par transfert de résine thermodurcissable imprégnant fibres longues et le moulage par compression d'un thermoplastique pré-imprégné de fibres courtes.

Acknowledgement

This project was possible because of the help of Concordia University, the Concordia Center for Composites (CONCOM), the Consortium for Research and Innovation in Aerospace in Quebec (CRIAQ) and, Pratt and Whitney Canada. The support of Barry Barnett from Pratt and Whitney Canada through this project is very appreciate.

I would like to express my sincere gratitude to Dr. Hoa. I feel very lucky to have been in is team and to have been under his guidance. Dr. Hoa was very present and available all along this journey. I will always appreciate the opportunity he gave me and all the knowledge he shared. I would also like to thank members of Dr. Hoa team, Daniel Rosca and Heng Wang.

I would also like to thank all the colleagues I had the chance to work with and which helped me; Hoang Minh Duc, Junfei Li, Hossein Ghayoor, Nima Shabani Jafroudi, Yasser Sami Elsherbini and all the others.

I would like to thanks all my close family; Francois, Manon, Simon and Amélie for their support and unconditional love. Finally, Rosalie Beaudoin-Vles for all the encouragements, the support and the love.

Table of contents

Chapter 1.	Introduction.....	12
1.1	Objectives	13
Chapter 2.	Literature Review.....	15
2.1	Thermoplastic Behavior.....	16
2.2	Pre-impregnated Thermoplastic & Thermostamping	19
2.3	Wrinkles.....	20
2.4	Shape distortions.....	22
2.5	Cost Analysis	26
Chapter 3.	Material Characterization.....	29
3.1	Introduction.....	29
3.2	Matrix Kinetics and Specific Heat.....	29
3.3	Coefficients of Thermal Expansion	34
3.4	Thermo-Mechanical Behavior	39
3.5	Conclusion	41
Chapter 4.	Finite element method for shape distortion prediction	42
4.1	Introduction.....	42
4.2	Thermal Simulation	45
4.3	Mechanical Simulation	50
4.4	Conclusion	60
Chapter 5.	Methodology for Wrinkles removal.....	61
5.1	Introduction.....	61
5.2	Methodology.....	63

5.3	Experimental	66
5.4	Simulation	67
5.5	Results and Discussion	69
5.6	Conclusion	78
Chapter 6.	Cost Analysis: Composite Manufacturing	79
6.1	Introduction.....	79
6.2	Methodology	80
6.3	Case study: Comparison of three manufacturing methods for an aerospace part.	86
6.4	Conclusion	98
Chapter 7.	Conclusion, Contributions & Future work.....	99
7.1	Conclusion	99
7.2	Contributions.....	100
7.3	Future work.....	100
Chapter 8.	References.....	102

List of figures

Figure 2.1: Thermoplastic Composites in Commercial Aircraft [1].....	15
Figure 2.2: Comparison between amorphous and semi-crystalline phase [2]	16
Figure 2.3: Graph of Modulus vs. Temperature of a typical semi-crystalline thermoplastic [6] .	18
Figure 2.4: Mechanisms during stamping and Inter-ply slip example [2].....	21
Figure 2.5: Skin-core effect [21].....	24
Figure 2.6: Thermal correction calculation [6].....	25
Figure 2.7: Cost estimation methods comparison, Adapted from [27].....	28
Figure 3.1: DSC signal of a typical semi-crystalline thermoplastic	30
Figure 3.2: DSC signal of TC1100	31
Figure 3.3: Impact of cooling rate on the final crystallinity	32
Figure 3.4: Relative crystallinity as function of cooling rate.....	32
Figure 3.5: Peak melting temperature as function of cooling rate	33
Figure 3.6: Heat flow and Heat capacity versus temperature	34
Figure 3.7: Reference direction for samples	35
Figure 3.8: TMA set-up	35
Figure 3.9: TC1100 thermal strain vs Temperature - Sample 2 Direction 1	36
Figure 3.10: Transition of linear thermal expansion – Sample 3.....	37
Figure 3.11: Linear thermal expansion vs Temperature - Out-of-plane. (a) Before deconsolidation (b) Melting of the matrix, deconsolidation of the sample. (c) Over crystallization. (d) Crystallization shrinkage. (e) After crystallisation (f) difference of sample thickness	38
Figure 3.12: DSC and TMA signals with a cooling rate of 1°C/min.....	38
Figure 3.13: DMA Storage modulus versus Temperature	41
Figure 4.1: Temperature profile.....	43
Figure 4.2: Process steps.....	44
Figure 4.3: Thermocouples	49
Figure 4.4: Comparison FEA and thermocouples data.....	50
Figure 4.5: References for shrinkage models	56
Figure 4.6: Experimental data from [45]	58

Figure 4.7: Experimental part[45].....	58
Figure 4.8: Finite element results.....	58
Figure 4.9: Model comparison.....	59
Figure 5.1: (a) Shape profile and (b) Final part	63
Figure 5.2: (a) Die assembly and (b) Springs positioning	67
Figure 5.3: Wrinkles on experimental part	68
Figure 5.4: Effect of mesh size on wrinkle detection	69
Figure 5.5:Reference springs stiffness and position	70
Figure 5.6: Taguchi’s results; (a) Shear angle, (b) In-Plane Fiber Stress X and (c) In-Plane Fiber Stress Y	71
Figure 5.7: Final set-up - (a) Upper view of the gripping set-up and (b) Isometric view of the complete set-up	72
Figure 5.8: Wrinkles mechanisms [57].....	72
Figure 5.9: Buckled region evolution (Stresses in y-direction)	73
Figure 5.10: Material removal "d"	74
Figure 5.11: Material removal comparison d=20 mm; (a) x stresses, (b) y stresses and (c) experimental.....	74
Figure 5.12: Stresses comparison for material removal.....	75
Figure 5.13: Added springs set-up	75
Figure 5.14: (a) y -stresses (b) x-stresses * Arrows show where the maximum stresses were taken.....	76
Figure 5.15: Stresses comparison for added springs.....	76
Figure 5.16: Stiffer spring’s set-up	76
Figure 5.17: (a) y -stresses (b) x-stresses for Case 3 * Arrows show where the maximum stresses were taken	77
Figure 5.18: Stresses comparison for stiffer springs.....	77
Figure 6.1: Overall project cost (Adapted from [10]).....	79
Figure 6.2: Manufacturing method versus volume [10]	86
Figure 6.3: Cross section overall shape	87
Figure 6.4: Process flows for the 4 manufacturing methods	88
Figure 6.5: Scrap percentage based on initial sheet geometry.....	89

Figure 6.6: Chart of cost summary	94
Figure 6.7: Thermostamping cost repartition.....	96
Figure 6.8: Total cost distribution based on Monte Carlo Simulation.....	97

List of tables

Table 2.1: Thermoplastic vs. Thermoset Composite	16
Table 2.2: Thermostamping steps	20
Table 2.3: CTE for various thermostamping related materials [6]	24
Table 3.1: CTE in-plane.....	36
Table 3.2: CTE out-of-plane.....	37
Table 3.3: CTE in direction 3 – Wide range.....	39
Table 4.1: CF T300 properties	46
Table 4.2: PPS TC1100 properties.....	46
Table 4.3: Density of TC1100 according to ASTM D702.....	46
Table 4.4: Summary of the thermal properties	48
Table 4.5: Summary of the thermal interaction properties	48
Table 4.6: Elastic orthotropic properties of TC1100	52
Table 4.7: Steel and TC1100 properties	53
Table 4.8: Contact properties.....	54
Table 4.9: Parameters and Levels for sensitivity analysis	55
Table 4.10: Properties and Temperatures for Radford and O'Neill model	57
Table 5.1: Constitutive models and parameters values for PPS/Carbon at 325°C from Aniform documentations [59] Calibrated on 17/02/2016.....	66
Table 5.2: Control Parameters and Alternative Levels.....	70
Table 6.1: Symbols for cost analysis	85
Table 6.2: Summary of labor cost.....	91
Table 6.3: RTM equipment and tooling cost	92
Table 6.4: Thermostamping equipment and tooling cost.....	92
Table 6.5: DLF equipment and tooling cost	93
Table 6.6: Summary of cost for all methods.....	94
Table 6.7: Manufacturing methods and obtained properties / *average between 0 and 90.....	95
Table 6.8: Inputs for Monte Carlo simulation	97

Chapter 1. Introduction

The use of composite materials in the aerospace industry has significantly increased in recent years and is still continuing its ascension. Commonly, thermosets are the preferred matrix to use but there is a growing interest in thermoplastics matrix. This is due to thermoplastics many advantages over thermosets such as welding possibility, infinite shelf life, good impact properties and fast manufacturing cycle time. However, the implementation of thermoplastic composites in the industry is slowed by the lack of knowledge on some few aspects including manufacturing defects. One of the most popular manufacturing methods to form thermoplastic composite is thermostamping. Thermostamping is a fast process where a pre-impregnated sheet of continuous fibers embedded in matrix resin is melted and reformed to the desired shape using a die. This method has many advantages and has been proven effective, yet manufacturing defects are still problematic.

One of the possible defects with thermostamping, as many other manufacturing methods, is shape distortion. Shape distortion is when the final part shape does not correspond to the expected shape or the tool shape. This has been an issue with composite parts for a long time and most of the work done have focused on thermoset since it is the most popular material in the industry. A common way to deal with this issue is the use of a rule-of-thumb or by trials-and-errors. Considering the cost of tooling, the cost of material and the available technologies, this method should not be used anymore. In order to obtain reliable results, it is important to have reliable inputs. Properties of thermoplastic are closely related to temperature. A common practice in FEA analysis is to use single value but it is clear that accurate simulations require temperature dependent constants over the range used during a thermostamping process. The second manufacturing issue is wrinkles formation. When forming a fabric into a complex shape, the inability of the fabric to stretch and deform can cause the appearance of wrinkles. This is mostly seen in double curvature shape because it requires more complex deformation mechanisms. Most studies available give solutions to their specific case but no procedure or methodology proposed is available to help reduce or remove wrinkles using a simulation approach. Finally, in order to implement a thermostamping process, it is important to evaluate if the process is cost effective. Cost analysis is useful for many things such as; to verify if the project fits in the budget, to give a quote to a client, to verify if a quote from a supplier is reasonable, to choose the less expensive

approach to use, and more. Cost is always critical in a competitive environment which makes an evaluation tool relevant.

1.1 Objectives

The following objectives are set according to the issues previously identified to accurately understand thermostamping of thermoplastic composite.

- (1) The first gap is the lack of reliable predictions of shape distortion of thermostamped long-fiber thermoplastic composites.
- (2) The second gap is the lack of thermal dependent properties for PPS/Carbon pre-impregnated composites over the thermostamping temperature range.
- (3) The third gap is the lack of a methodology to have an optimal set-up in order to reduce wrinkles in a thermostamped part.
- (4) A simplified cost analysis methodology applied to manufacturing of composite parts and a case study comparing thermostamping to other popular processes.

This thesis has the purpose of answering the gaps identified. This is done through seven chapters. The first chapter is the current introduction. The second chapter is a literature review on thermoplastic behavior, thermostamping, wrinkles, shape distortions, and cost analysis. The third chapter is a study helping to understand PPS/Carbon pre-impregnated material properties over a wide range of temperatures. The fourth chapter presents a finite element analysis using a sequential thermal-mechanical approach to predict shape distortions. The shape distortions obtained by the software are compared in the case of spring-in of an angled part. The fifth chapter is proposing a methodology to remove or to reduce wrinkles using commercial software, Aniform. The sixth chapter presents a cost analysis methodology to estimate manufacturing cost of a composite part. The methodology is evaluated through a case study comparing three manufacturing methods; resin transfer molding, compression molding of chopped fiber and thermostamping. Finally, the seventh

chapter presents the overall conclusion, the contributions and the future works suggested based on the assumptions made and results obtained throughout this work.

Chapter 2. Literature Review

The growing interest in long fiber thermoplastic composites brought new challenges for part manufacturers. Thermoforming is a commonly used manufacturing method for thermoplastic composites due to its ability to make complex shapes with a low process cycle time. The place of thermoplastic composites in aerospace is growing and it is used in many different applications (Figure 2.1) but there is still reluctance due to unknown aspects of the process. A literature review was performed in order to regroup the essential information regarding thermoforming of continuous fiber reinforced thermoplastics.

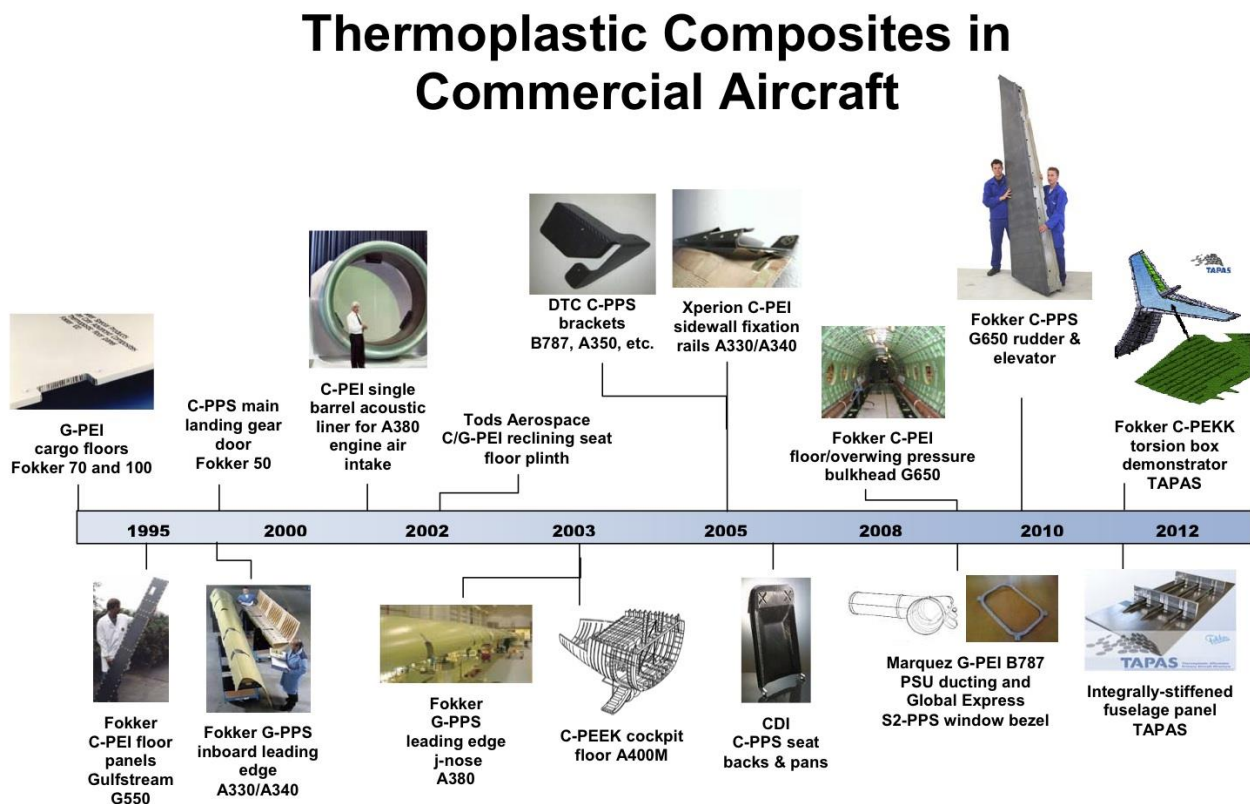


Figure 2.1: Thermoplastic Composites in Commercial Aircraft [1]

The composite materials are getting more and more accepted by the aerospace industry. However, the use of thermoplastic composite is still not as popular as thermoset; both have particular pros and cons as seen in Table 2.1.

	Pros	Cons
Thermoplastic Composite	<ul style="list-style-type: none"> -Infinite shelf life -Short processing cycle -Higher ductility and fracture toughness -Possibility to reform, weld 	<ul style="list-style-type: none"> -Stiff and boardy preform -High viscosity -High processing temperature
Thermoset Composite	<ul style="list-style-type: none"> -Low viscosity -Process at room temperature 	<ul style="list-style-type: none"> -Exothermic reaction -Irreversible reaction -Outgassing -Brittle

Table 2.1: Thermoplastic vs. Thermoset Composite

2.1 Thermoplastic Behavior

The different morphologies of thermoplastics can be separated into two families; semi-crystalline and amorphous. The difference between them is seen in the chain arrangements. The amorphous thermoplastic is made of randomly oriented and entangled chains and the semi-crystalline thermoplastic contains a ratio of region where the chains are organized and connected to the amorphous region (Figure 2.2).

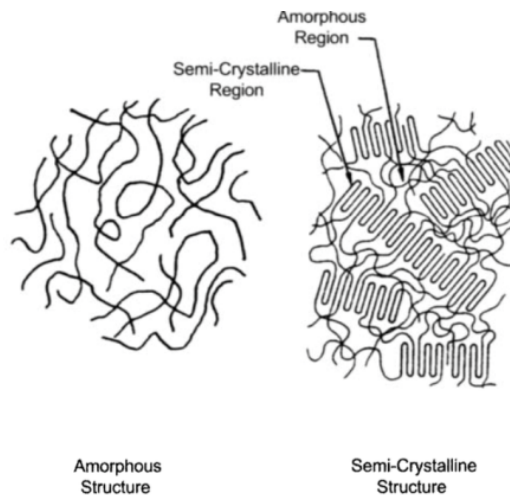


Figure 2.2: Comparison between amorphous and semi-crystalline phase [2]

The ratio of crystalline region determines the crystallinity of the material; also referred as degree of crystallinity. The augmentation of the crystallinity increases the strength, the stiffness, the creep resistance and the temperature resistance. On the other side, it decreases the toughness. The crystalline areas are created during the cooling. A slow cooling provides the necessary time for the chains to reorganize in order to minimize their energy and to obtain a good crystallinity.

The degree of crystallinity can also be improved by annealing the material between the melt temperature and the glass transition temperature [2]. Nohara, L. B. et al. [3] showed that isothermal crystallization from melted PPS can be described by Avrami kinetic modeling.

$$X_r = 1 - \exp(-kt^n) \quad (2.1)$$

The relative crystallinity (X_r) is a function of time (t), the crystallization rate (k) and the Avrami exponent (n). The value of the Avrami exponent is close to three when crystallization occurs from the melt and close to two for cold crystallization. In a composite, the value of "n" decreases which is caused by the presence of carbon fibers [4]. A simple experimental way to analyze material propriety change with temperature is by using Differential Scanning Calorimetry (DSC) or Modulated Differential Scanning Calorimetry (MDSC). When a DSC is used to determine the crystallinity of a neat resin and thermoplastic matrix composites, the following formula can be used [4, 5] to calculate the initial crystallinity.

Neat resin

$$X_c = \frac{\Delta H_f - \Delta H_c}{\Delta H_f^\circ} \quad (2.2)$$

Thermoplastic matrix composite

$$X_c = \frac{\Delta H_f - \Delta H_c}{(1 - W_f)\Delta H_f^\circ} \quad (2.3)$$

Where X_c is the crystallinity, ΔH_f is the heat flow of fusion, ΔH_c the heat flow of the crystallinity, W_f is the weight fiber fraction and ΔH_f° is estimated heat flow of a 100% crystalline sample.

The first transition of state during heating happens at the glass transition temperature (T_g). The T_g is the temperature that separates the polymer between a rigid glassy state and a rubber-like, flexible state. Above the T_g , the polymer chains are still continuous but the secondary bonds lose their strength. Figure 2.3 presents the relation between the modulus, the crystallinity and the temperature of an amorphous polymer (left), a semi-crystalline polymer (right). As seen in Figure 2.3, both graphs have a decrease in modulus under higher temperature but the shape of the curve is defined by the crystallinity of the initial material.

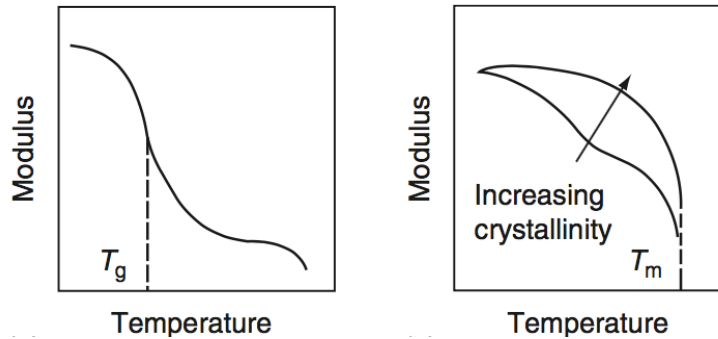


Figure 2.3: Graph of Modulus vs. Temperature of a typical semi-crystalline thermoplastic [6]

The commercial thermoplastics most suitable and popular for high-performance applications, including aerospace, are the following: PPS, PEI, PEEK, and PEKK. All of them are semi-crystalline except for PEI. Polyphenylene sulfide (PPS) is a popular material in aerospace and is used for multiple structural applications as seen in Figure 2.1. PPS has a glass transition temperature around 90°C and a melting point of 285°C . The T_g of PPS is relatively low compared to other semi-crystalline. PPS offers good toughness, excellent chemical and solvent resistance, and is cheaper than other semi-crystalline. The main disadvantages of PPS are low fracture toughness and low T_g , which required to be use in low temperature applications. Being a semi-crystalline thermoplastic, the understanding of the crystallization is important in order to go further with the manufacturing process. The maximum crystallization rate for an isothermal situation happens between the T_g and the T_m , where the combination of nucleation and crystal growth rates is optimal. For PPS, the optimal rate happens around 185°C [4].

Interesting points are raised by Jog, J. P. et al. [7] during a study on the crystallization of PPS. The study compares the crystallization behavior for a PPS resin from two different major suppliers. A comparison between Ryton V-I (called PPS1) supplied by Philips Petroleum and Fortron W203 (PPS 2) supplied by Hoechst Celanese showed few differences between their behavior:

- (1) *Melting peak temperature* was 284°C for PPS1 and 293°C for PPS2
- (2) *Heat fusion* of PPS1 was 45.8 kJ/kg and 55.4 kJ/kg for PPS2
- (3) *Crystallization temperature* during cooling was 246°C for PPS1 and 253°C for PPS2

Even when reheat and crystallized under the same condition, the two PPS had different behaviors when they are retested again (melting temperature, crystallization). The possible reason for those differences are attributed to the molecular architecture. This conclusion demonstrates that when using a new material, it is important to characterize it in order to obtain the right information.

2.2 Pre-impregnated Thermoplastic & Thermoforming

The fast manufacturing of thermoplastic composites is possible because of the utilization of pre-impregnated materials commonly referred to as prepregs. Pre-impregnated materials have their fibers already impregnated with the matrix which eliminates the impregnation challenge using a high viscosity polymer. This allows decreasing the pressure and the time required to wet the fiber during the manufacturing of the part. Thermoplastic pre-impregnated materials can be found under different forms as tape, fibers with clinging powders, commingled fibers and reinforced sheet. For thermoforming, reinforced sheet is the most popular.

Composites with thermoplastic matrix are shaped using various manufacturing methods. Thermoforming is a method in the family of compression molding. Since thermoplastics do not cure like thermoset, it is possible to change the resin state really fast back and forth many times. The main advantages of this method are the rapidity of the manufacturing and the ability to manufacture complex shapes. The biggest disadvantage is the inability to form parts with thickness variation. This fabrication method uses a blank (a pre-consolidated thermoplastic laminate) and a thermoforming machine. The steps of the fabrication are the following; (1) pre-heating of the blank, (2) moving the blank between the lower and upper mold, (3) movement of the lower or upper mold and taking up the blank, (4) closing the tool, (5) holding the blank inside the tool, (6) cooling and demolding of the part.







Steps	1. IR heating	2. Moving the blank	3. Closing of the mold
			
Parameters	-Heating temperature (°C) -Time (s) -Speed of heating (°C/min)	-Time of transfer (s) -Speed of transfer (mm/min)	-Speed of closing (mm/min) -Mold temperature (°C)
Steps	4. Closing the tool	5. Holding	6. Cooling and demolding
			
Parameters	-Tool temperature (°C) -Pressure (MPa)	-Time (s) -Tool temperature (°C) -Pressure (MPa)	-Demolding temperature (°C) -Cooling Rate (°C/min)

Table 2.2: Thermostamping steps

The infrared heater heats the blank to a temperature higher than the melting temperature of the matrix. Once a uniform temperature is reached through the blank, it is transferred between the lower and the upper molds. Depending on the equipment, the lower or the upper mold moves and takes the blank with it. When it reaches the opposite mold, the tool is closed. The mold stays closed while maintaining a certain temperature and pressure on the blank. During this operation, many parameters can influence the quality of the part. A good understanding of the mechanical and chemical phenomena happening during the complete cycle is crucial. In this study, two kinds of manufacturing defects are more deeply analyzed; wrinkles and shape distortion.

2.3 Wrinkles

A good understanding of the mechanisms occurring during thermostamping is needed in order to identify the cause of wrinkles and how to avoid them. Based on previous documentation [2, 8-11] four main mechanisms occur during forming as seen in Figure 2.4 (a); (1) resin percolation, (2) transverse squeeze flow, (3) inter-ply slip and (4) intra-ply slip. The resin percolation is the movement of the resin between the fibers, this phenomenon is important in order to obtain a good bonding between the plies. The transverse squeeze flow is the displacement of

the resin and fibers in-plane; parallel or transverse to the fiber orientation. This flow is usually induced by the pressure; the flow tends to equalize the distribution of the resin according to the distribution of the pressure. The next mechanism is the inter-ply slip. This mechanism is the translation movement of a ply relatively to another ply. This is required when doing single curvature since the length of the curve is shorter for the inner ply and longer for the outer ply (Figure 2.4(b)). This mechanism is directly related to wrinkles because if the ply is not able to translate, it will have to accommodate the extra material and this will appear in the form of wrinkles. The last mechanism is intra-ply shear. This mechanism is the deformation within a ply. This is usually needed when doing double curvature since the ply itself needs to reorganize in order to conform to the double curvature. For woven laminates, the deformation is commonly identified as the shear angle which is the angle between the warp and the weft (initially 90°). The critical angle at which wrinkles are created is called the “locking-angle” [12] or maximum shear angle. It is accepted that deformation beyond this angle causes the fabric to buckle out-of-plane followed by an increase of stiffness and a thickening of the fabric. The locking-angle value can be determined by a shear-frame test or bias-extension test and it is specific to the weave pattern, the fiber volume fraction and the fiber type [13].

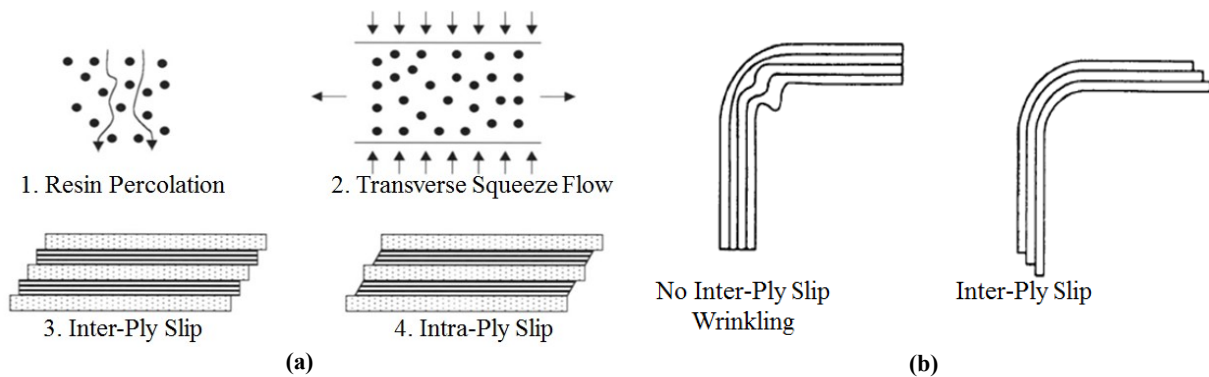


Figure 2.4: Mechanisms during stamping and Inter-ply slip example [2]

An early interest was developed for thermostamping and many studies have been made by M. Hou. In an early study [11], a 90-degree angle part was made from four different combinations of material; unidirectional carbon fiber/polypropylene, polyamide 12, poly(ether ether ketone) and woven glass fiber/polyetherimide. The predominant mechanism in this part, which is a single curvature, is the inter-ply slip. It was found that the right forming temperature allows having low enough viscosity to allow inter-ply slip which is needed to avoid wrinkles (or "kinking") in the

curved section. In this particular study, the forming temperature was related to the closing speed since the tooling was not heated. Similar results were obtained in a later study [14] when doing a half tube shape with a glass fiber/polypropylene laminate. Further studies [15, 16] were made on a three-dimensional hemisphere which required more complex deformations. Due to the complexity of the shape, a holder was used to constrain the laminate on the female mold while the male mold is pressing. It was shown that too low holder pressure did not restrict the laminate enough and let wrinkles appear and a too high holder pressure causes fiber breakage. The second aspect investigated is the impact of the initial area of the laminate where it is shown that a higher initial area (more excess material) tends to create more wrinkles. Five different cavity depths were used in which the deepest was a complete hemisphere. The deeper the mold was, the more wrinkling occurred.

2.4 Shape distortions

Manufacturing induced shape distortions have been a subject of interest considering their important impacts on the final part quality. The shape distortion is referred to as spring-in or spring-back for angled parts and as warpage for complex parts. A recent review made by Baran, I. and al. [17] separated the residual stresses in two different levels; micro and macro. Microscale behaviors are considered insignificant in term of shape distortion because it is assumed that the stresses are self-equilibrating. Macroscale is the level where the shape distortion occurs. The macroscale consists of: anisotropic behavior of individual plies, the tool-part relation, and the constraint effect of individual plies. This means, based on this review, a model able to predict shape distortion should include those three aspects. Depending on the situation, the temperature gradient can have a significant impact, therefore, it should be added to the phenomenon to include in the analysis.

2.4.1 *Anisotropy and constraint effect of plies*

A significant difference between the CTE of thermoplastics and carbon fibers is shown in Table 2.3. This difference combined with the anisotropy of the material structure create a large difference in the overall material properties. For woven fabrics, this can be translated by the large difference of in-plane and out-of-plane properties. Since out-of-plane is the dominant property, and is closely related to matrix behavior, it is important to have a good understanding of the impact

of crystallinity on the development of stresses and material properties. The effect of crystallization contraction has been studied by Unger, J.W. and Hansen, J. S. [18]. Their study showed experimentally that the initial contraction of the crystal phase has a small effect on the development of residual stress due to the compliance of the amorphous phase. For semi-crystalline matrices, the stress-free temperature can be found near the peak crystallization temperature during the cooling from melt. This is explained by the start of development of crystallinity which has load-bearing capability. The farther the steady state is from the stress-free temperature; the more residual stresses are built in the composite. In the same study made by Unger, J.W. and Hansen, J. S. [18], a process of quenching and annealing to minimize residual stresses in an APC-2 composite is presented. B. Landry [19] characterized a carbon/PEEK laminate using DMA. Under 3 points bending and a temperature cycle, it was shown that during cooling from melt, the laminate modulus starts increasing near the start of the crystallization range. The effect of crystallization shrinkage is also obtained by measuring the coefficient of thermal expansion during cooling. It was found that near the crystallization range, a large shrinkage occurs in the sample in the out-of-plane direction.

Each ply possesses an individual CTE, based on their orientations, which can cause non-uniform induced stresses. In a study made by J.A. Barnes and G.E. Byerly [20], the curvature of the non-symmetric laminate is tracked during heating and cooling showing the role of the plies anisotropy on residual stresses.

2.4.2 Tool-part interaction and temperature gradient

During the manufacturing process, it is most likely that the cooling of the material is not uniform; the region on the extreme tends to cool down more quickly than the middle. This causes a thermal “skin-core” effect. The gradient causes the skin to be in compression and the core to be in tension (Figure 2.5). For faster cooling rates and/or for thicker laminates, the distribution is more important and the residual stress is higher in the composite.. This gradient of temperature induces a gradient of cooling rate, which may create a crystallinity gradient.

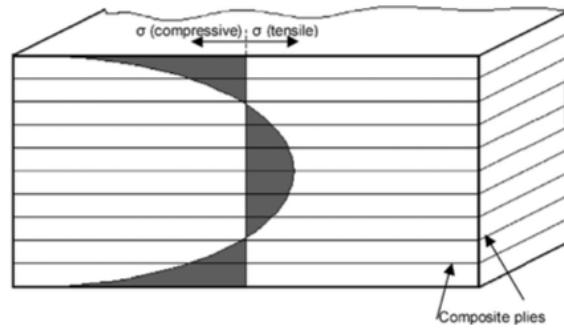
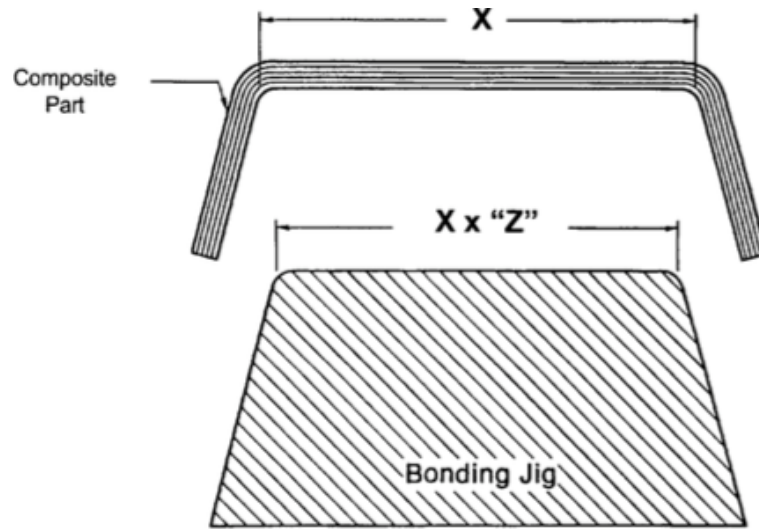


Figure 2.5: Skin-core effect [21]

Common materials for tools (steel, aluminum) for thermostamping have a lower CTE than thermoplastic and higher than carbon fibers as seen in Table 2.3. It is important to consider the tool geometry at the point where the thermoplastic starts to be able to take loads. This will allow obtaining the right geometry at room temperature and to avoid induced constraint to the part. To avoid this problem, it is important to consider a thermal correction factor while dimensioning the tool. The calculations are shown in Figure 2.6. The friction between the tool and the composite combined with the difference of CTE could cause interfacial stress which could induce additional residual stresses in the surface ply [21]. This shear interaction takes place at the tool-part interface while the middle of the composite does not experience any constraints; this gives a non-uniform stress distribution through the composite. The cooling of the composite “locks” this non-uniform stress distribution and cause shape distortion when demolding.

Material	CTE x 10 ⁻⁶ /°C
Plain carbon steel	11.7
Invar/Nilo	1.6
Aluminum alloys	23.5
Carbon fibers	-0.6 to -1.45
PPS	49
PEI	56
PEEK	47

Table 2.3: CTE for various thermostamping related materials [6]



X = Engineering Part Dimension
"Z" = Correction Factor

$$\text{Thermal Correction} = \text{Engineering Dimension} \times \underbrace{(\text{CTE}_p - \text{CTE}_T) \times (T_{\text{gel}} - T_{\text{RT}})}_{\text{"Z"}}$$

Where:

CTE_p = Coefficient of Thermal Expansion of Part
 CTE_T = Coefficient of Thermal Expansion of Tool
 T_{gel} = Temperature of Resin Gellation
 T_{RT} = Room Temperature

Figure 2.6: Thermal correction calculation [6]

2.4.3 Approach used for prediction

The previous paragraphs reviewed the most impactful phenomena causing shape distortions. The fundamental understanding of those phenomena set the base to predict the shape distortions. The most favored methods are numerical models and finite elements analysis.

2.4.3.1 Numerical

Numerical model can be quite powerful and easy to use. As shown before, the numerical model made by Radford [22] was shown effective to predict warpage. An earlier similar model was developed by N.Zahlan and J.M.O'Neill [23]. Both methods were initially developed for thermoset but considering the underlying theory, it is applicable to thermoplastic composite. Those models are only based on the initial angle, the change in temperature, the in-plane, and out-of-plane CTE. A recent study made by Salomi, A. and al. [24] used a modified Radford model which

is only based on in-plane and out-of-plane difference which gave a reasonable fit with experimental data. The addition made to the Radford model was made to account the fiber wrinkling at corners causing non-homogeneous properties at the corner. The disadvantages of those methods are their limitation to angled part, meaning they can only predict spring-in or spring-back of the part.

2.4.3.2 Finite elements

For more complex shape, finite element becomes a favored approach. Many studies use finite element approach to predict warpage for thermoset and thermoplastic composites. Only a few on thermostamping or similar processes of thermoplastic composites will be reviewed here.

J.A. Barnes et al. [20] investigated the experimental diagram forming of a quasi-isotropic AS4/PEEK thermoplastic composite. The experimental results were compared to the incremental O'Neill model and found good agreement. The stresses are evaluated using a stack of laminates separated by release film and by calculating the relation between stress and curvature for each individual ply. The results (tractions and point deflections) were used in a finite element model but poor agreement was obtained between the FE results and experimental. B.-S. Kim and al. [25] manufactured angled parts made of unidirectional polyamide/carbon commingled yarn fabric. The finite element model is based on three main material behaviors, the thermoviscoelastic behavior of the resin, the crystallization shrinkage of the resin and the thermomechanical behavior of the composite. The CTE is considered orthotropic and four temperature dependent values are used to represent the behavior over the wide temperature range. The measured and predicted residual stresses are in excellent agreement. A similar agreement is obtained for the spring-in value. C. Brauner [26] et al. built a finite element model to represent thermostamping of L-bracket made of PPS/Carbon. A model using crystallinity dependent properties was used to simulate the spring-in. A linear relation between relative crystallinity and matrix modulus was use to define mechanical properties and CTEs. A 3D finite element model is used to predicted deformation on a 92° tool, and a spring-in angle of 3.6 ° is obtained. The measured deviation on the experimental part was found to be 3.7°.

2.5 Cost Analysis

The goal here is to present what is available to the reader as cost analysis methods and to evaluate their potential according to the manufacturing of composite parts. Commonly, the cost

estimating methods are separated into three families: analogous, parametric and bottom-up. Many studies give a good overview of the methods available in an aerospace context [27-30]. A simplified review is made here to provide a background to the reader. The cost estimation methods presented can be used at different levels e.g. a part, a system or a project.

The analogous method estimates cost by comparison relatively to comparable historical situations based on their similarities and differences. It is a simple, quick and precise method if a good range of historical data of similar cases is available. This method is appropriate for the early stage of the project when not a lot of information is available and a good database exists. Few examples or case studies can be found in the literature [31-34]. For example, a simple formula can be represented as:

$$E = C_{ana-project 1} * F_1 + C_{ana-project 2} * F_2 \quad (2.4)$$

Where E the estimation of the project cost, $C_{ana-project 1}$ and $C_{ana-project 2}$ are cost of feature(s) from analogous projects, and F is a scaling factor based on the project size.

The parametric method is also based on comparison with historical data. The methodology is to develop a cost estimating relationship/equation based on various projects in the same family and to use it to estimate the unknown. This method required a good amount of historical data in order to make sure the relationship/equation is reliable. It has the advantage of being quick and precise but it could be erroneous to use it outside the available range of available data. For example, if based on historical data, the relation between the part cost and the part weight is linear, it is possible to estimate the unknown part cost based on its estimate weight. Few examples or case studies can be found in the literature [32, 35, 36]. An example of first-degree equations is:

$$E = C_1 * X + C_2 \quad (2.5)$$

Where E is the estimate, C_1 and C_2 are constants obtained from the equation developed based on historical data, X is the available or expected information that corresponds to the project.

The last method is bottom-up or engineering build-up method. This method is based on the actual process flow of the project and does separate estimation for each step. This method is the most precise but required a considerable amount of work and is not easily modifiable. The

understanding of the project needs to be advanced in order to have all the information available. This is the only method applicable when no historical data is available. Few examples or case studies can be found in the literature [37-40]. An additional example is the Advanced Composite Cost Estimating Manual (ACCEM)[41], which was made in order to provide input in a bottom-up estimation for composite manufacturing. The ACCEM presents formulas for different operations of composite manufacturing. Formulas are built by observing operators doing the task and obtaining the time taken to achieve the task. However, this manual was produced in 1976 which may have large degrees of uncertainty in the information available considering that the practice, technology, tools and the materials used have evolved.

Figure 2.7 regroups each method and provides the most appropriate method based on the actual phase of the project.

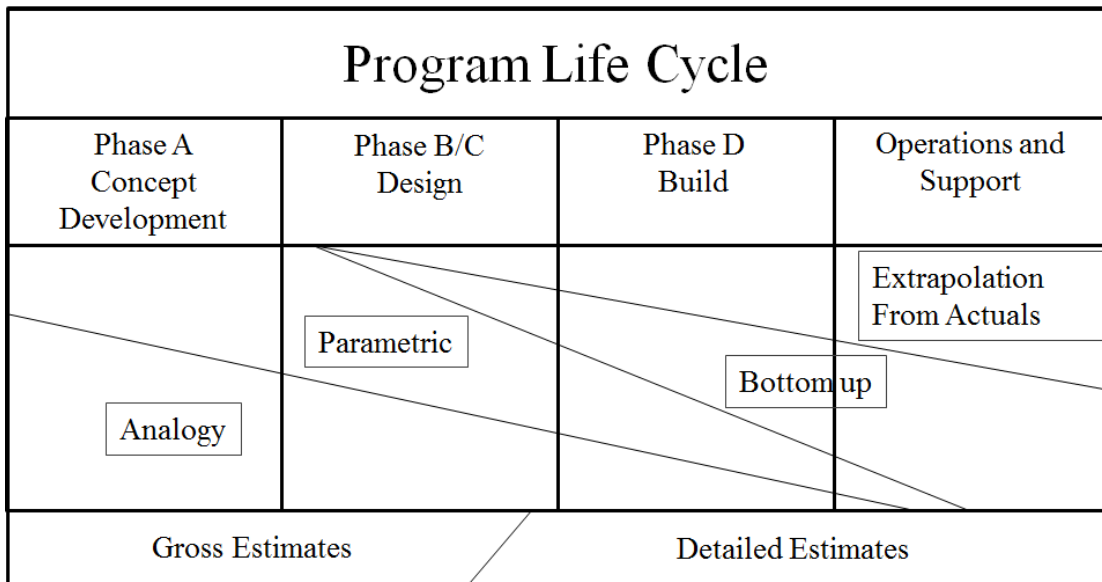


Figure 2.7: Cost estimation methods comparison, Adapted from [27]

Based on the goals, the information available for the period of the program life cycle, it is possible to accurately select the most appropriate cost modeling method. In the case of the manufacturing of a composite part, the availability of historical data is not assured but the project is advanced enough to be able to have all the information to do the bottom-up method. Also, because of the precision of this method, it is possible to identify the most influential steps and focused on optimizing them. For example, while doing a bottom-up method, the transfer time between stations is taking up the highest percentage of the labor time, the configuration of the manufacturing cell could be optimized to minimize the time lost.

Chapter 3. Material Characterization

3.1 Introduction

This chapter characterizes the material TenCate Cetex[®] TC1100 PPS (Polyphenylene sulfide)/ Carbon fiber (Toray T300 3K) 5-Harness satin woven fabrics. A thin layer of fiberglass type S is present on one side of the laminate for assembly purpose in order to avoid galvanic corrosion. The lay-up is $[(0, 90), (\pm 45), (0, 90)]_s + [(0, 90)]_{FG}$ and has a measured thickness of $1.916 \pm 3.10E-03$ mm. According to the datasheet [42], the resin weight content is 43 %, the T_g is 90°C and the T_m is 280°C . PPS is a high-performance thermoplastic and a semi-crystalline polymer. The goals of this chapter are to understand the thermo-mechanical behavior of this material and to provide input properties for manufacturing simulations. This chapter is separated into 3 sections; the matrix kinetics, orthotropic thermal expansion, and the dynamic thermal behavior.

3.2 Matrix Kinetics and Specific Heat

3.2.1 Introduction

This section uses Differential Scanning Calorimetry (DSC) and Modulated Differential Scanning Calorimetry (MDSC) to investigate the kinetic behavior of the material. DSC is used to investigate the glass transition temperature (T_g), the melting point (T_m), the impact of cooling rate on crystallization temperature range and final crystallinity. MDSC is used to obtain the specific heat capacity of the material as function of the temperature. The procedure for DSC is given by the standards ASTM D3418 and ASTM E1269 for MDSC.

3.2.2 DSC procedure

A TA Instruments MDSC Q200 is used for this series of experiments. Small circular samples were cut from the laminate received from TenCate using a hollow drill bit with an inside diameter of 4.32 mm (11/64 in). This procedure allows having a high contact area between the pan and the sample, which is highly recommended and allows keeping the laminate structure. Samples weighing between 12 and 15 mg are placed in Tzero hermetic aluminum pans. The samples were heated at a rate of $10^\circ\text{C}/\text{min}$ till 340°C and held for 2 minutes to remove thermal history. The

samples were then cooled at selected cooling rates. Each sample was tested at four different cooling rates. The cooling rates investigated were 1, 10, 20 and 50 °C/min. All these cooling rates were linear except 50°C/min where the function jump was used, making the cooling ramp exponential. The value of 50°C/min is the average of the overall rate. The degree of crystallinity of the resin was determined by the use of Equation (3.1). The exact value of the enthalpy of fusion of fully crystalline PPS is not in agreement by all studies because it is dependent of the extrapolation method used. According to [4], the values can vary from 50 J /g to 150.4 J/g depending on the technic used. For this study, the value of 150.4 J/g was used based on TenCate documentation [43].

$$X_c = \frac{\Delta H_f - \Delta H_c}{(1 - W_f)\Delta H_f^\circ} \quad (3.1)$$

X_c : Crystallinity

ΔH_f : Enthalpy of fusion (endothermic)

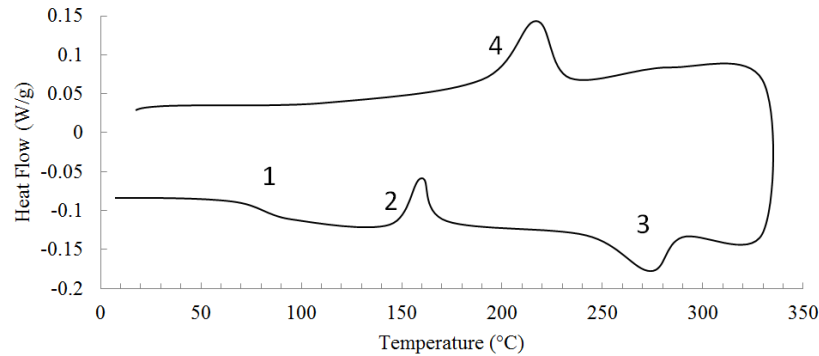
ΔH_c : Enthalpy of heating crystallization (exothermic)

ΔH_f° : Enthalpy of fusion of fully crystalline PPS (150.4 J/g)

W_f : Mass fraction of fiber in the composite

3.2.3 DSC results

Figure 3.1 shows a typical DSC curve for semi-crystalline thermoplastic composite and the important signals corresponding to matrix properties.



1. Glass transition of the amorphous fraction (heating)
2. Cold crystallization (heating)
3. Melting(heating)
4. Cooling crystallization (cooling)

Figure 3.1: DSC signal of a typical semi-crystalline thermoplastic

The DSC signals obtained with TC1100 (Figure 3.2) is compared to the typical signal for a semi-crystalline polymer (Figure 3.1). When a sample has very low crystallinity at room temperature, under a temperature ramp, the increase of temperature will help the chains move and reorganize which will cause energy change which will produce the cold crystallization peak. When the sample is already close the maximum crystallinity the heat ramp doesn't not produce an important change in the structure since it is already stable. The maximum crystallinity is different for each polymer but based on literature, a high crystallinity ratio for PPS is around 32% obtained by using a 0.4°C/min cooling rate [4]. Based on Figure 3.2, it is clear that the sample already has a high crystallinity; no T_g is visible and no cold crystallization occurs. Similar results were obtained by [4] for DSC curves of neat PPS. This is seen in both samples at every cooling rate. By definition, in each situation, a high crystallinity is achieved and the cooling rates of the equipment are not fast enough to quench the sample.

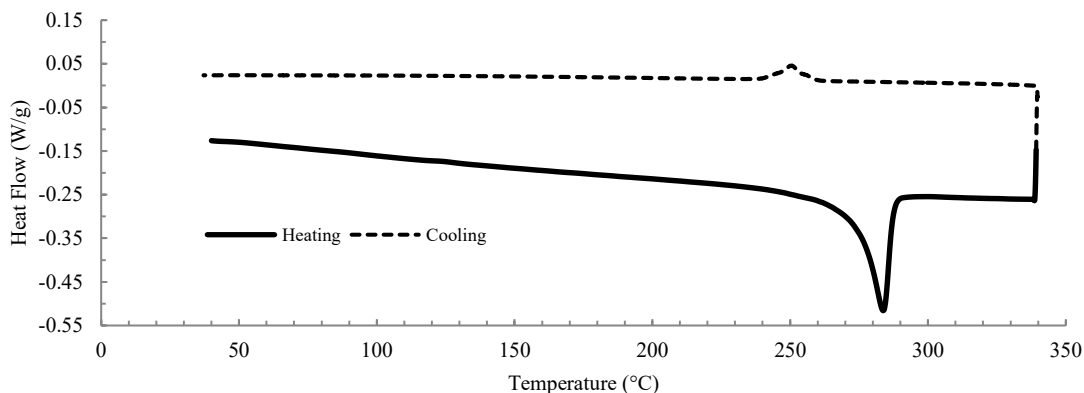


Figure 3.2: DSC signal of TC1100

3.2.3.1 First-Order Transition (crystallization and melting)

The impact of cooling rates on the final crystallinity and the crystallization zone is shown in Figure 3.3 and Figure 3.4 respectively. Figure 3.3 shows that a slower cooling rate gave a higher crystallinity. However, in the range possible with the Q200, the cooling rates are relatively slow and give a good crystallinity (over 20%) in each case. The data from the other studies are normalized with the value of 150.4 J/g and compared. The values found in this study are located in a similar range with the other studies. Figure 3.4 shows the evolution of the crystallinity during cooling. The graph shows the relation between the crystallinity and the temperature according to

the cooling ramp. The relative crystallinity is the ratio of the amount of instantaneous crystalline region over the maximum obtained under that temperature ramp. This can be calculated by using the instantaneous cumulated heat flow on the total heat flow of the crystallization. The trend shows that a faster cooling rate shifts the range to lower temperature. For example, at a fast cooling rate $\sim 50^\circ\text{C}/\text{min}$, the crystallization range is from 220°C to 170°C compared to a slow cooling rate $1^\circ\text{C}/\text{min}$ with a crystallization range from 265°C to 235°C .

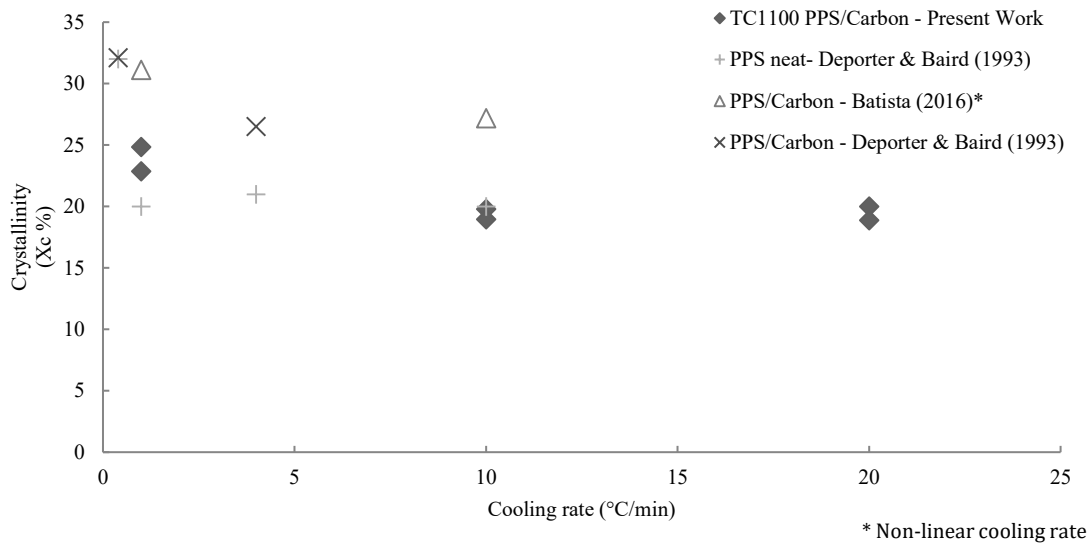


Figure 3.3: Impact of cooling rate on the final crystallinity

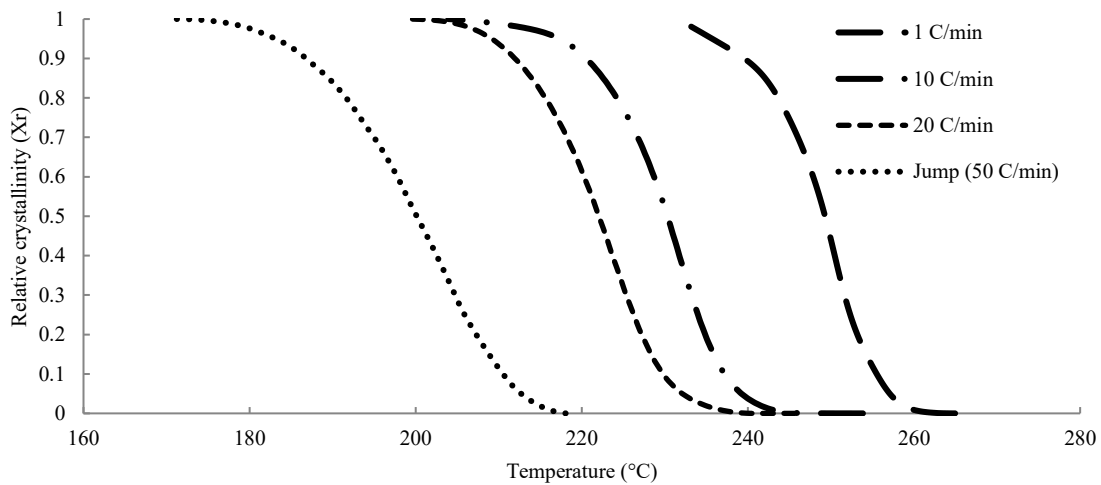


Figure 3.4: Relative crystallinity as function of cooling rate

The second characteristic evaluated is the melting temperature. According to the supplier datasheet, the melting temperature of PPS is 280°C. The values found in this study are impacted by the previous cooling sequence and are found to be between ~278°C and ~283°C. The relation between the peak melting temperature and the cooling rate is seen in Figure 3.5. A slower previous cooling rate (higher crystallinity) gives a higher melting point. A high crystallinity PPS/Carbon has a melting temperature of ~283°C.

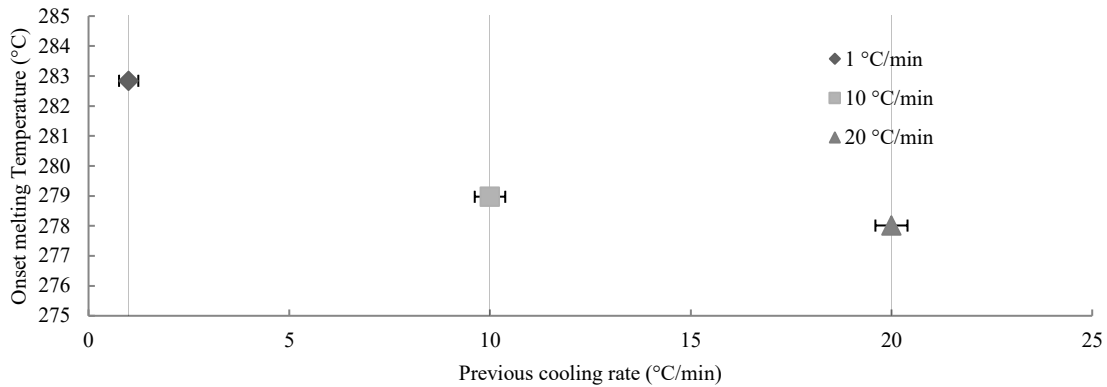


Figure 3.5: Peak melting temperature as function of cooling rate

3.2.4 MDSC procedure

An important property for thermal simulation is the specific heat capacity of a material. The specific heat capacity gives the direct relation to the energy required to raise a unit of mass by a unit of degree. An MDSC analysis is done on a sample in order to have the relation between the specific heat capacity and the temperature of the sample. The ASTM standard E1269 gives a procedure to do so. A sample of ~20 mg is used in a Tzero hermetic aluminum pan. The ratio between the modulate signal and the heating rate is really important to have representative data. The optimal procedure found is the following; modulated temperature of ± 1.00 °C every 110 seconds from 10°C to 320°C at a constant rate of 2 °C/min. Once 320°C is reached, the system is kept isothermal for 5 minutes before cooling down under the same modulated ramp.

3.2.5 MDSC results

Considering the specific heat capacity without the latent heat transition it is possible to consider for the cooling that the specific heat capacity varies linearly from ~1320 J/ Kg-°C at

310°C to $\sim 483 \text{ J/Kg}\cdot^\circ\text{C}$ at 23°C (Figure 3.6). The relation between the specific heat capacity and the temperature is different between heating and cooling. The linear trend is similar but the slope is different. The specific heat capacity at room temperature is the same, but at high temperature, they are different. This means that during the 5 minutes isothermal step at 320°C, the chemical arrangement keeps changing which increases the specific heat capacity causing the shift.

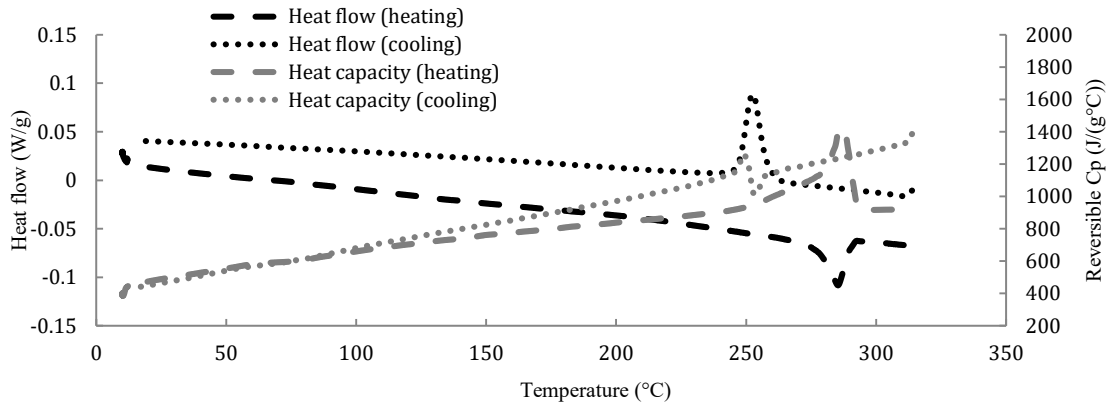


Figure 3.6: Heat flow and Heat capacity versus temperature

The conclusion is that the heat capacity is clearly dependent of temperature. In order to have a simple approximation, a linear behavior is considered and the value used at high temperature is the initial value for the cooling sequence.

3.3 Coefficients of Thermal Expansion

3.3.1 Introduction

A thermal mechanical analysis is done to determine the thermal expansion coefficient of small samples. The methodology used in this section is based on the ASTM standard E228 and the procedure used by B. Landry [19] on PEEK/carbon laminate.

3.3.2 TMA procedure

Three samples of 6 mm per 6 mm are cut from the initial laminate, with a thickness of 1.92 mm, using a diamond saw. Afterward, the samples are sanded in order to make the edges flat, defects free and smooth. A TA Instruments Q400 is used with the expansion probe. An MCA70 cooling system is used to have a controlled cooling. In order to have a stable procedure, two cycles

of heating-cooling are made for each sample. Figure 3.7 presents the reference directions of testing; the direction 1 is the one where the warp is visible on the top layer, direction 2 is the weft direction and direction 3 is out-of-plane.

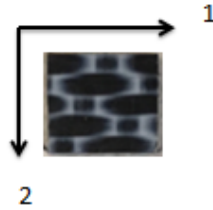


Figure 3.7: Reference direction for samples

Each sample is heated and cooled at a rate of $5^{\circ}\text{C}/\text{min}$ from 40°C to 180°C . The sample is held isothermally for 1 minute at the lowest and highest temperature. The probe applies a force of 0.05 N on the sample.

A second investigation is made to understand the behavior of the sample at higher temperatures (over the melting point). A different set-up is used to avoid penetration of the probe. A macro probe is installed on the TA Q400 to have a less important punctual force which gives more stable results. The sample is sandwiched between two quartz disks coated with Loctite® Frekote 44-NC™ demolding agent. A run is made with the quartz disk only and a CTE of $3\ \mu\text{m}/\text{m}^{\circ}\text{C}$ is found in the range of the experiment which is removed from the final CTE values. The sample is heated and cooled at a rate of $1^{\circ}\text{C}/\text{min}$ from 20°C to 320°C . The sample is held isothermally for 1 minute at the highest temperature and the probe applies a force of 0.1 N on the sample.



Figure 3.8: TMA set-up

3.3.2.1 In-plane (directions 1 and 2)

The linear CTEs are obtained from the graph of the linear thermal expansion versus the temperature. Figure 3.9 shows an example of sample 2 in direction 1. The values are shifted to

zero for the first point. The behavior is linear; the lowest R^2 obtained is 0.9967 and 0.9863 for direction 1 and 2 respectively showing the linear behavior of the in-plane CTE.

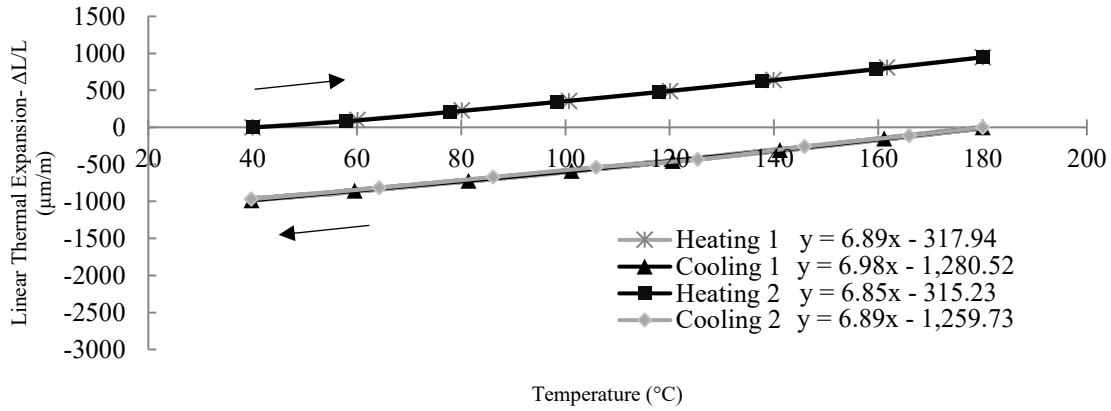


Figure 3.9: TC1100 thermal strain vs Temperature - Sample 2 Direction 1

	Dir. 1		Dir. 2	
	Heat	Cool	Heat	Cool
CTE ($\mu\text{m}/\text{m}^\circ\text{C}$)	5.99 ± 1.03	6.25 ± 0.91	7.01 ± 1.04	7.15 ± 1.21

Table 3.1: CTE in-plane

3.3.2.2 Out-of-plane (direction 3)

The behavior in direction 3 is driven mostly by the matrix instead of the fibers. Figure 3.10 shows the change of CTE near 100°C which is slightly above the T_g at 90°C. Each section is shifted to start with a zero strain. The problem is simplified by having only two linear coefficients of thermal expansion; one under the T_g and one over. The data of the three samples are compiled in Table 2.

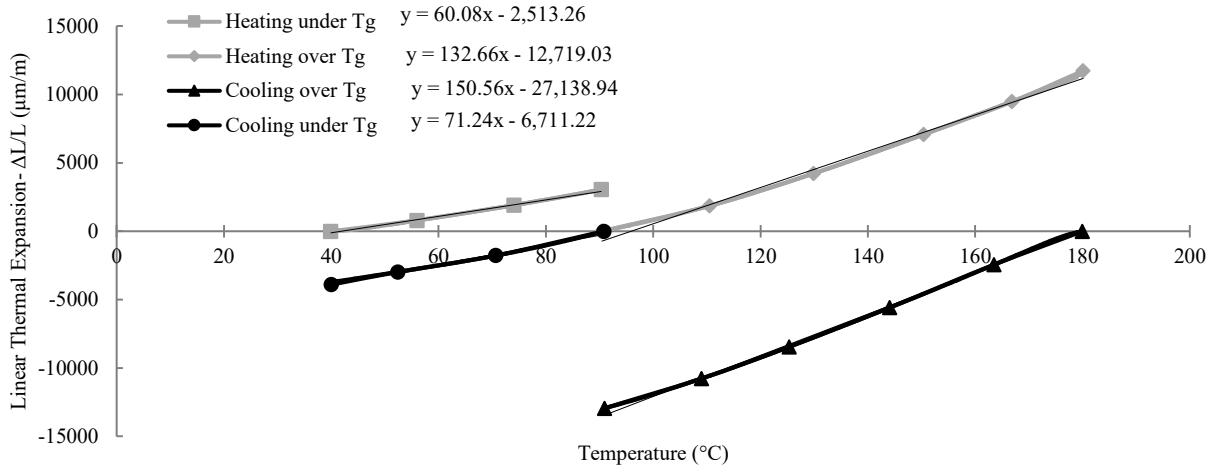


Figure 3.10: Transition of linear thermal expansion – Sample 3

	Dir. 3 under T _g		Dir. 3 over T _g	
	Heat	Cool	Heat	Cool
CTE (μm/m°C)	57.66 ± 4.56	65.50 ± 3.80	136.14 ± 7.84	137.91 ± 8.13

Table 3.2: CTE out-of-plane

According to TC1100 datasheet, the neat resin CTE is 52.2 μm/m°C which is close to the values under T_g in this experiment showing that the CTE out-of-plane is mostly driven by the matrix CTE.

3.3.2.3 Out-of-plane up to the melting point (direction 3)

Figure 3.11 shows the results of the out-of-plane linear thermal expansion at higher temperature. At less than 200°C the behavior stays the same as the previous analysis. The difference is near 280°C, where a large strain appears. This is related to the melting point of PPS. This large strain is caused by a deconsolidation of the laminate (Figure 3.11). The cooling has a plateau till 250°C; a large decrease is seen between 260°C and 235°C. This temperature range corresponds with the crystallization zone obtained by DSC under the same cooling rate. The comparison is shown in Figure 3.12. The large drop of CTE caused by the crystallization is located between 20% to 80% relative crystallinity. The rest of the cooling behave similarly as the heating and also to the previous samples investigated at lower temperature range.

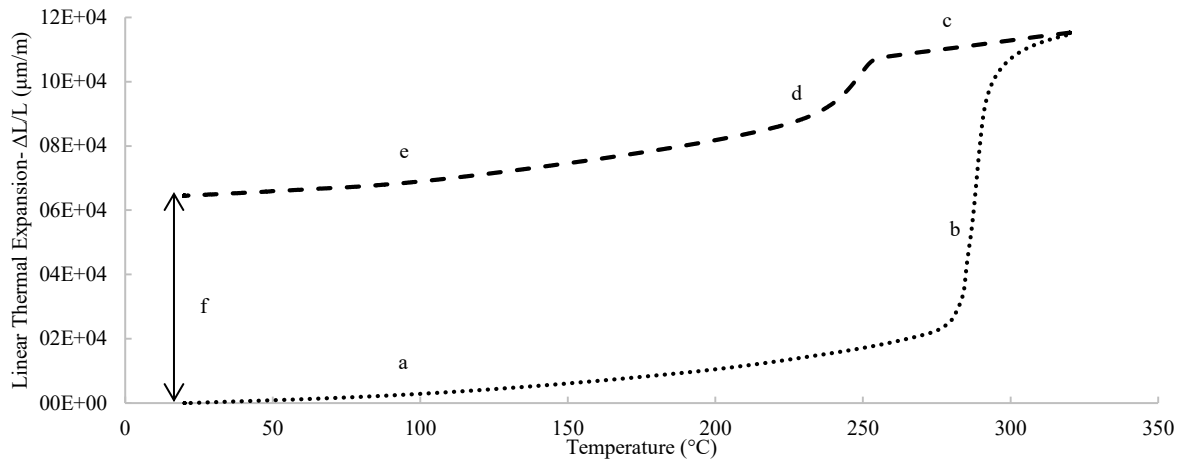


Figure 3.11: Linear thermal expansion vs Temperature - Out-of-plane. (a) Before deconsolidation (b) Melting of the matrix, deconsolidation of the sample. (c) Over crystallization. (d) Crystallization shrinkage. (e) After crystallisation (f) difference of sample thickness

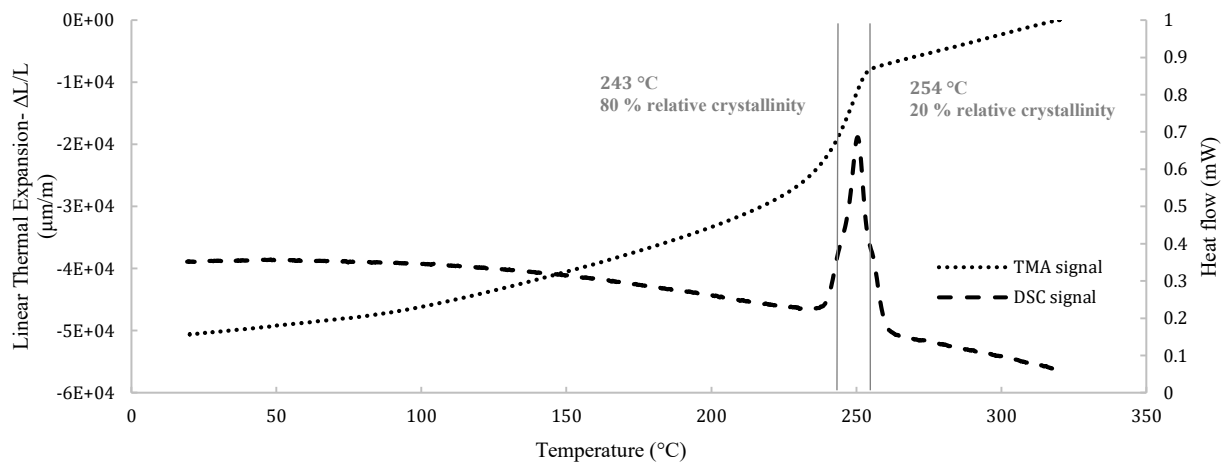


Figure 3.12: DSC and TMA signals with a cooling rate of 1°C/min

To simplify the behavior, the CTE during cooling can be separated into 4 values, presented in Table 3.3.

Cooling stage	Temperature Range (°C)	CTE ($\mu\text{m}/\text{m}^\circ\text{C}$)
Between crystallization and T_m	245 to 320	200
During crystallization	225 to 245	620
Between crystallization and T_g	90 to 225	130
Under T_g	20 to 90	60

Table 3.3: CTE in direction 3 – Wide range

3.4 Thermo-Mechanical Behavior

3.4.1 Introduction

The goal of this section is to measure the mechanical properties of the sample within a temperature range. TC1100 samples are solicited with a dynamic oscillatory load under 3 points bending while the temperature is varied. This experiment gives information on the change of modulus versus the temperature. Also, the phase difference between the stress and the strain provides information on the degree of viscoelasticity of the material. The methodology used is derived from the ASTM D4065, B. Landry [19] and TA Instruments recommendations.

3.4.2 DMA procedure

The Dynamic Mechanical Analyzer (DMA) used is the Q800 from TA Instruments. Two samples of 65 mm x 12 mm are cut from the received laminate with a thickness of 1.92 mm. They are wrapped in Kapton® tape with a thickness 0.06 mm to contain the sample. The testing method used is 3 points bending with a constant amplitude of 25 μm and a frequency of 1 Hz. The heating and cooling are made at a rate of 1°C/min between 50 °C to 300 °C.

3.4.3 DMA results

The first aspect investigated is how the material behaves (elastic or viscoelastic) as function of temperature. According to TA Instruments [44]; $\tan \delta$, which is the phase lag between stress/strain sinuses, will be 0 for purely elastic materials and 1 for purely viscous materials. In this experiment, $\tan \delta$ is under 0.1 from room temperature to 260°C during the heating and between 240°C to room temperature during cooling. The maximum value obtained is 0.35, still closer to an

elastic behavior than purely viscous, when the resin is in a melted state. Those results allow using an elastic model and to consider it as a reasonable approximation.

Figure 3.13 shows the change in storage modulus during the heating and the cooling of both samples. During the heating, the modulus drops near the T_g (90 °C). After, it decreases slowly till T_m (280 °C). TC1100 kept good properties after the T_g . For example, at 235°C, the modulus is still at ~70% of its initial value. The measurement and visual analysis of the sample after the bending test showed an increase of thickness and a permanent curvature of the sample. The calculations for cooling are adjusted using the final thickness. Equations 3.2 to 3.4 are available in TA instruments documentations for rectangular cross section.

$$\sigma_x = \frac{P * L * t}{4 * I} \quad (3.2)$$

$$\varepsilon_x = \frac{3 * \delta * t}{2 * L^2 * \left[1 + \frac{6}{10} (1 + \nu) \left(\frac{t}{L} \right)^2 \right]} \quad (3.3)$$

$$E = \frac{\sigma_x}{\varepsilon_x} = Ks \frac{L^3}{6 * I} \left[1 + \frac{6}{10} (1 + \nu) \left(\frac{t}{L} \right)^2 \right] \quad (3.4)$$

$$Ks = P / \delta \quad (3.5)$$

σ_x : Stress

P : Applied force

L : ½ Sample length

t : Sample thickness

I : Moment of inertia

ε_x : Strain

δ : Amplitude of deformation

ν : Poisson's ratio

Ks : Measured Stiffness

The deconsolidation affects the mechanical properties which cause the cooling curve to be shifted downward and to have a modulus lower than the initial. During cooling, the modulus drastically increases between 260°C to 240°C (from 2.2 GPa to 31.0 GPa), which corresponds exactly to the crystallization temperature at the same cooling rate.

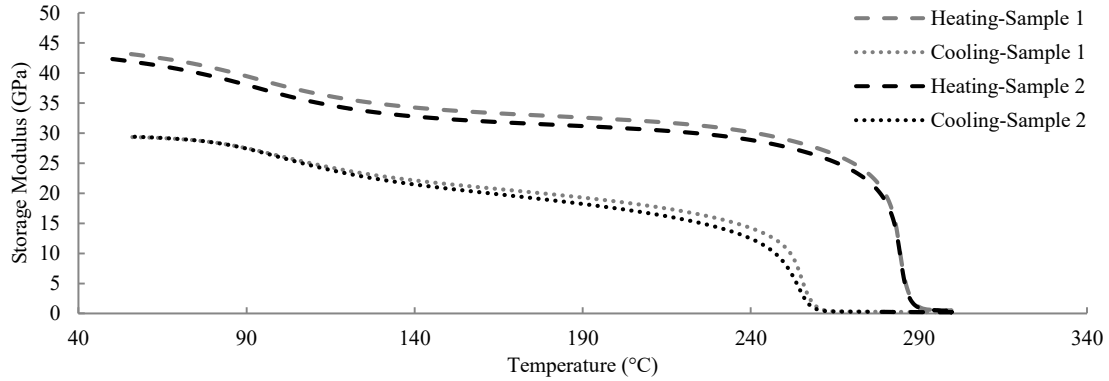


Figure 3.13: DMA Storage modulus versus Temperature

3.5 Conclusion

The goals of this section were to first have an overall understanding of the material behavior during a thermal loading and secondly to create data to use in further simulation. It was found that the crystallization affects every other behavior investigated. While using DSC, it was shown that no experimental cooling rates using Q200 were able to give pure amorphous polymer making it impossible to validate T_g and the cold crystallization zone with the approach used. It was also shown that the crystallization temperature range is affected by the cooling rate. When increasing the cooling rate, the crystallization occurred at lower temperature range. It was also shown that faster cooling rates (equivalent to lower crystallinity) gave lower melting temperatures in subsequent heating. The linear relation between specific heat and temperature was found using MDSC. TMA was used to find the coefficient of thermal expansion of the laminate in-plane and out-of-plane. The in-plane properties were found to be linear and the out-of-plane properties were found to be closely related to the matrix. Finally, DMA showed that the laminate had a mostly elastic behavior and showed the change of bending modulus in function of temperature. The aptitude for the sample to take load was found to be in direct correlation to the creation of crystal regions in the sample. In all experiments, the crystallinity was shown to have a large impact on the sample behavior.

Chapter 4. Finite element method for shape distortion prediction

4.1 Introduction

The formation of residual stresses during manufacturing is known to cause shape distortion. For angled parts, this phenomenon is known as spring-in or spring-back, depending on the direction of the deformation. For complex parts, shape distortion is usually referred to as warpage. A shape distortion is hard to predict and is usually minimized by compensating the tooling in the opposite direction in order to obtain a final part within the tolerance. However, this method is usually arbitrary and based on experience. Many efforts have been made in order to predict warpage of composite parts. Numerical models are commonly used but they are only applicable to simple geometry like angled part. The use of simulations to predict warpage allows avoiding a trial and error approach with costly tooling without regards of the part complexity. The popularity of thermoset has pushed researchers in that direction, and the gaining interest in thermoplastic has shifted the interest. The different chemical behavior between thermoplastic and thermoset does not always allow using similar methods and models for prediction. This chapter is proposing a finite element approach to simulate spring-in of long fiber thermoplastic composites manufactured with a thermostamping process.

The finite element model proposed in this study considers both thermal and mechanical behavior separately. A transient heat transfer analysis is done in order to obtain the temperature cycle of the part and the tool. The mechanical analysis uses the output of the thermal model as input and the corresponding properties in order to obtain stresses and deformations.

This chapter presents a methodology to build the model and the material properties used. The first step is the building and validation of the thermal model. The second step is the building and the validation of the mechanical model with a simple case, in this study a spring-in of an angled part is done. In addition, a sensitivity analysis is also made to have a better understanding of the impact of some input parameters on the model results.

The thermostamping process will be explained as function of the temperature profile as shown in Figure 4.1. The first step is the infra-red heating, the goal is to bring the matrix to the melting point and to maintain the temperature in order to remove all thermal history and in order to compensate the temperature lost during transfer. It is also important not to reach the degradation temperature of the matrix. The second step is the transfer and dies closing. The heated laminate is

transferred between the two dies and the upper die comes down. Usually, the dies temperatures are between the T_g and the T_m . The goal is to reach a high crystallinity by dwelling instead of controlling the cooling rate. To do so, the die temperatures should be in the cold crystallization zone. Once the die is closed, the pressure is applied and kept till the maximum crystallinity is reached. Afterward, the part is cooled in air till room temperature. The simulation window is shown in Figure 4.1. This window is selected because before it, almost no stresses are built because the matrix is still in a molten state.

Temperature profile in Thermostamping

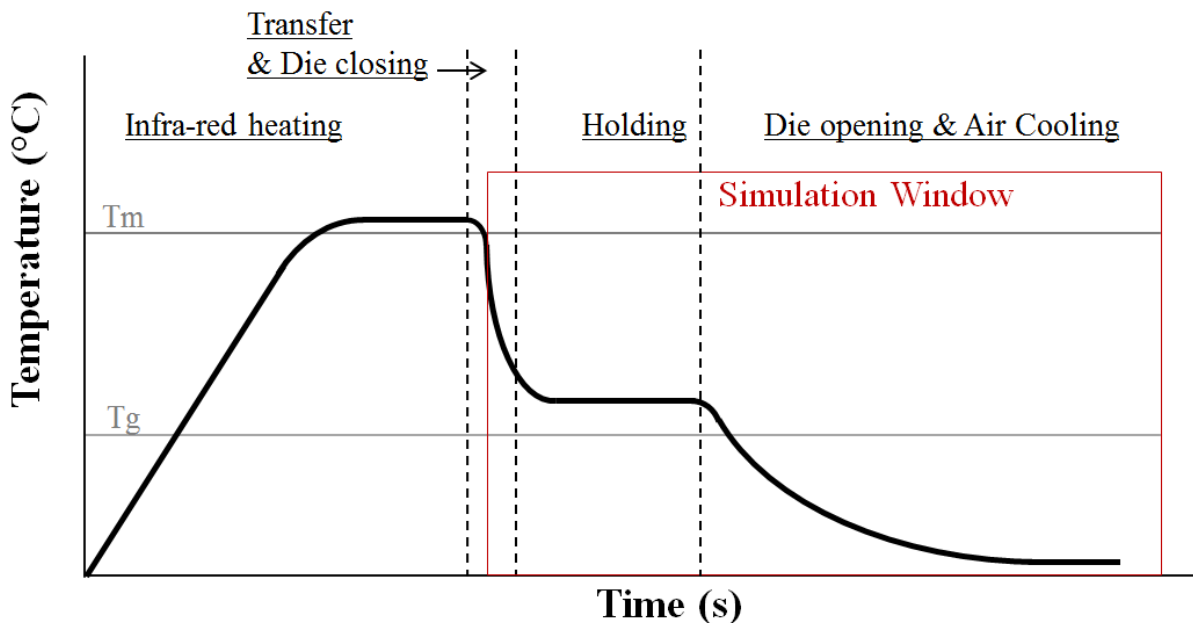


Figure 4.1: Temperature profile

Figure 4.2 shows steps that are simulated and the conditions for both thermal and mechanical step. The laminate temperature is set by a rule of thumb saying the laminate should be heated about 50°C over the melting point which gives a temperature around 330° . The tool temperature should be over the cold crystallization peak in order to perform annealing. Based on [4], the cold crystallization peak is around 110°C . Another common rule is to use the temperature between T_c and T_m which gives around 195°C . The time of 120 seconds was obtained by trial and errors and

by analysing DSC results till no cold crystallization peak were present. For the pressure, based on [45], they found that 3.3 MPa was the minimal value to obtained good curved beam strength.

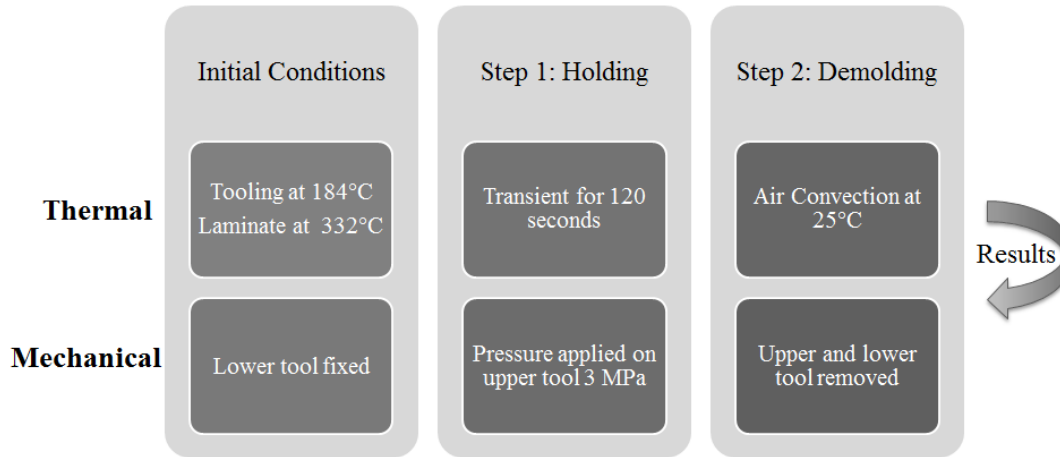


Figure 4.2: Process steps

The tool is not represented as a rigid body because this allows adding cooling channels in the model if needed. The meshing is done using 3D elements for both the laminate and the tooling. The composite lay-up function of Abaqus is used for the laminate, which creates layers within the elements. Abaqus solver uses Gauss quadrature at the layer plane and Simpson’s rule in the stacking direction. The laminate mesh is second order hexahedral elements and the tooling mesh is first order tetrahedral element. The meshing of the tooling is done to create a fine mesh on the contact surface and near the complex regions. The impact mesh size for the laminate is investigated in the sensitivity analysis section.

The assumptions made in this procedure will be presented individually in the respected section. Overall, it is assumed that the property versus temperature behavior will be the one obtained in the previous sections.

- The sequential thermal-mechanical model assumes that the mechanical solution is dependent on the thermal results but that the thermal results are independent of the mechanical results.
- The simulation represents the start of the cooling once the tooling is closed. The temperatures are assumed uniform through the laminate and the tooling. Also, the laminate is assumed stress-free at the beginning of the simulation. The previous steps which are infra-red heating and closing of the die are assumed to have no impact since the laminate is stress-free during those operations.

- Some studies talked about many factors influencing warpage like non-uniform fiber volume fraction, crystallinity gradient etc.. The model here does not consider those aspects since the model is a macro level model which assumes a uniform micro level structure.
- Some properties like thermal conductivity, thermal contact conductivity, etc.. are assumed independent of temperature.

4.2 Thermal Simulation

An accurate thermal simulation is the first step in having representative results. A transient heat transfer simulation is done to obtain the temperature profile seen by the laminate. This profile is later validated with experimental data. Having the right temperature profile gives information on the temperature through the laminate thickness and allows using temperature dependent properties which are both known to have an impact on shape distortion.

4.2.1 *Thermal Properties*

Thermal properties needed for the simulation are density, specific heat and orthotropic conductivity. Density and specific heat are found using experiments. Conductivities values are found using micromechanics models and are compared to experimental data from the literature. Constituent properties which are used for further calculation are presented in Table 4.1 and Table 4.2.

Carbon fiber T300 3K	
Density (kg/mm³)	1.760E-6
Young modulus -axial (N/mm²) [46]	230E3
Young modulus -radial (N/mm²) [47]	23E3
Poisson's ratio [47]	0.24
CTE L (mm/mm°K)	-0.41E-6
CTE R (mm/mm°K) [26]	12.5E-6
Thermal conductivity L (W/mm-°K)	10500
Thermal conductivity R (W/mm-°K) [48]	2000

Table 4.1: CF T300 properties

Thermoplastic PPS TC1100 [42]	
Density (kg/mm³)	1.35E-6
Tg (°K)	363
Tm (°K)	553
Young modulus (N/mm²)	3.8E3
Poisson's ratio	0.36
CTE (mm/mm°K)	52.2E-6
Thermal conductivity (W/mm°K)	190

Table 4.2: PPS TC1100 properties

The composite properties are considered isotropic for the density and the specific heat and, orthotropic for the thermal conductivity. The density of TC1100 was measured based on ASTM standard D792. The results obtained are the average of 6 samples and they are compiled in Table 4.3.

Sample	ρ (kg/m³)
Average	1590.76
Standard deviation	2.04

Table 4.3: Density of TC1100 according to ASTM D702

The specific heat values used are from the MDSC results presented in a previous section. The specific heat capacity is considered linear from ~ 1320 J/ Kg-°C at 310°C to ~ 483 J/ Kg-°C at 23°C. A temperature dependent table is imported into Abaqus.

Obtaining thermal conductivities of a woven composite layer is quite challenging and required an experimental set-up, a complex finite element or numerical model. However, for a unidirectional composite at the micro level, the rule of mixture is a simple and accepted model. In this study, the rule of mixture is used to obtain the conductivities needed for simulation. This assumption is based on the fact that a 5-harness satin has a very low waviness and could be seen as parallel 0° and 90° unidirectional plies. The conductivity properties are found using the rule of mixture in the case of a unidirectional material.

$$k_1 = V_f k_f + V_m k_m = 0.525 * 10.50 + 0.475 * 0.19 = 5.603 \text{ W/m}^\circ\text{C} \quad (4.1)$$

$$k_2 = k_3 = \frac{k_{fr} k_m}{V_f k_m + V_m k_{fr}} = \frac{2.0 * 0.190}{0.525 * 0.190 * + 0.475 * 2.0} = 0.362 \text{ W/m}^\circ\text{C} \quad (4.2)$$

In the case of the symmetric woven fabric, it is assumed that $k_1 = k_2$ and that the unidirectional layers are seen in series for out-of-plane and in parallel for in-plane. Similar to electrical circuit, the total conductance in parallel is equal to the sum of each conductance's.

$$k_{in-plane} = \frac{k_1 + k_2}{2} = \frac{5.603 + 0.362}{2} = 2.963 \text{ W/m}^\circ\text{C} \quad (4.3)$$

$$k_{out-of-plane} = \frac{2 * k_1 * k_2}{k_1 + k_2} = 0.362 \text{ W/m}^\circ\text{C} \quad (4.4)$$

Those values were obtained using many assumptions, in order to validate if the results obtained are in a probable range, the values are compared to experimental data from the literature. No values were found for the same material used in this study so similar situations are used to act as references. Based on experimental results obtained by Gowayed, Y. and al. [49], out-of-plane conductivity, for plain weave AS4/epoxy at 47.1% fiber volume fraction, is 0.373 ± 0.028 (W/m[°]C). The resin epoxy conductivity of this study is 0.196 W/m[°]C which is similar to the conductivity of PPS 0.19 W/m[°]C [46]. For the fiber properties, the paper used a value of 8.4 W/m[°]C along the fiber direction and 0.84 W/m[°]C in the transverse direction as compared to literature values found of 10.5 W/m[°]C along the fiber direction [50] and 2.0 W/m[°]C in the transverse direction [48] for the T300. The difference in the result for the out-of-plane conductivity is approximately 2.95%. Based on experimental data obtained by K. Woo et al. [51], 8-harness satin carbon fiber (Along fiber 8.4 W/m[°]C, radially 0.84 W/m[°]C)/phenolic (0.42 W/m[°]C) has an experimental value of 2.79 W/m[°]C, in-plane conductivity, compared to 2.96 W/m[°]C at a fiber volume fraction of 46.38 %. The experimental results show that the calculations of the in-plane thermal conductivities calculated are in a reasonable range. Table 4.4 presents the values used in the simulation.

	Thermal Conductivity (W/mm-°C)		Density (kg/m³)	Specific heat (J/ Kg-°C)
Steel	50200		8050	490
TC1100	Dir. 1 and 2	Dir. 3	1590.76	Figure 3.6
	2963	362		

Table 4.4: Summary of the thermal properties

4.2.2 Thermal Interactions

The interaction between the surfaces are set as a finite-sliding formulation. The tool surfaces are set as master and the laminate as a slave. The discretization method used is surface to surface contact. Abaqus used the thermal contact conductance which is the inverse of thermal contact resistance as the only thermal contact properties. This value is dependent on many aspects like the surface finish, the pressure, the clearance, the temperature and the state of the matrix. The characterization of this model is complex and hard to obtain. Based on experimental results and a literature review, Sridhar, L [52] compared the steady state thermal contact conductivities of many thermoplastics and they are found to be between 1E-2 and 1E-5 m² °C/W. This gives a conductance between 100 and 50 000 W/m² °C. This wide range shows the difficulty of using a single and right value. The value is chosen by trying the value in that range and it was found that 1500 W/m² °C gave a good fit with experimental data.

The natural convection coefficient is also considered in the interaction section as a surface film condition with a sink temperature of 23°C. A constant value of 10 W/m² °K is used [53]. Table 4.5 presents the values used in the simulation.

	Thermal conductance (W/m² °C)	Natural convection coefficient (W/m² °C)
TC1100/Steel	1500	-
TC1100/Air	-	10

Table 4.5: Summary of the thermal interaction properties

4.2.3 Thermal Validation

A trial blank has been monitored with 10 thermocouples placed on the top and bottom surfaces. Each TC (label from 101 to 110) was positioned according to the following layout (Figure

4.3) and their reading were recorded during the entire process with MEMOCAL equipment, from the heating station to the forming tool.

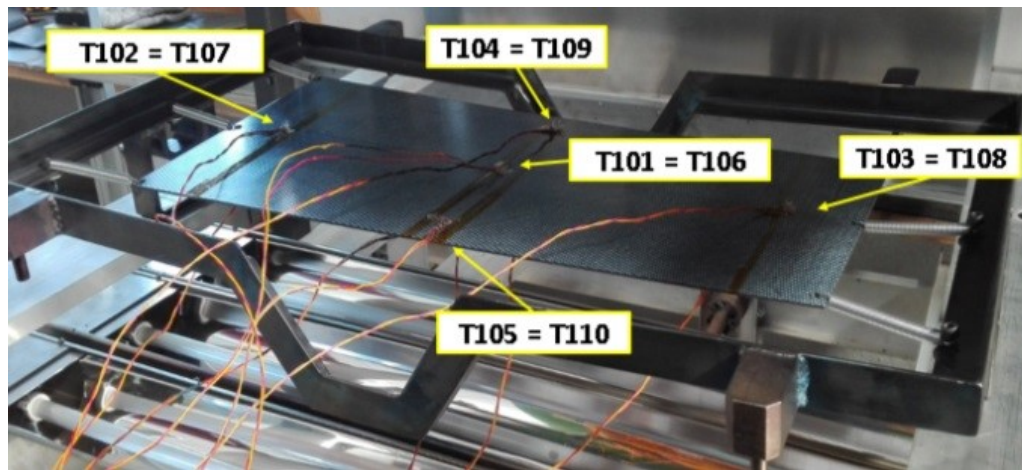


Figure 4.3: Thermocouples

Figure 4.4 shows the difference between the average of ten values from the actual thermocouples and the average of ten FEA values at the same locations. As seen in Figure 4.4, the thermal simulation has a good fit with the experimental data. The largest difference is observed when the mold is considered close on the high temperature laminate; this could be explained by the speed of the process and the rate of acquisition of the thermocouples. The thermocouples have their own thermal inertia which can cause difficulties to represent very fast process. The average of the thermocouples is used because the deviations in the experimental trial are due to hardly controllable factor like the non-uniform heating system, non-uniform tool temperature, thermocouple precision and etc. However, the size of the temperature deviation is negligible and their impacts on the warpage can be assumed as minimal. The temperature profile is accurate; the next step is built using those data in order to have corresponding properties.

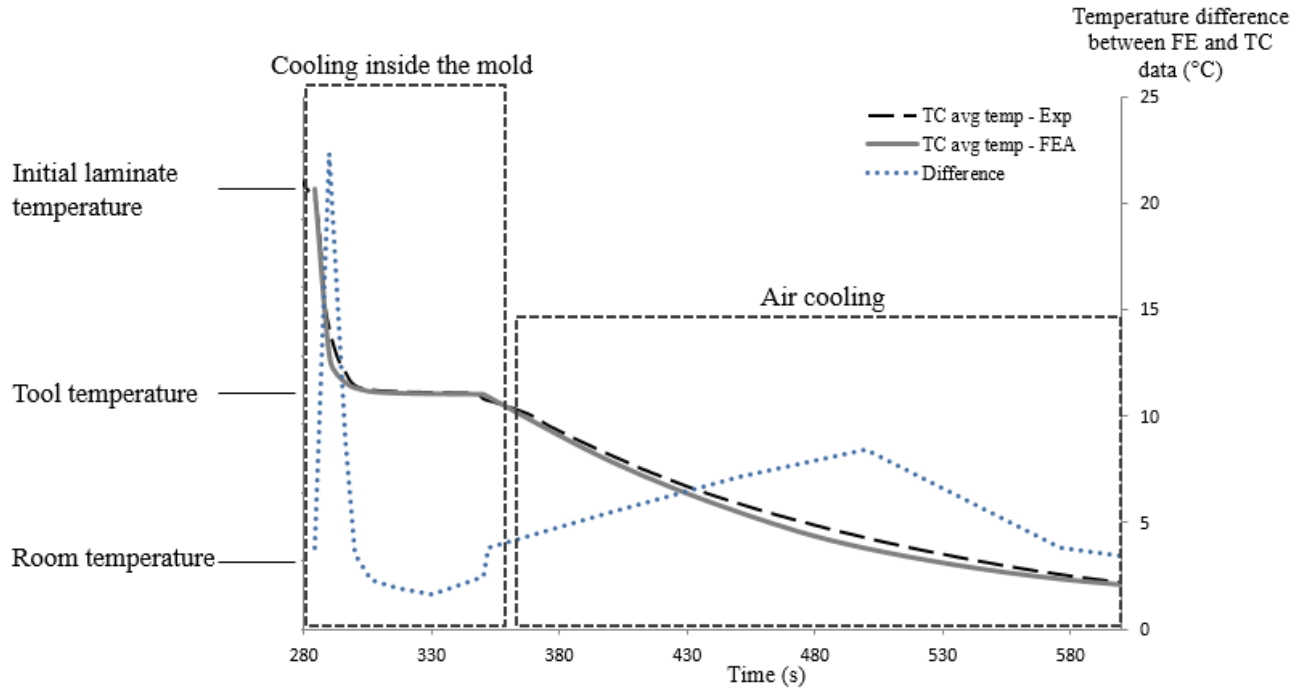


Figure 4.4: Comparison FEA and thermocouples data

4.3 Mechanical Simulation

The mechanical step is the critical step; this is where the residual stresses appear and where the expansion or shrinkage occurs. This step uses the output of the thermal step as an input to use the right thermal dependent properties. The model is then compare to two numerical models and one experimental part. The finite element model is built based on a study made by A.B. Kaganj and al. [45], which formed a S-Shape by thermostamping using PPS/Carbon.

4.3.1 Mechanical Properties

The properties needed for the mechanical simulation is the elastic behavior and the expansion behavior. As seen in the previous section, the material has a predominant elastic behavior which means it can be represented by an elastic model. The laminate is considered orthotropic and needs nine elastic constants. The composite lay-up is built using Abaqus 'composite lay-up' function using one integration point. For the thermal expansion, the behavior is also orthotropic and requires three constants. For steel, isotropic constant values are used.

CTE's obtained in the previous section were the properties for the whole laminate. However, Abaqus uses a composite laminate approach and the properties per ply are needed. An

inverse approach from the procedure detailed in *Stress analysis of fiber-reinforced composite materials* [54] is used to obtain the properties per ply. The methodology used is based on the classical laminate theory. The case is a free thermal response considering that the stresses during the characterization are negligible. The procedure proposed solves the in-plane and out-of-plane properties separately. A MatLab code is written to automatize the calculations; the equations used are 4.5 to 4.12. The material properties used for calculation are shown in Table 4.6. Equations 4.5 to 4.7 are used in 4.8 and 4.9. Afterward, 4.8 and 4.9 are used in 4.10 and 4.11. The value for $\bar{\alpha}_x$ and $\bar{\alpha}_y$ are taken from the experimental data of the previous chapter at each increment and α_1 and α_2 are isolated for each step. The same procedure is done for α_3 using equation 4.12. Equations 4.10, 4.11 and 4.12 are for symmetric and balanced laminate as in this study.

$$\alpha_x = \alpha_1 \cos^2 \theta + \alpha_2 \sin^2 \theta \quad (4.5)$$

$$\alpha_y = \alpha_1 \sin^2 \theta + \alpha_2 \cos^2 \theta \quad (4.6)$$

$$\alpha_{xy} = 2(\alpha_1 - \alpha_2) \cos \theta \sin \theta \quad (4.7)$$

$$\hat{N}_x^T = \sum_{k=1}^N (\bar{Q}_{11k} \alpha_{xk} + \bar{Q}_{12k} \alpha_{yk} + \bar{Q}_{16k} \alpha_{xyk}) (z_k - z_{k-1}) \quad (4.8)$$

$$\hat{N}_y^T = \sum_{k=1}^N (\bar{Q}_{12k} \alpha_{xk} + \bar{Q}_{22k} \alpha_{yk} + \bar{Q}_{26k} \alpha_{xyk}) (z_k - z_{k-1}) \quad (4.9)$$

$$\bar{\alpha}_x \equiv \frac{A_{22} \hat{N}_x^T - A_{12} \hat{N}_y^T}{A_{11} A_{22} - A_{12}^2} \quad (4.10)$$

$$\bar{\alpha}_y \equiv \frac{A_{11} \hat{N}_y^T - A_{12} \hat{N}_x^T}{A_{11} A_{22} - A_{12}^2} \quad (4.11)$$

$$\begin{aligned} \bar{\alpha}_z = \frac{1}{N} \sum_{k=1}^N [& \{S_{13}(Q_{11} m_k^2 + Q_{12} n_k^2) + S_{23}(Q_{12} m_k^2 + Q_{22} n_k^2)\} \bar{\alpha}_x \\ & + \{S_{13}(Q_{11} n_k^2 + Q_{12} m_k^2) + S_{23}(Q_{12} n_k^2 + Q_{22} m_k^2)\} \bar{\alpha}_y + \alpha_3 \\ & - \{S_{13}(Q_{11} \alpha_1 + Q_{12} \alpha_2) + S_{23}(Q_{12} \alpha_1 + Q_{22} \alpha_2)\}] \end{aligned} \quad (4.12)$$

Table 4.6 regroups the nine engineering constants needed for an orthotropic material. Some information is available from the supplier data sheet. Additional calculations are needed to obtain all constants. E_3 is assumed to be equal to the unidirectional rule of mixture from E_2 . This is based

that in both cases it is a matrix driven. The fiber behavior of 5 harness satin can be considered similar to UD material because of the low fiber waviness.

$$E_{1-UD} = V_f E_f + V_m E_m = 0.5 * 230 + 0.5 * 3.8 = 116.9 \text{ GPa} \quad (4.13)$$

$$E_{3-5HS} = E_{2-UD} = \frac{E_{fr} E_m}{V_f E_m + V_m E_{fr}} = \frac{23 * 3.8}{0.5 * 3.8 * + 0.5 * 23} = 6.522 \text{ GPa} \quad (4.14)$$

Based on lamina theory for ν_{12-UD} and laminate theory assuming a ply is two unidirectional at 0° and 90° for ν_{12-5HS} :

$$\nu_{12-UD} = \nu_f V_f + \nu_m V_m = 0.26 * 0.5 + 0.36 * 0.5 = 0.31 \quad (4.15)$$

$$\nu_{12-5HS} = 0.033$$

Based on [6] for unidirectional laminate.

$$\nu_{21} = \left(\frac{E_2}{E_1}\right) * \nu_{12} = 0.0173 \quad (4.16)$$

$$\nu_{13-5HS} = \nu_{23-5HS} = \nu_{13-UD} = \nu_{23-UD} = \nu_{12-UD} * \frac{(1 - \nu_{21-UD})}{(1 - \nu_{12-UD})} = 0.441 \quad (4.17)$$

$$G_{13-5HS} = G_{23-5HS} = G_{13-UD} = G_{23-UD} = \frac{E_2}{2(1 + \nu_{23})} = \frac{6.52}{2(1 + 0.441)} = 2.262 \text{ GPa} \quad (4.18)$$

Property	Values	References
E1 (MPa)	55800	Datasheet [46]
E2 (MPa)	53800	Datasheet [46]
E3 (MPa)	6522	Eq. (4.14)
ν_{12}	0.033	Eq. (4.15)
ν_{13}	0.441	Eq. (4.16)
ν_{23}	0.441	Eq. (4.16)
G12 (MPa)	4040	Datasheet [46]
G13 (MPa)	2262	Eq. (4.18)
G23 (MPa)	2262	Eq. (4.18)

Table 4.6: Elastic orthotropic properties of TC1100

Once the properties at room temperature are determined, the relation with the temperature for all those terms needs to be developed from the storage modulus versus temperature relation presented in the previous chapter. The terms $E_{1,2,3}$ and $G_{12,13,23}$ will change proportionally to the bending modulus and the Poisson ratios are assumed constant through the experiments. The next term to use is the expansion coefficients. The out-of-plane coefficient of thermal expansion varies as function of the temperature as presented in the section before. The CTE experiments results are very sensible considering the precision needed. To remove the noise of the experiment in the results a ten degrees mean of the instantaneous coefficient of thermal expansion (Eq. 4.19) is used for each temperature steps. The in-plane values for CTE are assumed constant and are the same as presented in the previous chapter.

$$\alpha_T = \frac{1}{L_0} \left(\frac{dL}{dT} \right)_T \quad (4.19)$$

	Young Modulus (MPa)	Poisson ratio (-)	Expansion Coefficient ($\mu\text{m}/\text{m}^\circ\text{K}$)
Steel	200,000	0.285	12.2
TC1100	As function of T($^\circ\text{C}$)	See Table 4.6	As function of T($^\circ\text{C}$)

Table 4.7: Steel and TC1100 properties

4.3.2 Mechanical Interactions

The interaction model used is the same as the thermal step. The properties needed are the normal behavior and the friction model. The normal behavior is a “hard” contact which gives an open or close contact without a soft transition [55]. The friction is dependent on many aspects of the demolding agent, the surface finish, the load and etc. H. Zeng et al. [56] results showed that a friction coefficient for a 55% carbon weight fiber content of short fiber at a load higher than 200 N is near 0.3 using pin-on-ring apparatus. The friction is assumed as constant and a value of 0.3 used. The friction model for a composite at different temperatures on a metal plate is more complex than a model at one constant but in this case, movement of the plies versus the metal plate is very small being mainly caused by the in-plane shrinking. Also, the impact of the friction value is later evaluated with the sensitivity analysis.

	Tangential Behavior - Coefficient Friction [56]
TC1100/Steel	0.3

Table 4.8: Contact properties

4.3.3 Mechanical Sensitivity Analysis

A sensitivity analysis has for goal to study the impact of the variation of the input parameters on the outputs of the model. The evaluation is made on the spring-in of a 90° angled part. The use of composite lay-up in the software discretizes the total thickness in the relative thickness of each ply with one integration point. According to Abaqus user manual [55]: "Solid composite layups are expected to have a single element through their thickness, and that single element contains multiple plies that are defined in the plies table. If the region to which you assign your solid composite layup contains multiple elements, each element will contain the plies defined in the ply table, and the analysis results will not be as expected." Different size elements and elements trough thickness are tested. Combination of size element between 0.5 mm to 2mm and a variation of 1 element to 3 elements through the thickness were tested and the values remain constant showing that in the range investigated the element size does not impact the final results.

Since there are many factors from the literature or developed with important assumptions, this method allows evaluating their impact with low computational resources. The next step is to evaluate the impact of the input values on the final results. A full factorial design of the experiment is used. A design of experiments allows structuring the test method and a full factorial design requires a lot of resources but give good conservative results. In this situation where the simulation time is reasonable, it is possible to do so. This step allows focusing the effort where it is most needed. However, this provides qualitative measures to rank the factors in importance order. Three factors are selected and 3 levels are used for each which requires 27 runs. MiniTab software is used to do compilation and calculations to obtain the analysis of variance.

A. Mechanical

A.1. Friction coefficient

A.2. CTE

A.3. Mechanical properties (Modulus and Poisson ratio)

Table 4.9 presents the range used for the sensitivity analysis, the goal is to vary inputs parameters and verify the impacts on the output. The medium range represents value from experiment and literature, which are the most realistic as possible. The small values used are half of the medium values and the high values are the double of the medium values. As shown earlier, the proprieties of a ply are derived from the experimental CTE and the mechanical properties.

	Small	Medium	High
Friction coef. tool - laminate	0.15	0.3	0.6
CTE	x 0.5	As previously presented	x 2
Mechanical properties	x 0.5	As previously presented	x 2

Table 4.9: Parameters and Levels for sensitivity analysis

The effect of the parameters can be determined as significant when the p-value is less than α which is 0.05 in this case. The p-value for the friction coefficient obtained was 0.393, for the Mechanical properties 0.410 and for CTE 0.000. This means that only the CTE was shown to have a significant impact on the warpage prediction. This shows that the approximation made for friction coefficient or for the mechanical properties can be assumed not impactful on the results obtained in term of spring-in simulation. The key aspect with thermoplastic composite is the crystallinity, it was previously seen that no load can be taken by the matrix before the start of crystallization meaning a very low amount a stress is built before the crystallization point. Since the part is demolded a bit below 200°C, low stress is present and the spring-in is mainly caused by the difference between in-plane and out-of-plane CTE during air cooling. The conclusion is not that only the CTE matters and has an impact on the model but it demonstrates that between mechanical properties, friction coefficient and coefficient of thermal expansion, the coefficient of thermal expansion is the only one with a significant impact. It also helps increase confidence in the model due to the uncertainty of the parameters used.

4.3.4 Mechanical Validation: Models comparison

The goal of the model is to represent the reality, in order to validate the model, it is important to compare the results to numerical model and/or experimental data. The goal here was to develop

a model for warpage. Whoever, warpage is usually complex and hard to compare. A simple form of warpage is spring-in or spring-back which is the change of angle of a v-shape. The first validation is made with a simple numerical model provided by N.Zahlan and J.M.O'Neill [23]. The second numerical model evaluated is the Radford model [22]. The third comparison is made by comparing the results to experimental data obtained from A.B. Kaganj and al. [45]. A numerical model has been developed by N.Zahlan and J.M.O'Neill [23] to theoretically estimate the spring-in of a thermoplastic composite. The model is validated with experimental data for a APC-2/AS4 [-45,0,45,90]_s. The problem is solved with 2 sets of parameters, over and under the T_g. They found that the calculated spring-in value of 1.28° was close to the experimental values.

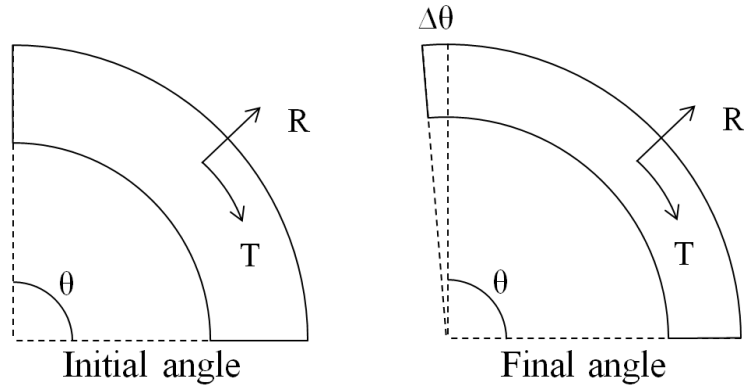


Figure 4.5: References for shrinkage models

$$\Delta\theta = (\alpha_R - \alpha_T) * \theta * \Delta T \quad (4.20)$$

$\Delta\theta$: Change in sector angle

θ : Sector angle

ΔT : Change in temperature from solidification

α_R : Radial coefficient of thermal expansion

α_T : Tangential coefficient of thermal expansion

Results for Radford and O'Neill will be applied to the PPS/Carbon. Based on the previous material characterization, the spring-in starts at the crystallization point which is near 220°C for a fast cooling rate.

< T _g			> T _g		
α _R (μm/m°C)	α _T (μm/m°C)	ΔT(°C)	α _R (μm/m°C)	α _T (μm/m°C)	ΔT(°C)
6.6	61.58	60	6.6	137.03	130

Table 4.10: Properties and Temperatures for Radford and O'Neill model

$$\Delta\theta = (\alpha_R - \alpha_T) * \theta * \Delta T = (6.6 - 137.03) * 90 * 130 * 10^{-6} = -1.526^\circ \quad >T_g$$

$$\Delta\theta = (\alpha_R - \alpha_T) * \theta * \Delta T = (6.6 - 61.58) * 88.47 * 60 * 10^{-6} = -0.299^\circ \quad <T_g$$

$$90^\circ - 1.825^\circ = 88.175^\circ$$

Radford model uses a similar approach and is a very common method for calculated spring-in angle [22]. It was initially developed for thermoset.

$$\Delta a = \frac{(\alpha_R - \alpha_T) * \theta * \Delta T}{(1 + \alpha_T * \Delta T)} \quad (4.21)$$

$$\Delta\theta = \frac{(\alpha_R - \alpha_T) * \theta * \Delta T}{(1 + \alpha_T * \Delta T)} = \frac{(6.6 - 137.03) * 90 * 130 * 10^{-6}}{(1 + 137.03 * 130 * 10^{-6})} = -1.499^\circ$$

$$\Delta\theta = \frac{(\alpha_R - \alpha_T) * \theta * \Delta T}{(1 + \alpha_T * \Delta T)} = \frac{(6.6 - 61.58) * 88.5 * 60 * 10^{-6}}{(1 + 61.58 * 60 * 10^{-6})} = -0.291^\circ$$

$$90^\circ - 1.79^\circ = 88.21^\circ$$

Both models are independent of many factors like the radius, the thickness, the lay-up sequence including modulus and individual CTE of each ply. Their main factor is the difference between out-of-plane and the in-plane CTE.

The finite element model of this study is then compared to experimental results using previous work made by A.B. Kaganj and al. [45]. This study used three different lay-ups of TC1100 5-harness satin which is the same material used in this study. The tooling properties are changed for the aluminum properties. The procedure is adapted to the one used in the paper; infra-red heating at 330°C, tool temperature at 200°C, holding time of 5 min and air cooled. The influence of Kapton film is neglected.

	Thin Quasi-iso	
	[[0,90]/(±45)] _s	
Laminate Thickness (mm)	1.24	
Tool radius (mm)	3.81	3.81
Tool Radi measured (mm)	3.77	3.63
Part Radi measured (mm)	87.42	87.31

Figure 4.6: Experimental data from [45]



Figure 4.7: Experimental part[45]

The model simulates the thin quasi-iso situation. The radius measured will be used for modeling since it corresponds to the actual tool. The results of the simulation are exported from Abaqus to Catia V5. Planes are fitted on the surfaces (in orange) and the angles are measured between those planes (Figure 4.8).

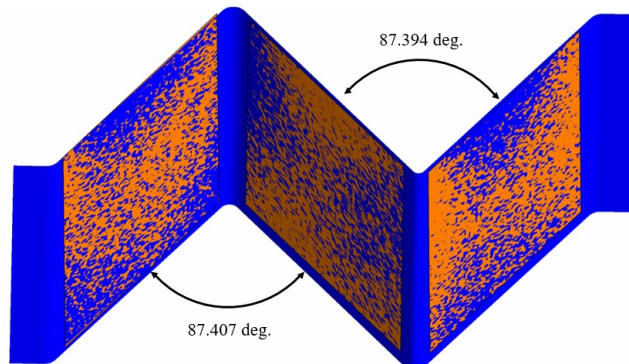


Figure 4.8: Finite element results

The results for each model are presented in Figure 4.9, both numerical models obtained similar values. However, it is important to consider that those models were calculated using only

two constant values of the CTE. The difference between Zahlan and Radford model from the experimental data is 0.92% and 0.97% respectively. The finite element model presented in this study obtained very close results to the experimental, difference of 0.04 %. Each model can be accepted as a successful method to approximate the spring-in in a reasonable margin of error. Without a doubt, the finite element model is more time consuming than the numerical model to predict the spring forward of a v-shape. However, the numerical models are based on the 2D geometry of the angled region and are not applicable to complex 3D shape. This step goal was to show how reliable the model was and if it was able to predict correctly a simple problem, which was successfully demonstrated. Also, an interesting result is that the numerical model has close results considering their simplicity. This can be explained by the results of the sensitivity analysis where it was found that the CTE was the only significant parameters compare to friction coefficient and the modulus on the output results. This allows us to conclude that a model that uses only the CTE and not the modulus can be accurate in situation where low stresses are built in the tooling.

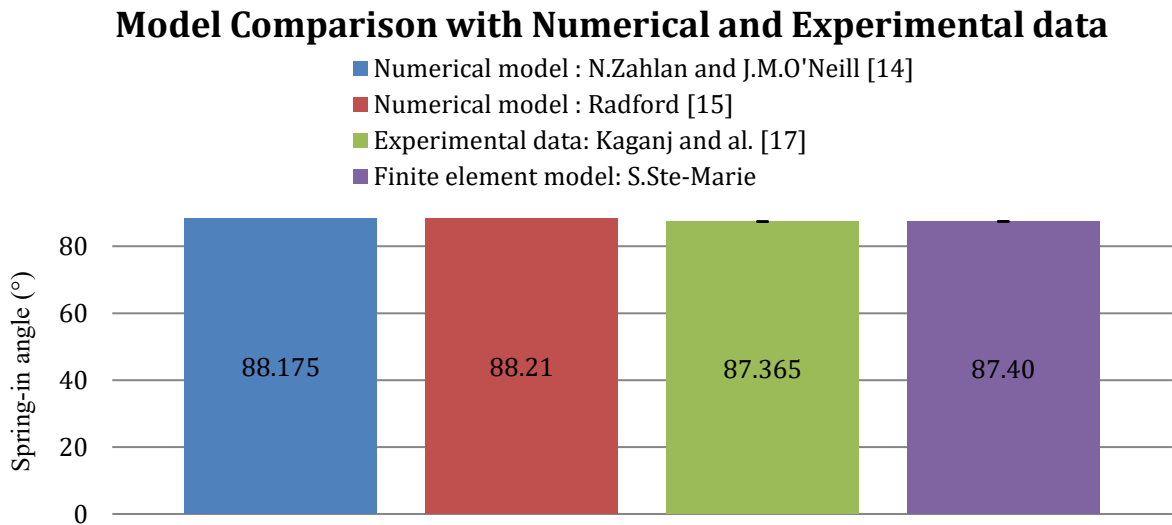


Figure 4.9: Model comparison

4.4 Conclusion

The complete procedure for warpage simulation is detailed through this chapter. A finite element model is built using a thorough material characterization, calculation of numerical models and value for literature. The thermal model is proven to be accurate when compared to experimental data. For the mechanical model, the impact of the friction coefficient, the mechanical properties and the coefficient of thermal expansion are evaluated through a sensitivity analysis. The results are compared using an analysis of variance and it is found that for those three input parameters, only the CTE can be identified as significant on the output. The mechanical results of the model are compared to numerical model and experimental data. In both case close results are obtained for the spring-in values.

Chapter 5. Methodology for Wrinkles removal

5.1 Introduction

Molds and materials are expensive and it is not economical to do many trials and errors to determine the best mold design and the best process parameters. This is because there are many permutations possible between the variables mentioned. It would be desirable if the prediction of wrinkle formation can be done using simulation. There are a few computer programs available. One commercial code is the AniForm software. More recent works made by Haanappel, S.P., and al [57], showed the forming of a wing fixed leading edge with UD CF/PEEK and 8HS GF/PPS. Experimental trials were done and validated with a finite element simulation using AniForm software. A good correlation is obtained between the simulation and the experimental trials. The elements size and a complete material characterization are identified as key aspects to have a good relationship between experimentation and simulation. Nguyen H.-D. and al. [58] showed that for an S-shape and a complex 3D shape made from a CF/PPS laminate simulation with AniForm represents well the thickness variation and the shear angle obtained with experimental trials. The impact of the tooling position is also investigated and it was found that it is possible to remove wrinkles by using the right positioning.

Based on representative results obtained from previous studies, AniForm was chosen as software to simulate the thermostamping process

However, for prediction, the user needs to be aware of the assumptions used:

- To run the program, it is necessary to enter input parameters. These include the properties of the composite laminate at high temperature, the friction coefficients between the laminate and the mold and between the layers themselves. These are scarcely available and it is time-consuming and expensive to determine them.
- To date, the program does not consider the heat transfer effect. The properties at constant temperature are used meaning that it is assumed that the experimental forming at high tool closure rates occurs at a uniform and a constant temperature.
- Friction is characterized using one material, surface finish, and demolding agent, but the real set-up could be different than the one used for characterization. To have the exact data, more experiments are required to fit the specific condition.

Due to the above uncertainty on input parameters, the user should be aware of the assumptions and assess how these could affect the prediction. Simulations can be used to detect trends in the development of critical areas, as done in this study. In terms of avoiding or eliminating the wrinkles, various process configurations can be studied using computer simulations. Based on previous reviews, many methods are available in order to eliminate wrinkles:

1. Removing redundant materials. In some situations, the existence of some material in the part may create compression stresses in surrounding regions and this may create wrinkles in the neighboring regions. The word “redundant materials” is used to indicate their removal does not affect the performance of the part or would have been removed by the final trimming.
2. Varying the stiffness of the holding springs. By changing the stiffness of the holding springs, the tension distribution within the part can be optimal so wrinkles are eliminated.
3. Adding more springs to locations close to where the wrinkles occur.
4. Varying the curvature of the part. In situations where it is possible, reducing the curvature of the parts (particularly for parts with double curvatures) can reduce or eliminate wrinkles.
5. Changing the thickness of the part. In situations where it is possible, reducing the thickness of the part can reduce or eliminate the wrinkles.
6. Changing the friction coefficient. Lower friction allows more freedom for the layers to move. This may or may not facilitate the formation of wrinkles. Friction coefficient can be reduced by applying some release agent on the surface of the mold (for part/mold friction), and/or better mold finish. The friction coefficient between layers of the composite can be reduced by reducing the viscosity of the resin. Increasing the temperature (at the beginning of the process) can reduce the viscosity. However, prolonging the high temperature can speed up the degradation of the resin, which can increase the viscosity.

Within the possible solutions proposed the three first are the most feasible since they require a minimum cost investment, they do not involve changes in the initial part requirements or modification of the tooling. For those reasons, this study will investigate: removing redundant materials, varying stiffness of the springs, and adding more springs to the locations close to where the wrinkles occur.

5.2 Methodology

Each method of the three presented previously will be investigated by the use of simulation. However, because of cost and time constraints, only one will be validated through experimental trial. The material removal method was selected.

The shape selected is a typical complex shape which has a double curvature. The double curvature requires inter- and intra-ply slip which regroups common challenges faced. The geometry of the part was selected in order to be able to obtain parts both with wrinkles and without wrinkles depending on the set-up used. The profile (Figure 5.1.a) is rotated by 40° around an axis located at 385 mm of the profile parallel to x axis on the xy plane. Once revolved, the straight section (70 mm) becomes a single curvature segment and the curved section (160 mm) becomes a double curvature segment (Figure 5.1.b).

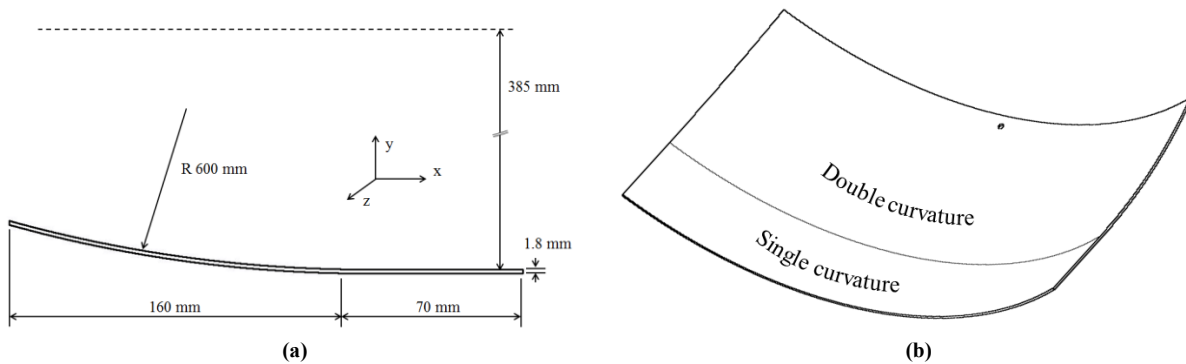


Figure 5.1: (a) Shape profile and (b) Final part

The material used in this study is a pre-impregnated thermoplastic composite for aerospace industry which is a 5-harness satin carbon fiber (T300) fabric impregnated with polyphenylene sulfide (PPS). According to the datasheet, the T_g is 90°C , the T_m is 280°C and the fiber volume fraction is 50%. The lay-up of the laminate is $[(0, 90), (\pm 45), (0, 90)]_s + [(0, 90)]_{FG}$. The material has an additional thin layer of fiberglass (FG) which is used to avoid galvanic corrosion in further assembly. The thin fiberglass scrim is not included in the simulation. Formability properties of the PPS/Carbon are available in the AniForm database [59].

5.2.1 Finite elements and constitutive model inputs

The software uses an implicit solver and the theory behind the software is detailed by Ten Thije et al. [60]. It uses custom three-node triangular shell elements to represent each ply of the laminate.

The properties per shell are separated into 3 groups; in-plane, bending and interface. This means, each ply is separated into 4 elements; contact elements on top and bottom (2x); DKT to represent bending behavior and membrane to represent in-plane behavior. The constitutive models used and their respective constants are represented in Table 5.1. Deformation behavior of the plies soft state at forming conditions is acquired by an extensive characterization program [57]. The characterization data is input for the various parts of the AniForm shell element by means of calibrated constitutive models. In-plane shear and bending responses at various deformation rates have been calibrated using a combination of elastic and shear rate dependent material models available in AniForm. The friction responses at various sliding velocities and normal pressures are calibrated using AniForm interface models that describe the hydrodynamic lubrication effects.

In-plane shear is characterized using the bias extension method [61], which extends a 45° oriented rectangular specimen using one static and one movable clamp. The in-plane constitutive model is a mixed model of the Cross model and Mooney-Rivlin. The mixed model is defined as the Eq. 5.1.

$$\tau = (2C_{10}(B - I) - 2C_{01}(B^{-1} - I)) + 2\eta(\dot{\gamma})D \quad (5.1)$$

Where B is the left Cauchy-Green deformation tensor, I is the identity tensor, $\eta(\dot{\gamma})$ the equivalent shear rate, D the rate of deformation tensor and C_{01} , C_{10} material constants. C_{01} and C_{10} constants are obtained through a model fit of the experimental data. The viscosity dependent of the shear rate is defined as the Eq. 5.2.

$$\eta(\dot{\gamma}) = \frac{\eta_0 - \eta_\infty}{1 + m\dot{\gamma}^{(1-n)}} + \eta_\infty \quad (5.2)$$

With $\dot{\gamma} = \sqrt{2D:D}$

η_0 and η_∞ are the Newtonian plateaus at low and high shear rates respectively. The constants n and m are the Cross constant which is derived from the Power-law.

Out-of-plane bending is characterized using a tailored bending fixture in a torsional rheometer, which secures a rectangular specimen. One of the clamps is subjected to a rotation in order to bend the specimen into a shape of constant curvature. The detailed methodology and calculations can be found in [62]. The test is performed at three different rotation velocities to capture the rate

dependent material behavior as well. The model obtained is a mixed model using the combination of an elastic and a Cross viscosity description. The constants are fitted from the experimental trial.

Inter-ply and tool-ply slip are characterized using a friction test set-up [63], which allows testing at different normal pressures and pull-out velocities. A specimen consists of three plies: two outer plies to be secured during the test, and one center ply that will be pulled-through the outer plies. The center ply is the composite material, whereas the outer plies consist of the composite material in case of inter-ply testing, and in case of tool-ply testing comprise metal shims that represent the tooling material. The test is performed at three different speeds to capture the rate-dependent response. For friction, the penalty model with polymer friction is represented by as Eq. 5.4 which is used in Eq. 5.3.

$$\tau_f = \eta \begin{Bmatrix} \dot{\gamma}_x \\ \dot{\gamma}_y \\ 0 \end{Bmatrix} \quad (5.3)$$

$$\eta = \eta_c c_p \quad (5.4)$$

Where τ_f is the traction due to the fluid deformation, $\dot{\gamma}_x$ and $\dot{\gamma}_y$ are the shear rates.

η_c is obtained by Eq. 5.5 and c_p by Eq. 5.6

$$\eta_c = \frac{\eta_0}{1 + (C * \dot{\gamma}_q)^{1-n}} \quad (5.5)$$

Where η_c is the viscosity of the polymer film, $\dot{\gamma}_q$ is the equivalent shear rate and η_0 , C , n , are fitting parameters.

$$c_p = a * (p_0 + p)^b \quad (5.6)$$

Where p is the contact pressure and where a , b and p_0 are fitting parameters. The contact pressure is obtained by multiplying the penalty stiffness and the penetration depth. The penalty stiffness can be adjusted in the simulation in order to keep the penetration less than half of the thickness of a ply. U. Sachs [63] gives a detail overview of the models of friction and bending and the important assumptions. The thickness of the resin-rich inter layers is considered constant; this has an important effect on boundary lubrication, hydrodynamic lubrication and, wall slip. For the

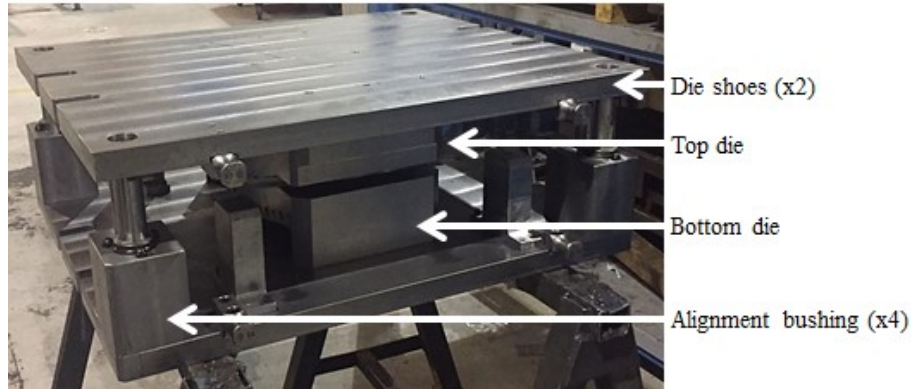
bending constitutive model, the increase of bending rigidity caused by the interlocking of the fiber, which is more severe at low temperatures or high deformation rates, is not included in the constitutive model.

Elements (model)	Behavior	Parameters	Values
Contact (Penalty with polymer friction)	Ply-ply and tool-ply	<i>Penalty</i>	
		Penalty stiffness (N/mm ³)	100.0
		<i>Polymer friction (tool-ply)</i>	
		C	0.24929
		η_0 (MPa s)	0.0011096
		film thickness (mm)	0.1
		N	0.25782
		<i>Polymer friction (ply-ply)</i>	
		C	6.92E-6
		η_0 (MPa s)	8.6425E-4
		film thickness (mm)	0.1
		N	0.079249
Membrane (Mixed model)	In-plane	<i>Elastic</i>	
		Elastic fiber model (GPa)	10.0
		<i>Mooney Rivlin</i>	
		C10 (MPa)	0.006
		C01 (MPa)	0.0
		<i>Cross model</i>	
		η_0 (MPa s)	0.51652
		η_∞	0.048469
		m (s ⁽¹⁻ⁿ⁾)	80.1286
		n	-0.15
DKTs (Mixed model)	Bending	<i>Isotropic Hooke</i>	
		E (Mpa)	161.1821
		ν (-)	0.33
		<i>Cross model</i>	
		η_0 (MPa s)	1620.9181
		η_∞	11.5334
		m (s ⁽¹⁻ⁿ⁾)	8000
		n	0.0346

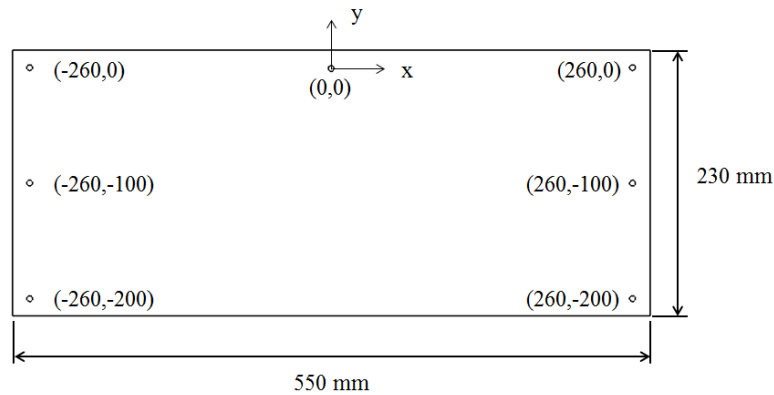
Table 5.1: Constitutive models and parameters values for PPS/Carbon at 325°C from Aniform documentations [59] Calibrated on 17/02/2016

5.3 Experimental

The panel is manufactured at Dema – Design Manufacturing SpA in Italy. The press used is a Muraro 250 tons with heated platens of 1200 mm x 1200 mm. The die assembly is made of steel and both dies are installed on die shoes. Alignment pins and bushings are used to ensure the alignment between the top and bottom dies.



(a)



(b)

Figure 5.2: (a) Die assembly and (b) Springs positioning

The pre-impregnated blank has 3 holes drilled on each side (as seen in Figure 5.2.b) where springs with a constant of 0.045 kg/mm are attached from the laminate to a frame. The infra-red system is made of 6 infrared lamps, 3 on top and 3 on the bottom with a capacity 2000 Watts each. The blank is heated in the infra-red heater till $350^{\circ}\text{C} \pm 10^{\circ}\text{C}$ (which is $\sim 70^{\circ}\text{C}$ over the melting point of PPS) then manually transferred between the dies which were pre-heated at $185^{\circ}\text{C} \pm 2.5^{\circ}\text{C}$. The top die goes downward at a speed of 60 mm/s till a distance of 1.76 mm between the lower die is reached. The die is kept closed for 66 seconds, and then the formed part is cooled in air. A trial blank has been monitored with 10 thermocouples (TC) placed on the top and bottom surfaces in order to obtain the temperature profile which is used to select the corresponding material model.

5.4 Simulation

The tooling is represented as a rigid surface with triangle elements. The count of elements is 1912 for the top die and 1907 for the bottom die. The laminate is represented by shell elements as described previously. It is assumed that the laminate is formed at the same constant temperature at

which it was characterized. Based on TC data, the forming occurs around 330°C and the material model used is characterized at a constant temperature of 325°C. The simulation set-up is based on the actual constraint of the press and tooling; the same distance between components, and the same closing speed. The presence of a problematic area in simulation results can be identified by many indicators. In this study, they can be seen in two ways, as out-of-plane excess material or as in-plane alternating compressive and tension stresses. The occurrence of alternating stresses does not necessarily mean wrinkles will appear but it identifies the critical zone where the stresses should be minimized.

Figure 5.3 shows where the wrinkles occurred in the experimental formed part. The wrinkles are located at the extreme of the double curvature and are visible on the fiberglass scrim. They are light wrinkles, mostly in-plane. The affected zone is symmetrically distributed around the middle and has dimensions of 106.55mm x 58 mm.

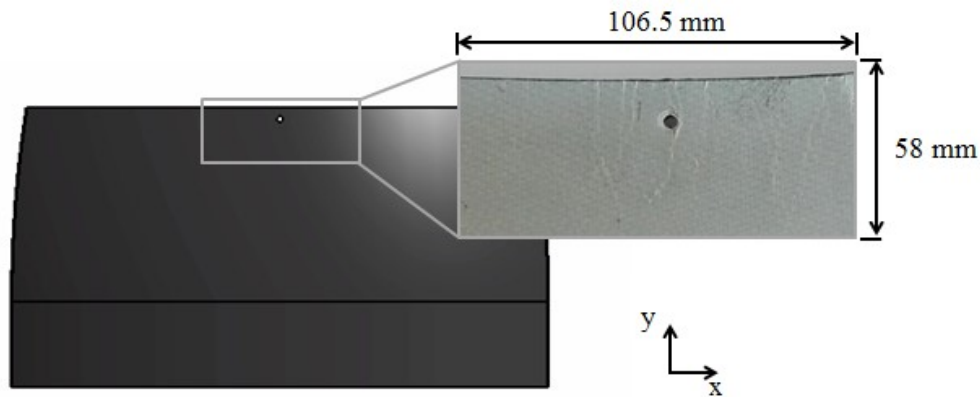


Figure 5.3: Wrinkles on experimental part

As addressed in the review, the mesh size is critical to have representative results. Too coarse meshes do not give the accuracy needed to highlight small wrinkles. Figure 5.4 shows the impact of the mesh size versus the representability of the results at the wrinkles location. For each trial, the left images represent the stresses in the x-direction and the images on the right represent the stresses in the y-direction. An element size of 14 mm only shows the compressive stresses but it does not show any trend causing wrinkles. Element size of 7.4 mm is small enough to highlight the problematic zone; however, the stress zone obtained is much bigger than the experimental results. The sensitivity of the results shows that element size of 3.8 mm and 2.7mm gave similar results as the experiments. Both show the compressive stresses near the edge in the x-direction and

alternating tension and compression stresses in y are caused by the movement of material in-plane. The size of 2.7 mm is the most accurate because it gives a similar zone dimension as the experimental part.

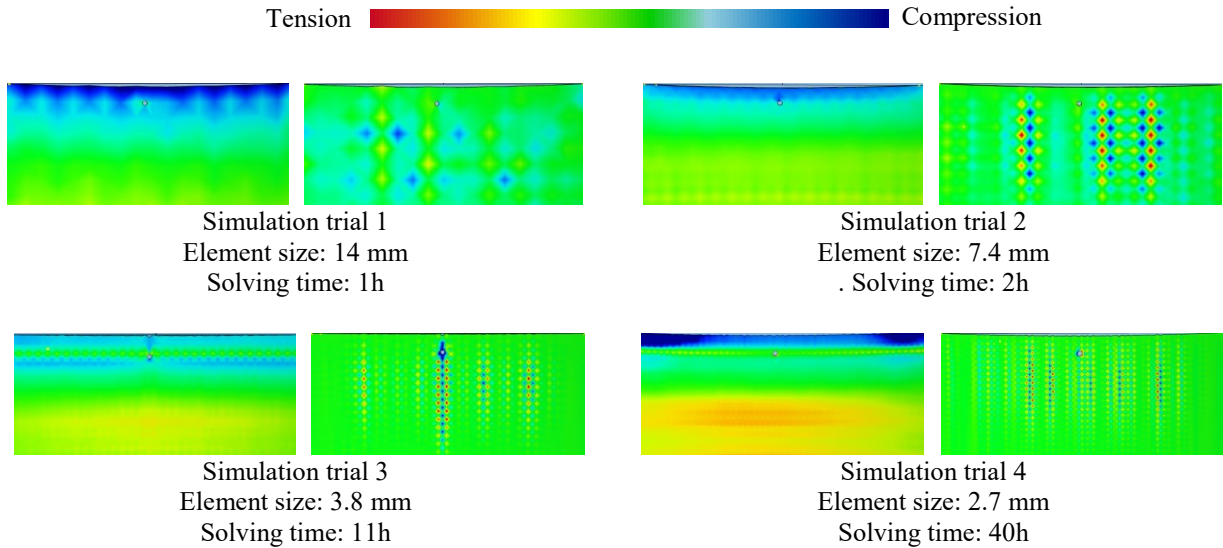


Figure 5.4: Effect of mesh size on wrinkle detection
Left: stresses in x-direction Right: stresses in y-direction

5.5 Results and Discussion

5.5.1 Preliminary DOE

A preliminary design of experiment (DOE) was made before coming up with the experimental set-up. The goal was to investigate the impacts of the initial control parameters (spring stiffness, spring position and forming temperature) on the final quality characteristics (in-plane stresses x and y-direction, and shear angle). AniForm material database has the material model of PPS/Carbon calibrated at three temperatures: 290°C, 325°C and 350°C. Each material model has its specific constants; the values for 325°C are presented in Table 5.1 and the values for 290°C and 350°C are available in AniForm documentation [59].

To assess the optimal processing parameters, different levels of each parameter are investigated. A DOE of 3 controls parameters with 3 levels was built. The approach used is a Taguchi's analysis using an orthogonal array. This approach allows reducing the computational cost by doing 9 runs instead of 81 and helps to identify the effect of factors on the response mean and variation. In this case, the control parameters selected are shown in Table 5.2 with their respective levels.

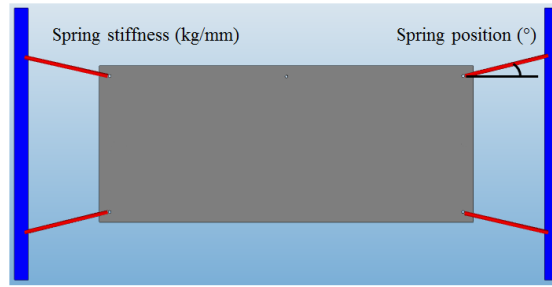


Figure 5.5: Reference springs stiffness and position

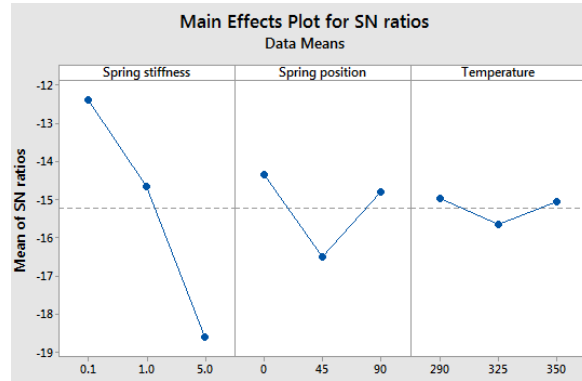
Parameter	Units	Levels		
		A	B	C
A- Spring Stiffness	kg/mm	0.1	1	5
B- Spring Position	°	0	45	90
C- Temperature	°C	290	325	350

Table 5.2: Control Parameters and Alternative Levels

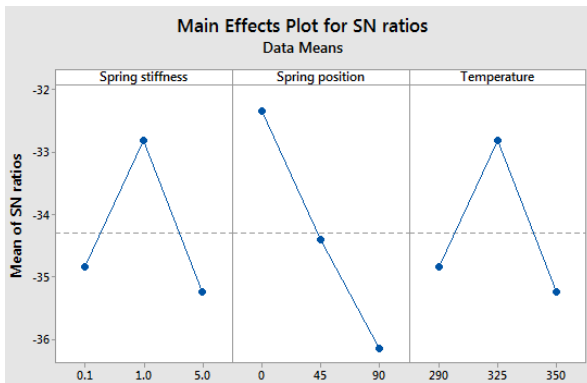
The results are analyzed using Minitab 17 statistical software [64]. The signal-to-noise ratio (S/N) is used with “smaller-is-better” which has the goal to minimize the maximum shear angle and maximum stresses. The S/N graphs are produced and are presented in Figure 5.6. Two aspects need to be observed on the graphs; the slope and the highest value. The slope gives information on the importance of the factor. For example, a steep slope means that the parameter is very impactful on the output. The higher a value is on the graph, the more it is appropriate to minimize the quality characteristics.

The springs stiffness has a big impact on the shear angle and in-plane fiber stress in y-direction but the impact is opposite. For the shear angle, the values of 1 kg/mm and 5 kg/mm is so stiff that it creates stresses even before the forming. This is also caused by the fact that the springs are located at the corners which create shearing effect when the spring stiffness is too high. This is why a lower springs stiffness and additional springs are recommended since the laminate should not be under high stresses or deformed before forming. The spring’s position is optimal at 0° for the shear angle and in-plane stress in the x-direction and optimal at 45° for in-plane stress in the y-direction. A middle value should be used. This can be explained by the fact that in order to avoid wrinkles, a pre-tension should be applied to the fibers. This springs position allows having tension

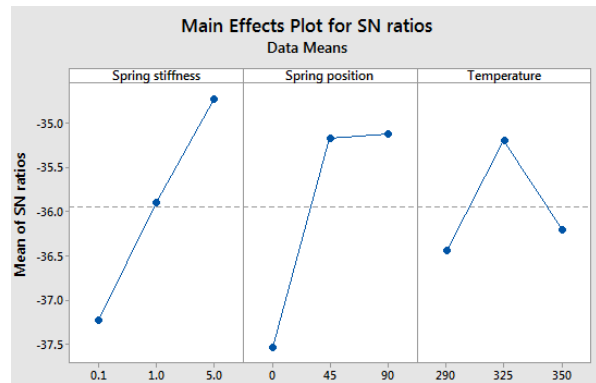
in all the fiber directions and mostly in the direction where the large curvature happen. For the temperature, the impact for all quality characteristics is small but in the in-plane situation (x- and y-directions), 325°C is best and should be used.



(a)



(b)



(c)

Figure 5.6: Taguchi's results; (a) Shear angle, (b) In-Plane Fiber Stress X and (c) In-Plane Fiber Stress Y

Based on the preliminary DOE, the experimental set-up was built. The springs positioning and tension are closely related and are critical to have a good stress distribution. Based on the previous conclusion, low stiffness springs 0.045 kg/mm are used at 22.5° and new springs are added in the middle to create a more uniform tension within the laminate. The laminate should be formed at a temperature close to 325°C. The results of the simulation analysis helped to build the preliminary set-up without using any experiments and without historical data (Figure 5.7).

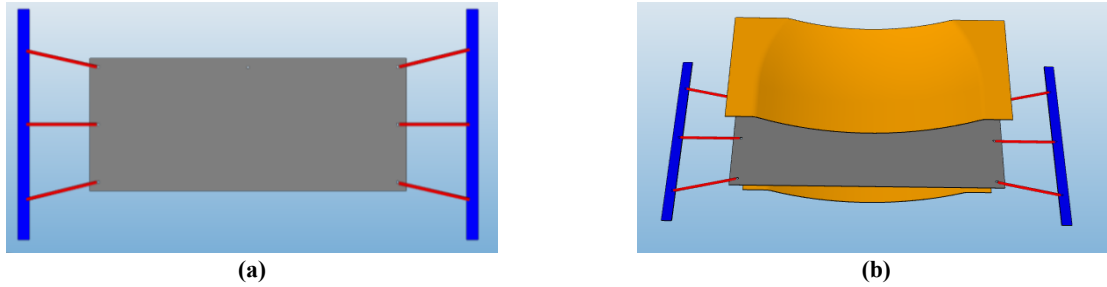


Figure 5.7: Final set-up - (a) Upper view of the gripping set-up and (b) Isometric view of the complete set-up

5.5.2 Mechanism causing wrinkles

Laminate deformation is directly related to wrinkles formation. A good understanding of the laminate deformation will provide information on where the wrinkles come from and how to avoid them. In a case of a double curvature, excess materials need to be reorganized by inter-ply and intra-ply shear.

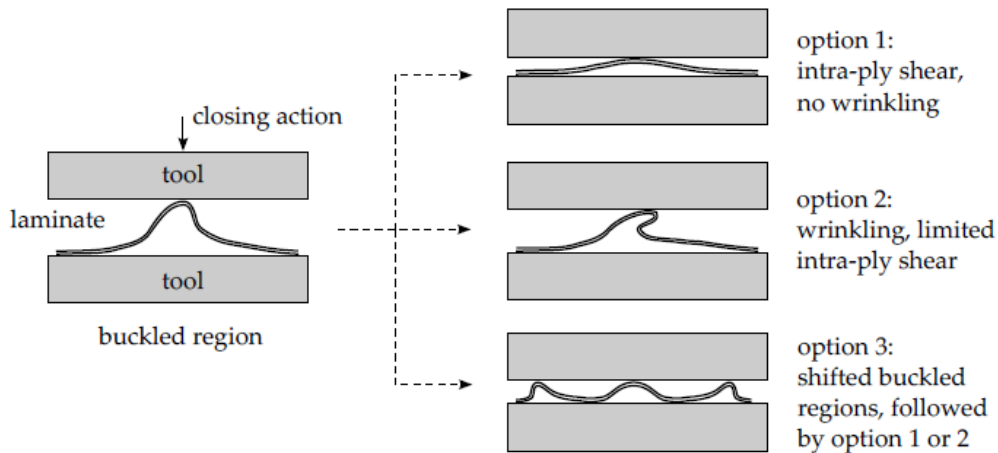


Figure 5.8: Wrinkles mechanisms [57]

The simulation is stopped at different distances from the final position between the top and bottom tool which is the final thickness of the part (1.76 mm). This allows seeing the evolution of the excess material; results are presented in Figure 5.9. Similarly, to the third option of Figure 5.8, the large buckled region is transformed in smaller regions from 3 mm to 2 mm before the full closing. At this point, the stresses in the material are still low. At 0.5 mm, stresses appear because the material is forced in the plane causing intra-ply shear which is reflected by in-plane stresses. As seen in the experimental part, it causes buckling of the fiberglass scrim and waviness in the carbon fiber layer.

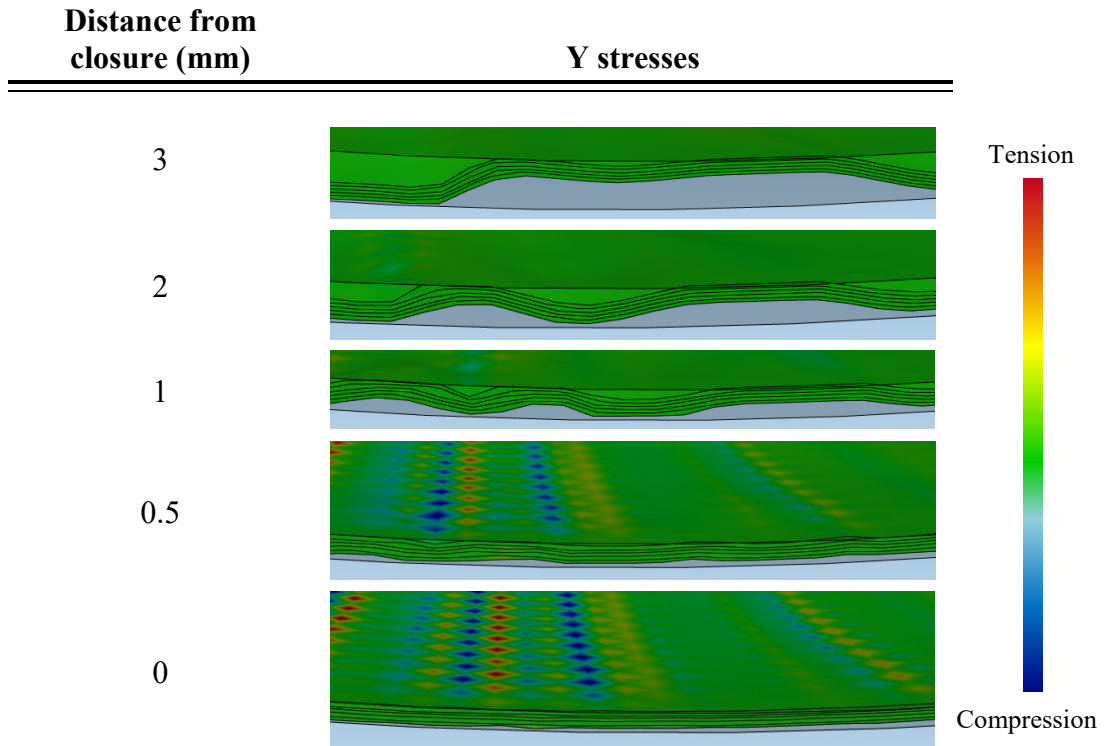


Figure 5.9: Buckled region evolution (Stresses in y-direction)

5.5.3 Method 1: Material removal

This method is applicable if the initial blank is larger than the expected final part, which is the case in this paper. Based on the previous section, it is seen that the wrinkles are created by the excess material being pushed in-plane. The solution investigated is to remove material in the critical area in order to reduce the stresses when the tool is closed. Lips of material of different size "d", varying from 10 mm to 30 mm, are removed on the edge of the double curvature region in order to understand how this change affects the result (Figure 5.10). A small section in the middle is kept because the drilled hole is needed as a positioning reference. Figure 5.11 shows the comparison of simulation and experimental results before and after a 20 mm material removal. The comparison of simulation results before (b.1) and after (b.2) material removal show that this method allowed reducing stresses in the y-direction. This reduction was enough to remove wrinkles, which is visible in the experimental part (c.1 and c.2).



Figure 5.10: Material removal "d"

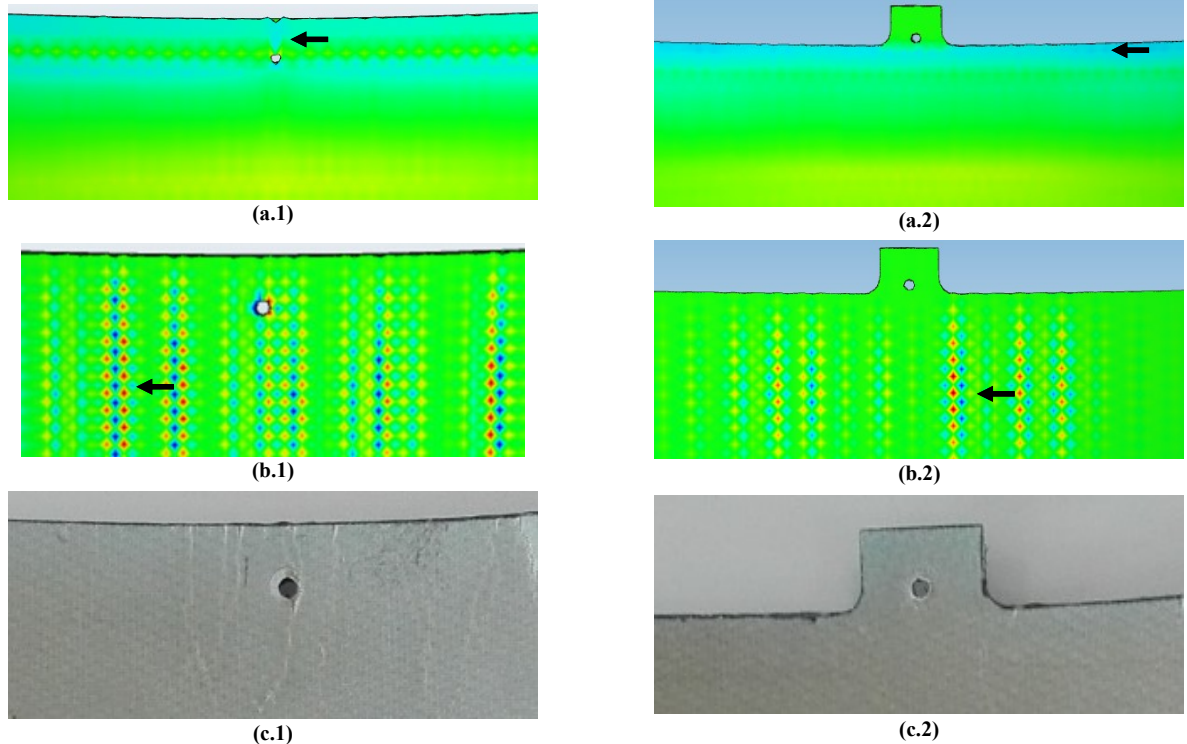


Figure 5.11: Material removal comparison $d=20$ mm; (a) x stresses, (b) y stresses and (c) experimental. (1) Without material removal and (2) with material removal.

*Arrows show where the maximum stresses were taken

Based on Figure 5.12, all value of "d" gave good results. This is explained by the fact that the excess material being pushed in-plane is always the most important at the edge of the double curvature. Based on the successful experimental results with 20 mm, it is possible to assume that 10 mm and 30 mm would have been successful methods also. This demonstrates that excess material removal in critical zone allows reducing the stresses under the threshold value at which wrinkles are created. It also proved that the simulation model is able to accurately represent reality.

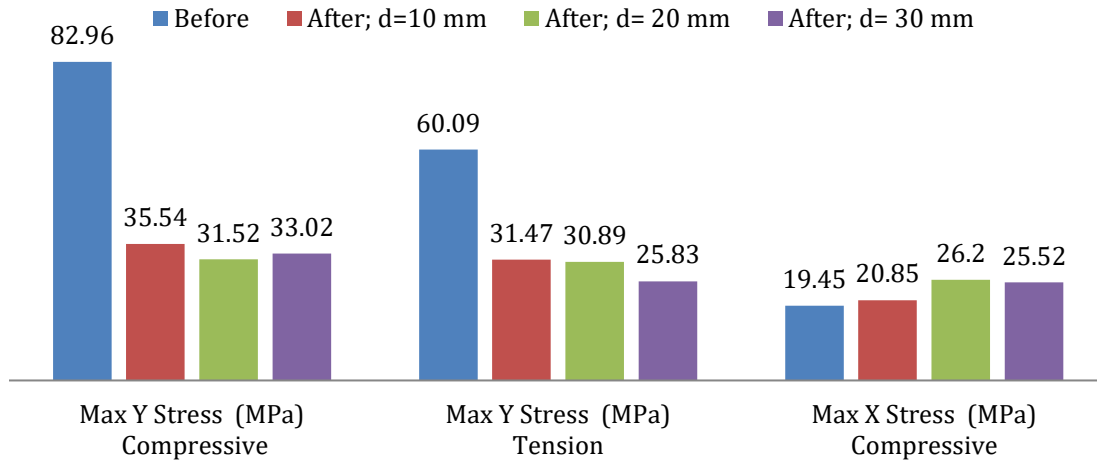
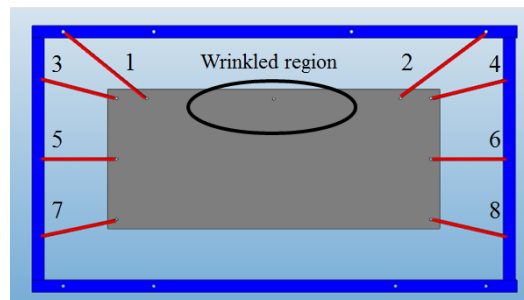


Figure 5.12: Stresses comparison for material removal

5.5.4 Method 2: Additional springs

This method is one of the most common because of the simplicity of adding spring(s) where needed. The locations where to position the additional springs are usually decided by common sense, trial-and-error or experience. In this case, wrinkles are created by high compressive force in the excess material area. By adding springs with the same stiffness constant as the other ones near the wrinkled region with a force opposite to the one creating wrinkles, it is possible to counter that effect. The two springs are added are 1 and 2 as seen in Figure 5.13.



Springs 1 and 2 are added with a constant of 0.45 kg/mm

Figure 5.13: Added springs set-up

Figure 5.14 shows where the max stresses were taken after the addition of springs. Figure 5.15 shows that the addition of springs allowed reducing the stresses to around 25 MPa in y-direction which was previously shown as a successful threshold to avoid wrinkles. The compressive and tensile stresses in y are reduced by 68.06% and 61.91% respectively. The

compressive stresses in the x-direction did not change much but, this was shown to have a low impact on wrinkles creation. A visualization of where the wrinkles came from and trying to oppose the force creating them is a good approach in this case. Even then, it can be challenging to visualize it in a complex case and this is why a simulation approach is useful since it allows trying different positioning according to the specific case without wasting any material.

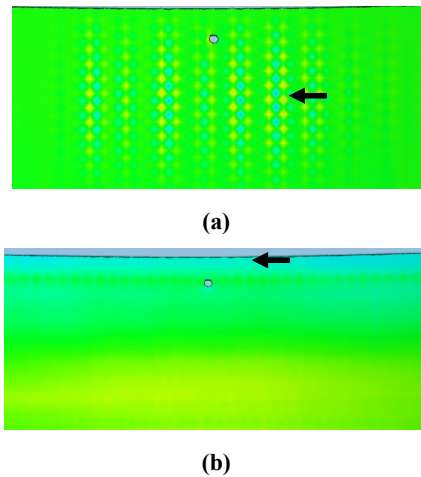


Figure 5.14: (a) y -stresses (b) x-stresses * Arrows show where the maximum stresses were taken

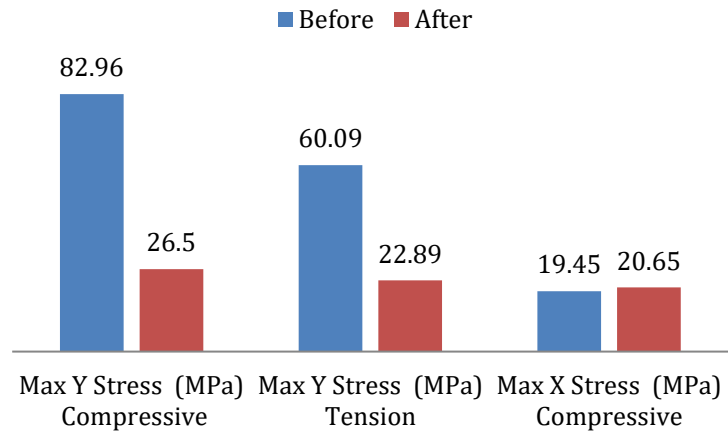


Figure 5.15: Stresses comparison for added springs

5.5.5 Method 3: Springs stiffness

This method provides a solution which allows keeping a similar set-up and simply changing the stiffness of the springs used. Three different cases are investigated. The initial case has all the springs stiffness 0.045 kg/mm. Case 1 increases all the springs stiffness (1 to 6) to 0.1 kg/mm. Case 2 increases the springs stiffness close to the wrinkles region (1 and 2) to 0.1 kg/mm and all the others springs stiffness (3 to 6) to 0.075 kg/mm. Case 3 increases the springs stiffness close to the wrinkles region (1 and 2) to 0.15 kg/mm and all the others springs stiffness (3 to 6) to 0.075 kg/mm.

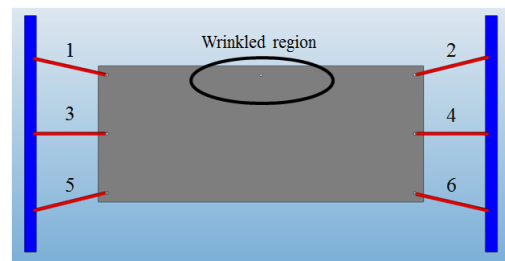


Figure 5.16: Stiffer spring's set-up

Case 1 results show that increasing all the springs stiffness did not help to reduce the stresses considerably. The case 2 results show that using springs stiffness of 0.75 kg/mm for springs 3 to 6 and higher springs stiffness, 0.1 kg/mm, for springs 1 and 2, near the wrinkled region allowed reducing the initial stresses. The last solution, case 3, gave low stresses and equilibrate results which can be identified as the best scenario. Figure 5.18 shows that the case 3 helped reduce the stresses of 38.90% and 27.76% in the y-direction in compression and tension respectively. Figure 5.17 shows where the max stresses were taken after the change of springs tension in case 3.

Those results show that in the case of a wrinkled region caused by compression of the excessive material, using stiffer springs near that specific region help having a more uniform deformation which results in fewer or no wrinkles. It is common practice to use the same stiffness for all springs. However, the results obtained show that when the part is not symmetric a custom distribution of the springs stiffness gives the best results.

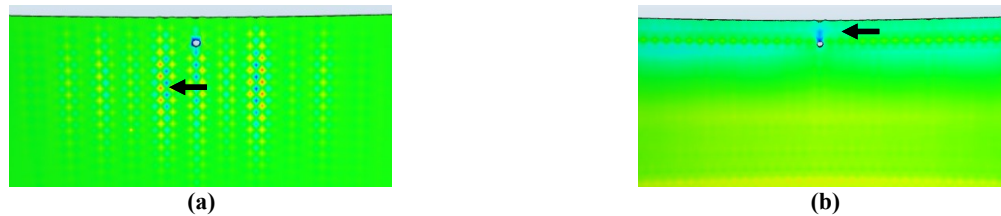


Figure 5.17: (a) y -stresses (b) x-stresses for Case 3 * Arrows show where the maximum stresses were taken

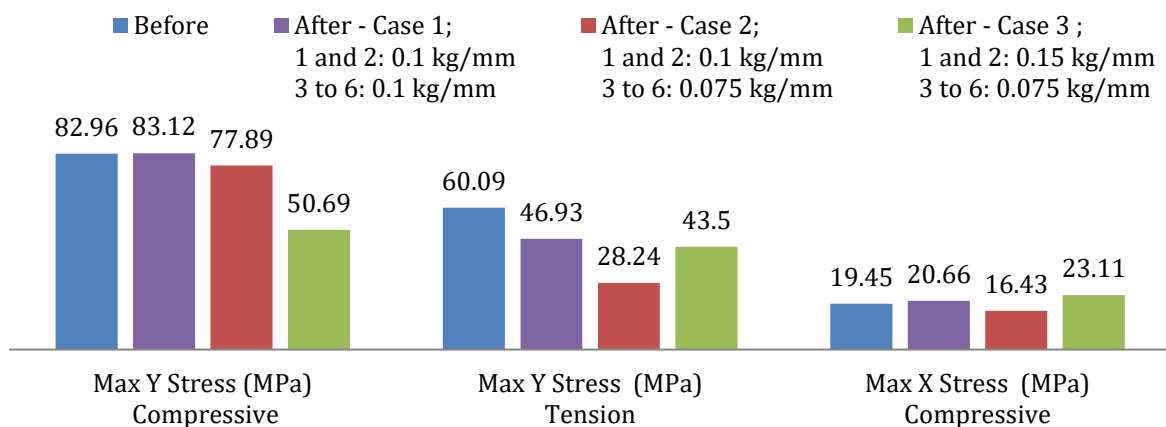


Figure 5.18: Stresses comparison for stiffer springs

5.6 Conclusion

The goal of this study was to propose methods to remove wrinkles in thermostamped structural laminates and to use a finite element approach as an alternative to the traditional trials and errors. More precisely, this study investigated three methods to remove wrinkles occurring in the double curvature region of a thermostamped part. The results presented the use of a Taguchi design of experiments to optimize the initial experimental set-up. Afterward, a first experimental part was made with thermocouples in order to use the material model characterized at the right forming temperature. A second part was formed in order to identify the defect zone. Wrinkles were visible on the top ply of the double curvature area. A sensitivity analysis showed that the right size of mesh was able to represent accurately this critical area using AniForm. Three methods are then identified as solutions to remove wrinkles and were explored using AniForm software. The first method, material removal, was validated with the manufacturing of an experimental part. The simulation was able to show that this method allowed reducing the stresses under the critical value and giving a good part quality without any defects. Two other methods, using additional springs and adjusting springs stiffness, were simulated and were shown as successful methods to reduce stresses. Different options were tested for each method in order to give a better understanding of the impacts made by those change. This paper provides solutions to part manufacturers which need to remove wrinkles and shows the capability of AniForm to optimize the thermostamping set-up before doing any experimental trials. By doing so, a crucial gain in cost and time can be made toward obtaining defect-free parts.

Chapter 6. Cost Analysis: Composite Manufacturing

6.1 Introduction

The aerospace industry is highly competitive, encouraging companies to be as cost-efficient as possible. Caused by new environmental regulations and to lower operation cost, aerospace companies are attracted to lightweight composite materials. The shift from a metallic to a composite part is complex and can increase considerably the cost of the part. In order to make a judicious decision, cost needs to be estimated. This estimation is referred as cost estimation or cost analysis. Cost estimation can have many purposes; to verify if the project fits in the budget, to give a quote to a client, to verify if a quote from a supplier is reasonable, to choose the less expensive approach to use, and more. In any case, it plays a critical role in terms of decision making. A cost analysis can be very complex and broad. This particular chapter focuses on the estimation of manufacturing cost for advanced composite parts. This narrowing of a complete cost analysis requires ignoring revenue from sales, distribution costs, taxes and profit margin which can make the situation much more complex (Figure 6.1). The decision to include General and Administrative (G&A) and overhead in this cost analysis are detailed further. In this study, a methodology is presented to estimate the price per part considering the manufacturing process. The methodology is applied to a case study comparing three different manufacturing methods; RTM, compression molding and thermostamping. Finally, a deeper study on cost repartition is made on the thermostamping manufacturing method.

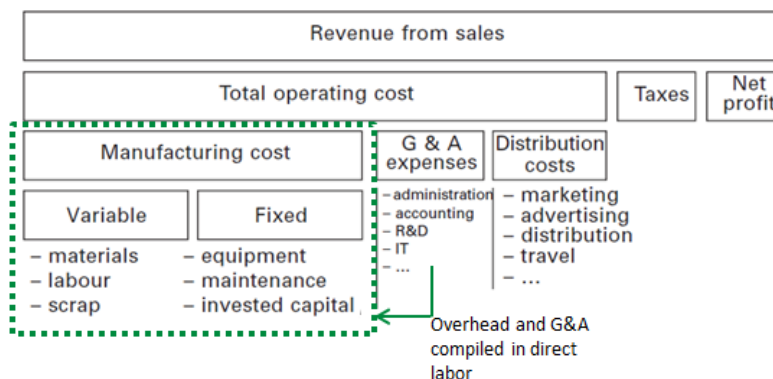


Figure 6.1: Overall project cost (Adapted from [10])

6.2 Methodology

Based on a bottom-up methodology, the cost obtained is in function of: material cost, the actions and their respective time, the labor rate including overhead and G&A and, on equipment and tooling cost. All the information is acquired with the closest approximation and is updated continually as the project advances. The methodology proposed here is separated into 5 steps.

6.2.1 *Set-up context*

In order to start the estimation, the manufacturing context needs to be set. Depending on the location of the company, the number of working day per year, the number of hours of work per year can be very different. Information to define are:

- Number of parts per year
- Duration of the project
- Number of working days per year
- Length of a working day
- Number of shifts per day

This information helps to identify if the capacity of the company is able to reach the expected number of parts per year. It also allows establishing the amortization and the maintenance of the equipment and tooling based on the expected number of parts.

Part information like material, expected fiber volume fraction, expected weight, lay-up sequence, volume, and overall dimensions should be available at this point and need to be defined clearly.

6.2.2 *Build process flow, including required equipment and tooling*

A bottom-up method is based on a detail estimation of each step of the process. The process flow is the way used to build the chronological series of events or actions required during the manufacturing process.

For this step, a minimum of knowledge, expert help or good literature is required. In order to facilitate the separation, the actions are split into three groups: preparation, part consolidation, and finishing. All the steps are written down even if some steps may not require time as labor time. For example, curing of the resin is a long step but it is not required to have an operator present for

all the curing period. This helps to have a consistent process flow and allows validating the total manufacturing cycle time. The advantage of the bottom-up method is the precision; however, the estimation is as precise as the information inputs. All the actions including, set-up times and movement times need to be included and be as close as possible to reality. It is also important to mention the assumptions and if possible to add a standard deviation of the values.

As the process flow is built, a list of equipment and tooling is done in parallel. Equipment is standard and is bought as is from a supplier/manufacturer, for example, a press or an oven. Toolings are custom made for the project and are made in-house or subcontracted to a specialist, for example, a mold or a fixture for trimming.

6.2.3 Develop cost estimate

6.2.3.1 Material

The calculation of the material cost considers the amount required for the part ($C_{material\ part}$) and the excess that is removed or not used. The bought material which was not used is referred as scrap ($\%_{scrap}$) and it will be estimated as a percentage of the part material. Because of environmental regulation, scrap materials need to be disposed the appropriate way, this involves disposal costs which are counted as percentage of scrap cost ($\%_{disposal}$). The most common way is to deal with a company or send it to a specialized landfill. The total cost of material is referred as C_m and is in \$.

$$C_m = C_{material\ part} + (\%_{scrap} * C_{material\ part}) + (\%_{disposal} * (\%_{scrap} * C_{material\ part})) \quad (6.1)$$

6.2.3.2 Actions and Labor rates

In order to manufacture a part, many steps are needed. A step is separate into three; the time required to move the part to the station (t_{moving}), the time required to set-up (t_{set-up}) and the time to complete the action (t_{step}). Also, the number of operators ($n_{operators}$) for each step needs to be considered as some step may require more than one. This is summarized by equation 2 where t is the time in hours and j is the number of the steps. The sum of each step time gives the total labor time (t_{labor}) required to manufacture the part.

$$t_T = \sum ((t_{step(j)} + t_{set-up(j)} + t_{moving(j)}) * n_{operators(j)}) \quad (6.2)$$

To obtain cost, the total time (t_T) needs to be multiplied by total labor rate (R_T). The labor rate (R_{labor}) needs to be defined and the overhead ($\%_{overhead}$) and G&A ($\%_{G\&A}$) are included as a percentage of the labor rate. The labor rate is in \$/hours. Equation 6.2 summarizes the man hours needed in total and equation 6.3 the labor rate corresponding to these man hours. The G&A includes managing team, legal service, accounting, public relation and similar expenses, and the rest of the general expenses. The overhead is the rest of the indirect cost which includes building and building maintenance, electricity, cleaning, insurance, payroll taxes and etc. Based on a publication made by RAND on the effect of lean manufacturing in an aerospace context [65] the overhead costs are between 150 and 250 % of the direct labor cost per hour, and the G&A cost is between 10 and 25 % of the direct labor cost per hour. Another study made by N. Bernet et al. [66] arrives at a total overhead between 75 and 115 % of the labor cost per hour based on the compilation of diverse sources. In this case, the overhead and G&A are considered but depending on the situation, it is possible to ignore them depending on the situation.

$$R_T = R_{labor} + (\%_{G\&A} * R_{labor}) + (\%_{overhead} * R_{labor}) \quad (6.3)$$

The total cost for man-hours is referred as C_{labor} and is presented in equation 4.

$$C_{labor} = t_T * R_T \quad (6.4)$$

6.2.3.3 Equipment and tooling

The difference between tooling and equipment is that tooling is made specifically for the project and equipment could be used in the further project. For example, a mold has a specific shape for a specific part and cannot be used for other parts. Oppositely, a press can be used with different molds for different projects. The equipment can be separated in two families, the dedicated (C_{E-d}) and non-dedicated (C_{E-nd}). The dedicated are equipment that will be used only for this particular project and the non-dedicated is equipment available in the plant that is shared between projects since it does not require a full-time usage.

For the tooling, it is necessary to calculate the price at the beginning of the project ($C_{E(I)}$), the price at the end ($C_{E(F)}$), the maintenance cost (M), installation cost (I) and the number of part

made with this piece of equipment (n_{parts}). The non-dedicated equipment usage is defined as time of usage (t_{n-d}) and rate per hours (R_{n-d}). Together, the non-dedicated and dedicated are the total equipment cost (C_E). The total tooling cost ($C_{T\ total}$) is obtained by the summation of all individual tool cost (C_T) including maintenance (M) over the number of part (n_{parts}) made with that tooling.

With this information, it is possible to reduce all this information by a price by part.

$$C_{E-d} = \sum \left(\frac{C_{E(I)} - C_{E(F)} + M + I}{n_{parts}} \right)_i \quad (6.5)$$

$$C_{E-nd} = \sum (R_{n-d} * t_{n-d})_i \quad (6.6)$$

$$C_E = C_{E-d} + C_{E-nd} \quad (6.7)$$

$$C_{T\ total} = \sum \left(\frac{C_T + M}{n_{parts}} \right)_i \quad (6.8)$$

After the entire prices are combined and a price per part is obtained which allows obtaining an easy comparison method.

$$Total\ price\ per\ part = C_m + C_{labor} + C_E + C_{T\ total} \quad (6.9)$$

6.2.3.4 Other factors & Data gathering and Assumptions

This step has the goal to estimate a time for the activities and price of the material and equipment. This is without a doubt the most challenging part due to many reasons. Mostly, it is hard to have a single and definite value of time and price. For example, different operators have different speed of working, the quote can vary a lot from different suppliers, the value of the currency of raw material varies in time, and this list could go on. Since prices can vary a lot from suppliers, it is important to get few quotations and to identify why price difference occurs. Negotiations are also important factors that could affect the price, long-term deal or volume rebate can be obtained. This is why no exact answer is valid; the importance is to have a close enough estimate and also to be able to update the information easily as the project advances. This requires a certain amount of time because a lot of correspondences are needed with experts, suppliers, and sub-contractors. Based on all those uncertainties, two conclusions can be derived. First, the methodology needs to be modular and easily modifiable. This is referred as the Cost Estimation

Lifecycle. Secondly, an additional study can be done to measure the range of possible cost instead of a single value.

6.2.3.5 Integrated non-cost factors

An important consideration when taking a decision is also a non-cost factor. For example, costs related to minimizing pollution are hard to evaluate in terms of return on cost. In composite structure, those factors can be the final weight, the mechanical strength, and etc. The importance of that factor can be estimated, weighted proportionally to their importance and included in the final decision.

Parameters for complete cost analysis		
Definition	Symbol	Units
Cost material	C_m	\$
Cost material used for the part	$C_{material\ part}$	\$
Scrap material	$\%_{scrap}$	-
Disposal	$\%_{disposal}$	-
Total labor time	t_T	hours
Action time	$t_{step(j)}$	hours
Set-up time	$t_{set-up(j)}$	hours
Moving time	$t_{moving(j)}$	hours
Number of operators	$n_{operators}$	-
Total labor rate	R_T	\$/hours
Labor rate	R_{labor}	\$/hours
Total cost labor	C_{labor}	\$
G&A as percentage of labor	$\%_{G\&A}$	-
Overhead as percentage of labor	$\%_{overhead}$	-
Total cost dedicated tooling	C_{E-d}	\$
Initial value dedicated tooling	$C_{E-d(I)}$	\$
Final value dedicated tooling	$C_{E-d(F)}$	\$
Maintenance	M	\$
Installation	I	\$
Number of part for the amortization	n_{parts}	-
Total cost non-dedicated tooling	C_{E-nd}	\$
Rate non-dedicated tooling	R_{n-d}	\$/hours
Time of usage of non-dedicated tooling	t_{n-d}	hours
Total cost equipment	C_E	\$
Cost tooling	C_T	\$
Total cost tooling	$C_{T\ total}$	\$

Table 6.1: Symbols for cost analysis

6.3 Case study: Comparison of three manufacturing methods for an aerospace part.

The goal of this case study is to compare three different manufacturing methods and to find which is the most cost-effective for a particular part. This case study uses the previously introduced methodology to help to make the best decision in terms of cost. The methods selected are some of the most popular manufacturing methods in the aerospace industry. Also, it is possible to consider three types of reinforced composites; thermoset long fibers, thermoplastic long fibers, and thermoplastic short fibers. The selected manufacturing methods respectively are resin transfer, thermostamping and compression molding. Those three methods give a good overview comparison of some popular manufacturing methods. The data, values, and results obtained here are not absolute answers and are used as a guideline.

Those methods are widely different; they all have their own advantages and disadvantages. The selection can be made on a different aspect as the shape of the part, the rate of production and the cost. Figure 6.2 shows the more appropriate method based on annual volume and nature of the matrix.

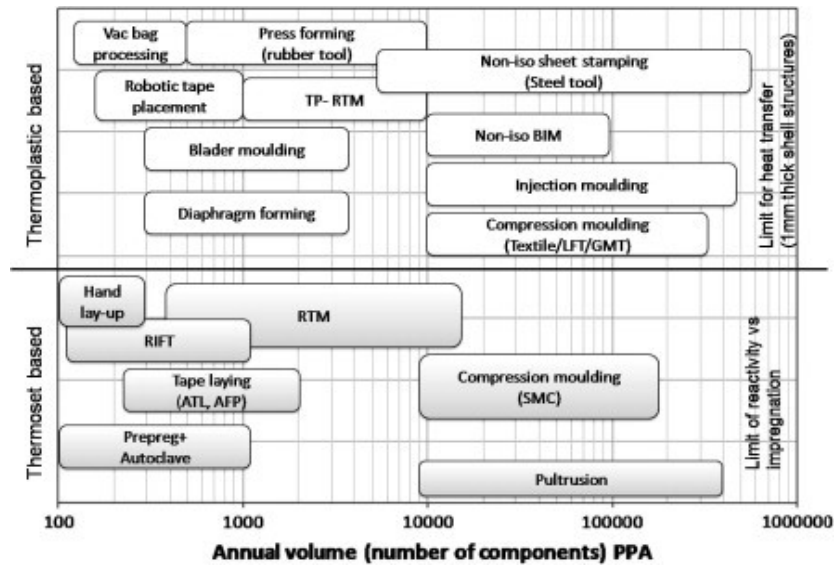


Figure 6.2: Manufacturing method versus volume [10]

The part used for this study will be the same as the one presented in a previous chapter. It is a complex shape with a double curvature and has a constant thickness. This shape is selected as a

generative composite part (Figure 6.3). More information on the shape was presented in Chapter 5. The shape size overall is approximately 260.0 mm x 233.3 mm x 35.7 mm. In the case of RTM and Thermoforming, the lay-up is $[(0, 90), (\pm 45), (0, 90)]_s$. In the case of DLF, this is equivalent to a thickness of 1.8 mm. The calculations are based on 5000 parts a year for the duration of 7 years. For a total of 35 000 parts will be manufactured. Based on 260 working days per year, it is approximately 20 parts per day. The hours worked per day are 7.5 hours.

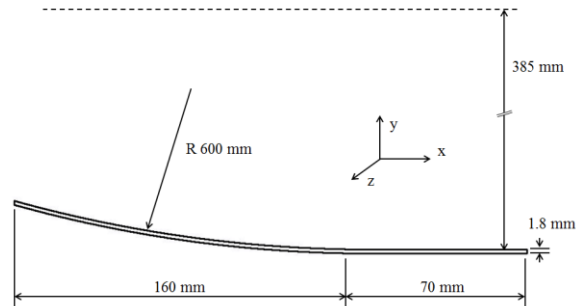


Figure 6.3: Cross section overall shape

Before starting this case study, it is important to understand that the values used are variables and that they are not absolute values. They are obtained by the best of the available information and knowledge. The goal of the case study is to put the methodology in a practical context. The second part of this case study considers the uncertainty and addresses the impact and probabilities of those uncertainties.

Step 1: Process flow and Equipment/Tooling list

Based on the literature, personal knowledge and experts, the process flow of each manufacturing method is regrouped in Figure 6.4. The list of tooling and equipment is added at the end. The inspection is not considered because it is based on comparative results.

Manufacturing methods			
	<u>Thermostamping</u>	<u>Compression Molding</u>	<u>Resin Transfer Molding</u>
Preparation	-Trimming of the blank -Mold heating	-Weighting of the strands -Mold preparation -Dropping the strands	-Mold preparation -Preform cutting -Layering -Preforming -Mold heating -Closing mold -Plugging system
Part Consolidation	-Heating of the blank -Forming and holding -Cooling	-Heating -Pressure application -Cooling -Demolding -Cleaning	-Injection -Curing -Opening Mold -Demolding -Cleaning
Finishing	-Trimming -Deburring	-Deburring	-Trimming -Deburring
Tooling Equipment	-Press -Mold -Trimming machine -Trimming fixture	-Press -Mold (with heating system) -Trimming machine -Trimming fixture	-Injector(s) -Mold -Trimming machine -Trimming fixture

Figure 6.4: Process flows for the 4 manufacturing methods

Step 2: Data and assumptions

A spreadsheet is done with all the activities and all the inputs are obtained from supplier and experts.

Material

a. Thermostamping

The thermostamping material comes in pre-impregnated sheets. This study will use a PPS/Carbon with a 5HS woven fabric at around 57% fiber weight fraction. During thermostamping process, there are two trimming steps where scraps are produced. The first one is the initial trimming from a large sheet and the second is the finishing trimming. The first trimming can create

a lot of scraps because sheets come in standard sizes so depending on the shape dimension and the number of parts per sheet the scrap can be quite high. The size needed for a part is approximately 550mm x 230mm. Figure 6.5 shows standard sheet size from two different suppliers and the amount of scrap obtained in each case. The rest of the scrap is obtained by the second trimming which in this case is only the area outside the curved section (used for gripping). Based on the 3D model it is around 13.5% per part. The total scrap per part is between 13.7 and 17.6%.

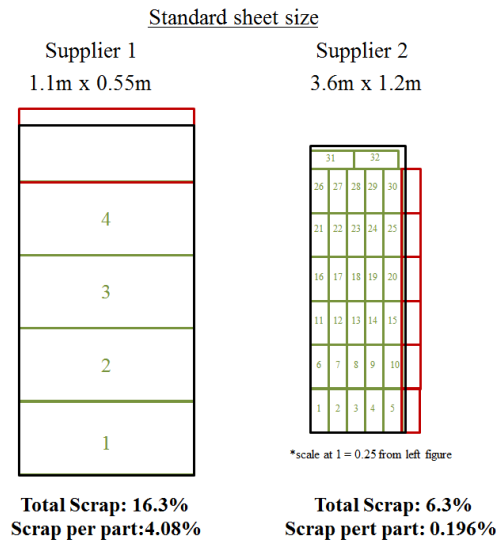


Figure 6.5: Scrap percentage based on initial sheet geometry

The price for the 1.2m x 3.6 m sheet is approximately 2400 \$ for a PPS/Carbon. This gives a total price of 75.00 \$ including the scrap. In this case, the scrap material is around 4.73 \$ per part from the first trimming and 9.49 \$ from the second trimming.

$$C_s = 4.73 + 9.49 = 14.22 \$$$

$$C_{material\ part} = \frac{2400}{32} - 14.22 = 60.78 \$$$

$$C_m = 60.78 + 14.22 = 75.00 \$$$

b. RTM

For RTM, the material is obtained in two forms, the woven fiber, and the resin. Similarly, as the previous situation, the carbon fiber weave comes in a roll with a defined width. The width obtained from two suppliers is 1.25 m. With an RTM process, it is possible to obtain a net shape after the injection removing the second trimming process. The only scrap fiber will be produced

by the first trimming. In this case, the loss of unused material at the edge is approximately 1.6% per ply, giving a total of 9.6% per part. A small amount can also be obtained at the end of the roll but it is negligible on the number of parts obtained in a roll. The resin scrapped is in the equipment (hose, injector) and during the bleeding. The amount of resin lost per part is estimated at 5%.

The price for a carbon fiber 5 hardness satin obtained from two suppliers is between 53.20 CAD\$/m² and 61.845 CAD\$/m². The resin system is an epoxy at 166 CAD \$/kg. The volume of the part is 1.098E-4 m³ and the fiber weight fraction is at 57%. Based on resin density of 1220 kg/m³ (density of cured resin), 0.0576 kg of resin is used which gives 9.56 \$. The fiber required an area of 0.062 m² six times. The fiber price is between 19.79 \$ and 23.01 \$.

$$C_{material\ part-supplier\ 1} = 9.56 + 19.79 = 29.35 \$$$

$$C_{material\ part-supplier\ 2} = 9.56 + 23.01 = 32.57 \$$$

$$C_{s-supplier\ 1} = 9.56 * 0.05 + 19.79 * 0.096 = 2.38\$$$

$$C_{s-supplier\ 2} = 9.56 * 0.05 + 23.01 * 0.096 = 2.69\$$$

$$C_{m-supplier\ 1} = 29.35 + 2.38 = 31.73\$$$

$$C_{m-supplier\ 2} = 32.57 + 2.69 = 35.26 \$$$

c. DLF

The use of strands form helps using the right amount of material each time, so it is possible to achieve a net shape with this process. This allows estimating the scrap at 0%. The price for Carbon/PEEK unidirectional fiber is around 294.76 \$/kg. The volume of the part is 1.098E-4 m³ and density of the Carbon/PEEK with 34% resin content is 1620 kg/m³. This gives a total price of 52.43 \$.

$$C_m = 52.43 \$$$

Action time and Labor rates

a. Labor rate

In Canada, the means salary for a technician in composites is approximately 20 CAD\$/hours according to [67]. The overhead and G&A percentages selected are the mid value from the RAND publication [65].

$$R_T = 20 + (17.5\% * 20) + (200\% * 20) = 63.5 \text{ \$/hours}$$

b. Action time

To keep it concise, the times are summarized in three groups; preparation, consolidation, and finishing. The estimated time where obtained from discussions with experts. The non-intensive labor times are considering in order verifying if the goal of 20 parts per day is achievable. The RTM is a long process so it is considered that the mold could do five parts at the time considering the small dimensions of the part.

	RTM	Thermostamping	DLF
Time preparation (min)	62	8	12.5
Time consolidation (min)	0	6.5	5
Time finishing (min)	8.5	8	8
Total labor-intensive time (min)/(hours)	70.5/1.17	22.5/0.375	25.5/0.425
Labor cost (\$)	74.55	23.63	26.65
Total labor non-intensive time (min)/(hours)	221/3.68	22.5/0.375	115.4/1.92

Table 6.2: Summary of labor cost

Equipment and Tooling

a. RTM

The challenge with RTM is the rate of production, as mentioned previously the labor times are considered based on an injection of five parts at the same time. However, the total time needed is 3.68 hours meaning that on a 7.5-hours working day; only 10 parts can be made. A second shift could increase it to 20, which makes it possible. The use of a second shift could increase the overhead. The other possibility is to double the equipment which will require a bigger initial investment and would reduce the amortization of both equipment since they will be used for 17500 parts each.

<u>Dedicated equipment</u>	Initial Price (\$)	Final Price (\$)	Maintenance (\$)	Number of part (-)
Injectors	20 000	4 000	1 500	35 000
<u>Tooling</u>				
Mold	75 000	-	10 000	35 000
Trimming fixture	5 000	-	500	35 000
<u>Non -Dedicated equipment</u>	Price per hours (\$/hours)		Hours required per part	
Oven	0.5		2	
CNC	50		0.10	
2D fabric cutting machine	0.5		2	

Table 6.3: RTM equipment and tooling cost

The total price for equipment per part is

$$\begin{aligned}
 C_E &= C_{E-d} + C_{E-nd} + C_{T \text{ total}} \\
 &= 1.11 + (1 + 5 + 1) + (2.43 + 0.16) \\
 &= 10.70\$
 \end{aligned}$$

b. Thermostamping

Thermostamping is known to be effective for fast cycle time. There is no steps that required no labor-intensive work. Meaning it is possible to achieve 20 parts a day with one tool. Usually, for thermostamping, a specialized tool can be used with an integrated heating system and automatic transfer which reduce the total manufacturing time.

<u>Dedicated equipment</u>	Initial Price (\$)	Final Price (\$)	Maintenance (\$)	Number of part (-)
Press with heating system	290 000	80 000	2000	35 000
<u>Tooling</u>				
Mold assembly (die shoe, pins)	30 000	-	3000	35 000
Trimming fixture	5 000	-	500	35 000
<u>Non -Dedicated equipment</u>	Price per hours (\$/hours)		Hours required per part	
Water jet	30		0.10	
CNC	50		0.10	

Table 6.4: Thermostamping equipment and tooling cost

$$\begin{aligned}
C_E &= C_{E-d} + C_{E-nd} + C_{T \text{ total}} \\
&= 10.63 + (3.0 + 5.0) + (0.94 + 0.16) \\
&= 19.73\$
\end{aligned}$$

c. DLF compression molding

A similar issue as the RTM process is faced with the compression molding of short fiber, the total time needed for one part is 1.92 hours because the mold needs to be cooled down and reheated for each part. In this case, a similar approach can be used, 2 molds or a mold with 2 cavities should be used. In this study a second mold is preferred. This required a bigger press and a larger heating system.

<u>Dedicated equipment</u>	Initial Price (\$)	Final Price (\$)	Maintenance (\$)	Number of part (-)
Press	100 000	40 000	2 000	35 000
Heating device	15 000	3000	1 000	35 000
<u>Tooling</u>				
Mold 1	20 000	-	3000	17 500
Mold 2	20 000	-	3000	17 500
Trimming fixture	5 000	-	500	35 000
<u>Non -Dedicated equipment</u>	Price per hours (\$/hours)		Hours required per part	
CNC	50		0.10	

Table 6.5: DLF equipment and tooling cost

$$\begin{aligned}
C_E &= C_{E-d} + C_{E-nd} + C_{T \text{ total}} \\
&= (4.06 + 0.54) + (5) + (1.31 + 1.31 + 0.16) \\
&= 12.38\$
\end{aligned}$$

Comparison

All three methods are compared and summarized in Table 6.6, in order from the most expensive to the least; RTM, DLF, and Thermostamping.

	RTM	Thermostamping	DLF
Cost material used for the part (C_m)	29.35	60.78	52.43
Cost scrap material (C_{scrap})	2.38	14.22	0
Labor cost (including G&A and Overhead) – (C_{labor})	74.55	23.63	26.65
Total cost equipment (C_E)	8.11	18.63	9.6
Total cost tooling ($C_{T\ total}$)	2.6	1.1	2.78
Total price per part	116.99	118.36	91.46

Table 6.6: Summary of cost for all methods

Figure 6.6 helps to put the comparison of costs in perspective. RTM is similar to thermostamping even if it has the lowest material cost, the amount of labor required cause the process to be as expensive. Thermostamping also has a high cost mainly because of the very high material cost and the high scrap ratio. The pre-impregnated sheets require a high amount of work to produce which causes the high cost. DLF has also a high material cost, which can be expected because it required many steps to obtain the short impregnated chopped tape and because the price of PEEK is quite high. However, the low labor and the minimal scrap keeps the process cheaper. For the labor and equipment, DLF and thermostamping are similar. Overall, RTM and thermostamping has similar price and DLF is the least expensive. One interesting aspect for thermostamping is its fast manufacturing time which allows to do a part five times quicker than DLF and 9 times quicker than RTM. The results presented and the conclusions obtained, are only valuable in this particular case study. The change of any inputs parameters will results in different conclusions.

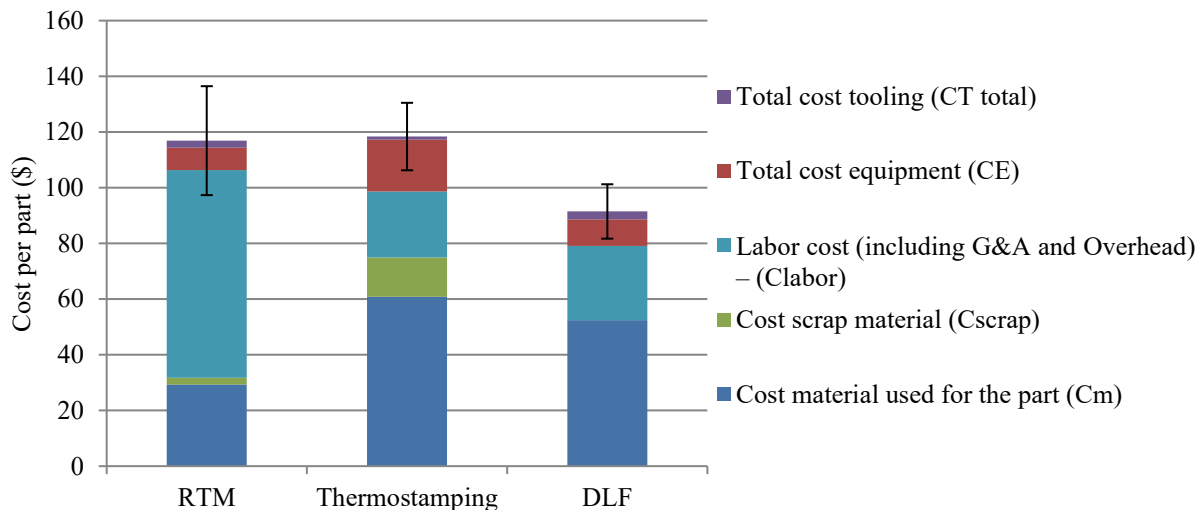


Figure 6.6: Chart of cost summary

In conclusion, in the situation of a relatively small part with a constant thickness and with the parameters set (number of parts per year, etc.), it was found that DLF is the most cost-effective manufacturing method. RTM and thermostamping were identified as costliest methods. RTM because of the high labor required but if the process is able to be automatized, it could be a very interesting option because the material cost is the lowest. For thermostamping, the high cost was mainly caused by the high material cost. Table 6.7 shows the mechanical properties and the density obtained in each situation. RTM and thermostamping materials have similar values but DLF material has much lower mechanical properties even if a more performant thermoplastic is used.

	RTM	Thermostamping	DLF
Material	CYCOM 890 RTM/T650 5HS woven carbon fabric	PPS/T300 5HS woven carbon fabric	PEEK/AS4-12K Carbon
Resin Content (%)	43	43	34
Density (g/cm³)	1.53	1.55	1.62
Tensile Strength (MPa)	834.0*	755.5*	288.9
Tensile Modulus (GPa)	69.3*	54.8*	43.4
Compressive strength (MPa)	99.1*	640*	312.3
Compressive modulus (GPa)	17.75*	51.7*	48.3

Table 6.7: Manufacturing methods and obtained properties / *average between 0 and 90

6.3.1 Thermostamping detailed analysis

The specific cost for the thermostamping situation is analyzed separately. Figure 6.7 represents the repartition of the cost for each part. The material cost, including scrap, takes up most of the total cost. However, few impacts can be made in order to reduce manufacturing cost. Rebates for large volume orders are available and should be negotiated with the material supplier. Thermoplastic is a recyclable material so a recycle avenue should be investigated. Also, as mentioned earlier, using a gripping system that uses less material for gripping could have a significant impact. The second most impactful cost is the labor cost. Manufacturing cells using robots are gaining a lot of place in the industry. This avenue is gaining a lot of interest because it is precise and has a very good repeatability but also because it decreases the cost related to labor.

Thermostamping detailed cost

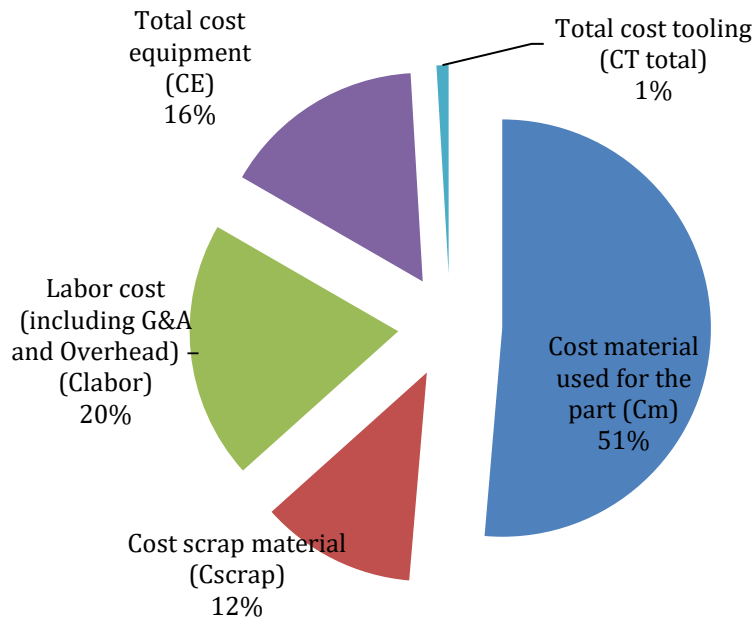


Figure 6.7: Thermostamping cost repartition

The results are based on the closest estimations possible of the real values but the input values used can have an important variation. To better understand the impact of risk and uncertainty of this cost analysis, a Monte Carlo simulation is done on the thermostamping process. A Monte Carlo simulation is a simple way to evaluate the possible outcome of a simulation using random sampling to build a range of answers considering their probability. The first step is to define the domain for the input variables and their distributions. In this case, it is assumed that the estimation follows a normal distribution. The second step is to create random data based on the initial values, the standard deviations and the types of distribution. The third step is to run the simulation by using the random data values into the transfer equation. The transfer equation is the sum of the cost.

$$Total\ cost = (C_m + C_s) + (t_{labor} * R_T) + \left(\sum \left(\frac{C_T + M}{n_{parts}} \right)_i \right) + C_{E-d} + \sum \left(\frac{C_{E(I)} - C_{E(F)} + M + I}{n_{parts}} \right)_i$$

The parameters used and their range is presented in Table 6.8.

	Best estimation	% Range
Cost material used for the part (C_m)	60.78	10
Cost scrap material (C_{scrap})	14.22	10
Total time labor (t_{labor})	0.375	30
Labor rate (R_T)	63	10
Total cost equipment dedicated (C_{E-d})	372 000	20
Total cost equipment non-dedicated (C_{E-nd})	8	20
Total cost tooling ($C_T total$)	38500	10
Number of parts	35 000	15

Table 6.8: Inputs for Monte Carlo simulation

A Monte Carlo simulation is done with 100,000 samples using the data from Table 6.8: Inputs for Monte Carlo simulation

. The results show that the mean is located at 118.63 CAD\$.

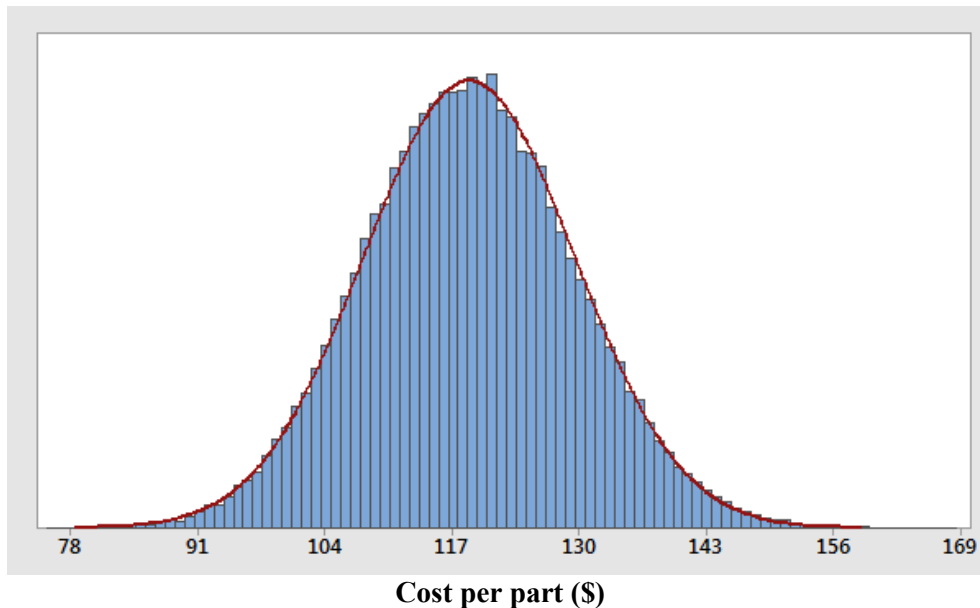


Figure 6.8: Total cost distribution based on Monte Carlo Simulation

The extreme values are between 76.43 CAD\$ and 168.14 CAD\$. The standard deviation is 10.84 \$CAD meaning that there 95.45% of the chance that the price is located between 111.25 CAD\$ and 125.86 CAD\$.

6.4 Conclusion

This chapter presents a cost estimation method adapted from the bottom-up estimation method. In order to estimate the cost for a composite part, impactful costs and steps are considered and regrouped in order to obtain a single cost per part. This is very useful to negotiate a quote, to plan the feasibility of a change of manufacturing method, selecting the cheapest manufacturing method and more. A case study was made to compare the price of using RTM, thermostamping or compression molding as manufacturing methods for a composite part. The results showed that for the particular case of high volume rate and constant thickness, RTM and thermostamping had similar price for similar mechanical properties and that DLF had lower price but lower mechanical properties. The results obtained are in function of the selected part and the expected conditions (volume per year, labor rate, etc.). The change of any of those parameters will produced a different output. Thermostamping was decorticated and analyzed more profoundly. As mentioned earlier, the two goals of this custom method were to be easily modifiable and to consider uncertainties. The first criterion is answered by putting the data and formulae on a spreadsheet making the calculation automatics. The second criterion is investigated through a Monte Carlo simulation. Based on the distribution of the inputs parameters, the simulation gives the final expected range of price.

Chapter 7. Conclusion, Contributions & Future work

7.1 Conclusion

This thesis provides an introduction and a literature review in the first and second chapter respectively. The third chapter identified the chemical and mechanical behavior of a PPS/Carbon pre-impregnated thermoplastic under a wide range of temperature. The correlation between the melting temperature and the initial crystallinity showed that higher crystallinity gave a higher peak melting temperature. The relation between the cooling rate and the final crystallinity were shown using cooling rates achievable with the DSC. Faster cooling rate tends to shift the crystallization range to lower temperature. The results allowed having a better understanding of the crystallization behavior during a thermostamping process. An MDSC was used in order to have the heat capacity in function of temperature. It was shown that the use of a single value may not be the most precise way since a linear correlation is seen between heat capacity and temperature. The second characterization of the material was made on the CTE. The in-plane and out-of-plane CTE were obtained. Under the melting point, it was shown that in-plane values are linear and out-of-plane values can be separate under and over the T_g. The CTE out-of-plane was investigated over the melting temperature range showing the four stages of CTE during cooling; over crystallization, crystallization shrinkage, over the T_g and under the T_g. The last characterization using DMA brought two conclusions. It was shown that for a heating ramp the modulus is mostly kept until the melting point but for the cooling ramp the modulus starts increase around the crystallization zone. This shows that the material has no rigidity until the start of the crystallization. The second conclusion is that under the melting point, the material has an elastic behavior and over the melting a more viscous-elastic behavior but still mostly elastic.

The fourth chapter detailed the procedure to use of a 3D finite element model using a sequential thermal and mechanical approach with temperature dependent properties to predict shape distortion of a thermoplastic composite. First, a thermal model was built and validated with experimental data. For the mechanical step, a sensitivity analysis was made on the modulus, the coefficient of friction between the mold and the CTE showed that only the CTE was impactful on the results obtained. This was explained that a few residual stresses are create in the mold and that most of the warpage happen after the crystallization which is usually close to the demolding. Finally, the mechanical model was compared to numerical models (O'Neill and Radford) and experimental data from literature showing accurate results.

The fifth chapter is the wrinkles prediction study, where three methods to remove wrinkles were investigated using finite element commercial software called Aniform. The three methods selected for this study were removing material, varying springs tension and adding springs. The first one was validated through experimental trial. For each proposition, different configurations were tested to have a wider understanding of their impacts. All three methods with the right set-up were found to be successful to eliminate wrinkle for a double curvature part. This study shows that simulation is a powerful tool to optimize a thermostamping set-up before investing in expensive tooling.

The sixth chapter proposed a method to estimate the cost of manufacturing composites part. The method is then applied to a case study comparing thermostamping to RTM and compression molding. In the specific case of high production rate and a small part, it was found that RTM and thermostamping had similar price per part and that DLF had a lower price per part. Propositions to reduce the cost of the thermostamping process are also done.

7.2 Contributions

1. An approach using a 3D finite element model and a thorough material characterization was used to predict spring-in behavior of thermoplastic composites manufactured with thermostamping.

2. A methodology was proposed using a simulation to investigate different set-up solutions to minimize or eliminate wrinkles. The focus was made on wrinkles removal and offered different solutions applicable to a wide variety of cases using a simulation based approach.

3. A cost estimating method for manufacturing of complex aerospace parts was proposed allowing obtaining a single price per part and to include the uncertainty of the price range.

7.3 Future work

It was shown that properties like bending modulus and CTE are closely related to crystallinity. In this study, the values used are temperature dependent and are characterized at precise rates. The use of a slow cooling and annealing both help obtaining a final maximal

crystallinity. However, the rate is different which causes the change of properties to happen at different temperatures. Two avenues could be explored; to characterize the material at similar rate than under the manufacturing thermostamping cycle or to use crystallinity dependent properties. The challenge is to characterize the material under extreme heating and cooling rate while characterizing properties that required a lot of precision. It was shown in a few studies that the process parameters affect the final shape distortion, which is not investigated in this study.

1. An evaluation of the impact of the process parameters on experimental spring-in and a same evaluation with the model could help evaluate more accurately the strength of the model of this study.

2. The integration of crystallinity dependent properties instead of temperature dependent properties would better represent the extreme cooling rate of thermostamping.

The wrinkles prediction in this case was found effective compared to the experimental part. The part selected was relatively simple. It was the simpler case of geometry known to create wrinkles. Also, the effects of processing parameters (mold temperature, speed of closing, pressure) were not investigated and their impact on the agreement with FE results would be interesting.

3. Study the effect of processing parameters and more complex part geometries on the ability of results prediction.

The cost analysis model is based on a simple model using a bottom-up approach. The analysis is made at a practical level and does not include the economical context.

4. In order to bring the estimation to a more complex level, the model could include the inflation rate, the interest rate, taxes and government grant.

Chapter 8. References

1. Gardiner, G., *Thermoplastic composites: Primary structure?* Composite World, 2011.
2. Campbell, F.C., *Manufacturing Processes for Advanced Composites*. 2003: Elsevier Science.
3. Nohara, L.B., et al., *Study of crystallization behavior of poly(phenylene sulfide)*. Polímeros, 2006. **16**: p. 104-110.
4. Spruiell, J.E.J., C.J., *A review of the measurement and development of crystallinity and its relation to properties in neat poly (phenylene sulfide) and its fiber reinforced composites*. 2005, Oak Ridge National Laboratory for U.S. Department of Energy.
5. Lee, T., F. Boey, and K. Khor, *On the determination of polymer crystallinity for a thermoplastic PPS composite by thermal analysis*. Composites Science and Technology, 1995. **53**(3): p. 259-274.
6. Mallick, P.K., *Fiber-Reinforced Composites: Materials, Manufacturing, and Design, Third Edition*. 2007: CRC Press.
7. Jog, J.P. and V.M. Nadkarni, *Crystallization kinetics of polyphenylene sulfide*. Journal of Applied Polymer Science, 1985. **30**(3): p. 997-1009.
8. Hoa, S.V., *Principles of the Manufacturing of Composite Materials*. 2009: DEStech Publications, Incorporated.
9. Cogswell, F. and D. Leach, *Processing science of continuous fibre reinforced thermoplastic composites*. SAMPE J., 1988. **24**(3): p. 11-14.
10. Long, A.C., *Forming textile composites*. Design and Manufacture of Textile Composites, 2006: p. 149.
11. Hou, M., K. Friedrich, and R. Scherer, *Optimization of stamp forming of thermoplastic composite bends*. Composite Structures, 1994. **27**(1-2): p. 157-167.
12. Nowacki, J. and M. Neitzel, *Thermoforming of reinforced thermoplastic stiffened structure*. Polymer Composites, 2000. **21**(4): p. 531-538.
13. Sherwood, J.A., et al., *6 - Fabric thermostamping in polymer matrix composites A2 - Advani, Suresh G*, in *Manufacturing Techniques for Polymer Matrix Composites (PMCs)*, K.-T. Hsiao, Editor. 2012, Woodhead Publishing. p. 139-181.
14. Friedrich, K. and M. Hou, *On stamp forming of curved and flexible geometry components from continuous glass fiber/polypropylene composites*. Composites Part A: Applied Science and Manufacturing, 1998. **29**(3): p. 217-226.
15. Hou, M., *Stamp forming of fabric-reinforced thermoplastic composites*. Polymer Composites, 1996. **17**(4): p. 596-603.
16. Hou, M., *Stamp forming of continuous glass fibre reinforced polypropylene*. Composites Part A: Applied Science and Manufacturing, 1997. **28**(8): p. 695-702.
17. Baran, I., et al., *A Review on the Mechanical Modeling of Composite Manufacturing Processes*. Archives of Computational Methods in Engineering, 2016: p. 1-31.
18. Unger, W.J. and J.S. Hansen, *The effect of cooling rate and annealing on residual stress development in graphite fibre reinforced PEEK laminates*. Journal of composite materials, 1993. **27**(2): p. 108-137.
19. Landry, B., *Compression moulding of complex parts with randomly-oriented strand thermoplastic composites (Doctoral disseration)*, in *Mechanical Engineering*. 2015, McGill: Montreal.

20. Barnes, J.A. and G.E. Byerly, *The formation of residual stresses in laminated thermoplastic composites*. Composites Science and Technology, 1994. **51**(4): p. 479-494.
21. Parlevliet, P.P., H.E.N. Bersee, and A. Beukers, *Residual stresses in thermoplastic composites—A study of the literature—Part I: Formation of residual stresses*. Composites Part A: Applied Science and Manufacturing, 2006. **37**(11): p. 1847-1857.
22. Radford, D.W. and T.S. Rennick, *Separating sources of manufacturing distortion in laminated composites*. Journal of Reinforced Plastics and Composites, 2000. **19**(8): p. 621-641.
23. Zahlan, N. and J.M. O'Neill, *Design and fabrication of composite components; the spring-forward phenomenon*. Composites, 1989. **20**(1): p. 77-81.
24. Salomi, A., et al., *Spring-in angle as molding distortion for thermoplastic matrix composite*. Composites Science and Technology, 2008. **68**(14): p. 3047-3054.
25. Kim, B.-S., et al., *Numerical analysis of the dimensional stability of thermoplastic composites using a thermoviscoelastic approach*. Journal of Composite Materials, 2002. **36**(20): p. 2389-2403.
26. Brauner, C., et al., *Analysis of process-induced deformations in thermoplastic composite materials*. Journal of Composite Materials, 2014. **48**(22): p. 2779-2791.
27. NASA, N., *Cost estimating handbook*. Washington, DC, 2008.
28. Hueber, C., K. Horejsi, and R. Schledjewski, *Review of cost estimation: methods and models for aerospace composite manufacturing*. Advanced Manufacturing: Polymer & Composites Science, 2016. **2**(1): p. 1-13.
29. Curran, R., S. Raghunathan, and M. Price, *Review of aerospace engineering cost modelling: The genetic causal approach*. Progress in Aerospace Sciences, 2004. **40**(8): p. 487-534.
30. Zaloom, V. and C. Miller, *A review of cost estimating for advanced composite materials applications*. Engineering Costs and Production Economics, 1982. **7**(1): p. 81-86.
31. Kellogg, R., E. Mahr, and M. Lobbia. *An analogy-based method for estimating the costs of spacecraft*. in *Aerospace Conference, 2005 IEEE*. 2005. IEEE.
32. Duverlie, P. and J. Castelain, *Cost estimation during design step: parametric method versus case based reasoning method*. The international journal of advanced manufacturing technology, 1999. **15**(12): p. 895-906.
33. Rush, C. and R. Roy, *Expert judgement in cost estimating: Modelling the reasoning process*. Concurrent Engineering, 2001. **9**(4): p. 271-284.
34. Rehman, S. and M.D. Guenov, *A methodology for modelling manufacturing costs at conceptual design*. Computers & Industrial Engineering, 1998. **35**(3): p. 623-626.
35. Watson, P., et al., *Cost estimation of machined parts within an aerospace supply chain*. Concurrent Engineering, 2006. **14**(1): p. 17-26.
36. Salam, A., N. Bhuiyan, and G.J. Gouw, *Parametric Cost Estimating Relationships for Design Effort Estimation*. World Academy of Science, Engineering and Technology, International Journal of Mechanical, Aerospace, Industrial, Mechatronic and Manufacturing Engineering, 2013. **7**(7): p. 1359-1364.
37. Schubel, P.J., *Technical cost modelling for a generic 45-m wind turbine blade produced by vacuum infusion (VI)*. Renewable Energy, 2010. **35**(1): p. 183-189.
38. Schubel, P.J., *Cost modelling in polymer composite applications: Case study – Analysis of existing and automated manufacturing processes for a large wind turbine blade*. Composites Part B: Engineering, 2012. **43**(3): p. 953-960.

39. Pantelakis, S.G., et al., *A concept to optimize quality and cost in thermoplastic composite components applied to the production of helicopter canopies*. Composites Part A: Applied Science and Manufacturing, 2009. **40**(5): p. 595-606.
40. Cutcher-Gershenfeld, J., R. Paduano, and B. Barrett, *Employing Activity Based Costing and Management Practices within the Aerospace Industry: Sustaining the Drive for Lean*. Boeing Commercial Airplane Group, Wichita Division/IAM, Wichita, Kansas, 1999 and 2000. 2001.
41. LeBlanc, D.J., *Advanced Composite Cost Estimation Manual (ACCCEM)*. 1976, Report no. AFFDL-TR-76-87, Northrop Corporation, 1976, LA, CA, USA.
42. TenCate *Cetex TC1100 PPS Resin System Datasheet*.
43. TenCate, *Cetex - PPS Guide Lines*. 2003.
44. *TA instruments - Q800 Brochure*. 2010.
45. B. Kaganj, L.L.L., M. Hojjati, S.V. Hoa, *Stamp Forming of S-shape Thermoplastic Composites*, in *10th Joint Canada-Japan Workshop on Composites*. 2014, DEStech Publications, Inc: Vancouver, Canada.
46. *Product Datasheet: TenCate Cetex TC1100 PPS resin system*, TenCate, Editor. 2016.
47. Menessier, E., et al., *Axial and Radial Coefficients of Thermal Expansion of Carbon Fibers in the 20°–430°C Temperature Range as Derived from the Thermal Expansion in A Collection of Papers Presented at the 13th Annual Conference on Composites and Advanced Ceramic Materials: Ceramic Engineering and Science Proceedings*. 1989, John Wiley & Sons, Inc. p. 1426-1439.
48. Villière, M., et al., *Experimental determination and modeling of thermal conductivity tensor of carbon/epoxy composite*. Composites Part A: Applied Science and Manufacturing, 2013. **46**: p. 60-68.
49. Gowayed, Y. and J.-C. Hwang, *Thermal conductivity of composite materials made from plain weaves and 3-D weaves*. Composites Engineering, 1995. **5**(9): p. 1177-1186.
50. TORAYCA *T300 Datasheet*.
51. Woo, K. and N.S. Goo, *Thermal conductivity of carbon-phenolic 8-harness satin weave composites*. Composite Structures, 2004. **66**(1): p. 521-526.
52. Sridhar, L., *Investigation of thermal contact resistance at a plastic-metal interface in injection molding (Doctoral dissertation)*. New Jersey Institute of Technology, 2000.
53. Astrom, B.T., *Manufacturing of polymer composites*. 1997: CRC Press.
54. Hyer, M.W., *Stress analysis of fiber-reinforced composite materials*. 2009: DEStech Publications, Inc.
55. ABAQUS, *ABAQUS online documentation 6.14*. 2017, Dassault Systemes.
56. Zeng, H., G. He, and G. Yang, *Friction and wear of poly (phenylene sulphide) and its carbon fibre composites: I unlubricated*. Wear, 1987. **116**(1): p. 59-68.
57. Haanappel, S.P., et al., *Formability analyses of uni-directional and textile reinforced thermoplastics*. Composites Part A: Applied Science and Manufacturing, 2014. **56**: p. 80-92.
58. Nguyen, H.-D., M. Deshaies, and X.-T. Pham, *Simulation-Assisted Mold Design For Forming of Thermoplastic PPS/Carbon Fiber Composites*. Aero 2015 Conference, Montreal, 2015.
59. AniFormEngineering, *Material Calibration Sheet - Version 2.0*, AniFormEngineering, Editor. 2016.

60. ten Thije, R.H.W., R. Akkerman, and J. Huétink, *Large deformation simulation of anisotropic material using an updated Lagrangian finite element method*. *Computer Methods in Applied Mechanics and Engineering*, 2007. **196**(33): p. 3141-3150.
61. Cao, J., et al., *Characterization of mechanical behavior of woven fabrics: experimental methods and benchmark results*. *Composites Part A: Applied Science and Manufacturing*, 2008. **39**(6): p. 1037-1053.
62. Sachs, U., R. Akkerman, and S.P. Haanappel. *Bending characterization of UD composites*. in *Key Engineering Materials*. 2014. Trans Tech Publ.
63. Sachs, U., *Friction and bending in thermoplastic composites forming processes (Doctoral dissertation)*. 2014: University of Twente.
64. *Minitab 17 Statistical Software*. 2010, Minitab, Inc. (www.minitab.com): State College, PA.
65. Cook, C. and J. Graser, *Military Airframe Acquisition Costs: The Effects of Lean Manufacturing, 2001*. RAND MR-1325.
66. Bernet, N., et al., *An integrated cost and consolidation model for commingled yarn based composites*. *Composites Part A: Applied Science and Manufacturing*, 2002. **33**(4): p. 495-506.
67. Neuvoo. *Neuvoo Job Search* (<https://neuvoo.ca/salaire/technicien-en-composite/>). 17/10/2017.

